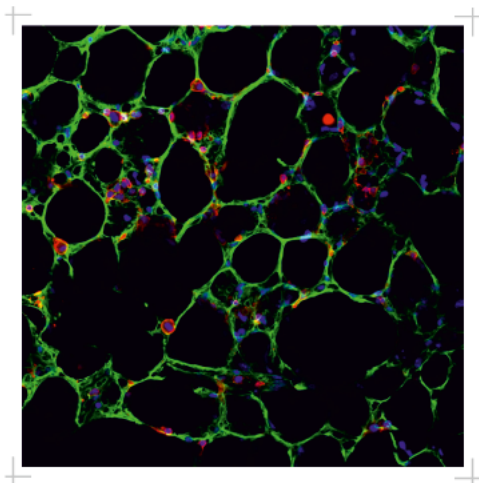


Determination of lung regeneration using an *ex vivo* tissue slice model

Franziska Uhl



Dissertation zum Erwerb des
Doktorgrades der Naturwissenschaften
an der Medizinischen Fakultät der
Ludwig-Maximilians-Universität München



édition scientifique
VVB LAUFFERSWEILER VERLAG

Das Werk ist in allen seinen Teilen urheberrechtlich geschützt.

Die rechtliche Verantwortung für den gesamten Inhalt dieses Buches liegt ausschließlich bei den Autoren dieses Werkes.

Jede Verwertung ist ohne schriftliche Zustimmung der Autoren oder des Verlages unzulässig. Das gilt insbesondere für Vervielfältigungen, Übersetzungen, Mikroverfilmungen und die Einspeicherung in und Verarbeitung durch elektronische Systeme.

1. Auflage 2015

All rights reserved. No part of this publication may be reproduced, stored in a retrieval system, or transmitted, in any form or by any means, electronic, mechanical, photocopying, recording, or otherwise, without the prior written permission of the Authors or the Publisher.

1st Edition 2015

© 2015 by VVB LAUFERSWEILER VERLAG, Giessen
Printed in Germany



édition scientifique
VVB LAUFERSWEILER VERLAG

STAUFENBERGRING 15, D-35396 GIESSEN
Tel: 0641-5599888 Fax: 0641-5599890
email: redaktion@doktorverlag.de

www.doktorverlag.de

Aus dem Comprehensive Pneumology Center Munich des
Institut für experimentelle Pneumologie
Direktor: Prof. Dr. med. Oliver Eickelberg

Determination of lung regeneration using an *ex vivo* tissue slice model

Dissertation zum Erwerb des Doktorgrades der Naturwissenschaften
an der Medizinischen Fakultät der Ludwig-Maximilians-Universität München

vorgelegt von

Franziska Uhl
aus Hof

München, 2014

Gedruckt mit Genehmigung der Medizinischen Fakultät der Ludwig-Maximilians-Universität München

| | |
|-----------------------------|---|
| Betreuer: | PD. Dr. rer. nat. Silke Meiners |
| Zweitgutachterin: | Prof. Dr. rer. nat. Sabine Marten-Steffens |
| Dekanin bzw. Dekan: | Prof. Dr. med. Dr. h.c. M. Reiser, FACR, FRCR |
| Tag der mündlichen Prüfung: | 01.07.2015 |

***Dedicated to all the people that
supported me during my journey***

TABLE OF CONTENTS

| | |
|--|-----------|
| Table of Contents | I |
| Abbreviations | V |
| 1 Zusammenfassung | 1 |
| 2 Summary | 2 |
| 3 Introduction | 3 |
| 3.1 Lung repair and remodelling | 3 |
| 3.1.1 Chronic obstructive pulmonary disease | 3 |
| 3.1.2 Pathogenesis of COPD | 4 |
| 3.2 Signalling pathways involved in lung repair | 6 |
| 3.2.1 The wingless/integrase-1 (Wnt) signalling pathway | 6 |
| 3.2.1.1 Canonical Wnt signalling | 6 |
| 3.2.1.2 Non-canonical Wnt signalling..... | 7 |
| 3.2.1.3 Wnt signalling in development | 7 |
| 3.2.1.4 Wnt signalling in disease and regeneration..... | 8 |
| 3.2.1.5 Pharmacological modulation of Wnt signalling..... | 8 |
| 3.2.2 The TGF-beta signalling pathway | 10 |
| 3.2.2.1 TGF-beta and epithelial-to-mesenchymal transition | 11 |
| 3.2.2.2 TGF-beta in COPD and lung cancer..... | 11 |
| 3.3 Translational medicine and preclinical models..... | 12 |
| 3.4 Precision cut tissue slices – 3D <i>ex vivo</i> lung tissue cultures | 13 |
| 3.5 Hypothesis and aims of this thesis | 15 |
| 4 Materials and Methods | 16 |

| | | |
|---------|---|----|
| 4.1 | Materials..... | 16 |
| 4.1.1 | Laboratory equipment and software..... | 16 |
| 4.1.2 | Chemicals and consumables..... | 18 |
| 4.1.3 | Buffers, solutions and media..... | 21 |
| 4.1.4 | Standards and Kits..... | 23 |
| 4.1.5 | Enzymes..... | 23 |
| 4.1.6 | Oligonucleotides..... | 23 |
| 4.1.7 | Antibodies..... | 25 |
| 4.1.8 | Animals..... | 27 |
| 4.1.9 | Human Tissue..... | 27 |
| 4.2 | Methods..... | 28 |
| 4.2.1 | Animal model of emphysema induced by elastase instillation..... | 28 |
| 4.2.2 | Generation of 3D-LTC (PCLS)..... | 28 |
| 4.2.2.1 | Generation of 3D-LTC from murine lungs..... | 29 |
| 4.2.2.2 | Generation of 3D-LTC from human lung segments..... | 30 |
| 4.2.3 | RNA expression analysis..... | 30 |
| 4.2.3.1 | RNA isolation..... | 30 |
| 4.2.3.2 | cDNA synthesis by reverse transcription..... | 31 |
| 4.2.3.3 | Quantitative PCR (qPCR)..... | 31 |
| 4.2.4 | Genotyping..... | 32 |
| 4.2.5 | Viability and proliferation assays..... | 33 |
| 4.2.5.1 | Live/Dead assay..... | 33 |
| 4.2.5.2 | WST-1 assay..... | 34 |
| 4.2.5.3 | BrdU assay..... | 34 |
| 4.2.5.4 | Lactate dehydrogenase (LDH) assay..... | 34 |
| 4.2.6 | Proteinbiochemistry..... | 35 |
| 4.2.6.1 | Protein isolation and concentration determination..... | 35 |
| 4.2.6.2 | Protein analysis with Western Blot..... | 35 |
| 4.2.6.3 | Enzyme-linked immunosorbant assay (ELISA)..... | 35 |
| 4.2.7 | Histology..... | 35 |

| | | |
|----------|--|-----------|
| 4.2.7.1 | Haematoxylin & Eosin (H&E) staining | 36 |
| 4.2.7.2 | Masson-Trichrome (MTC) staining | 37 |
| 4.2.7.3 | Elastin staining | 38 |
| 4.2.7.4 | LacZ staining..... | 38 |
| 4.2.7.5 | Immunofluorescence | 39 |
| 4.2.8 | Live cell imaging | 39 |
| 4.2.9 | Statistical Analysis | 39 |
| 5 | Results..... | 40 |
| 5.1 | Characterization of 3D-LTC from healthy/non-COPD tissue over time..... | 40 |
| 5.2 | Characterization of 3D-LTC from diseased lung tissue specimen..... | 42 |
| 5.2.1 | Morphology and viability of 3D-LTC after elastase induced emphysema | 43 |
| 5.2.2 | Morphology and viability of 3D-LTC from human patients..... | 46 |
| 5.3 | Characterization of Wnt/beta-catenin signalling in 3D-LTC..... | 49 |
| 5.4 | Wnt/beta-catenin activation in 3D-LTC from emphysematous mice and human patients 49 | |
| 5.4.1 | Toxicity of LiCl in 3D-LTC | 50 |
| 5.4.2 | Effects of Wnt/beta-catenin activation by LiCl in murine 3D-LTC | 51 |
| 5.4.3 | Effects of Wnt/beta-catenin activation by LiCl in human 3D-LTC..... | 56 |
| 5.4.4 | Wnt/beta-catenin activation by CT in 3D-LTC | 59 |
| 5.5 | TGF-beta activation in 3D-LTC..... | 62 |
| 6 | Discussion..... | 65 |
| 6.1 | Characterisation of 3D-LTC | 65 |
| 6.1.1 | Influence of the process of slice generation | 65 |
| 6.1.2 | Influence of the slice thickness and tissue density | 66 |
| 6.1.3 | Influence of the cultivation medium and culture conditions | 68 |
| 6.1.4 | Influence of the cultivation technique | 69 |

| | |
|--|-----------|
| 6.1.5 Benefits and limitations of the 3D-LTC | 69 |
| 6.1.5.1 Biosample preparation | 70 |
| 6.1.5.2 Reduction in sample material | 70 |
| 6.1.5.3 Natural environment and cellular composition in 3D | 71 |
| 6.1.5.4 Applications of 3D-LTC | 71 |
| 6.1.5.5 Translation to other animal models, organs, and diseases | 72 |
| 6.1.5.6 Limitations | 73 |
| 6.2 Pathway modulation studies with 3D-LTC | 74 |
| 6.2.1 Wnt/beta-catenin activation | 74 |
| 6.2.2 TGF-beta activation | 77 |
| 6.3 3D-LTC as a tool for preclinical testing | 78 |
| 6.4 Conclusion | 80 |
| 7 References | 82 |
| 8 Appendix | 95 |
| 8.1 Acknowledgements | 95 |
| 8.2 Curriculum vitae | 97 |
| 8.3 Publications and presentations | 98 |
| 8.4 Eidesstattliche Versicherung | 101 |

ABBREVIATIONS

A

| | |
|-----------|-----------------------------|
| A | adenosine |
| ABC | active beta catenin |
| AE | alveolar epithelial |
| Aqp5 | aquaporin 5 |
| APC | adenomatosis polyposis coli |
| APS | ammonium peroxodisulfate |
| alpha-SMA | alpha smooth muscle actin |
| AT I | alveolar epithelial type I |
| AT II | alveolar epithelial type II |
| ATP | adenosine triphosphate |
| Axin | axis inhibition protein |

B

| | |
|------|-----------------------------------|
| BALF | bronchoalveolar lavage fluid |
| BMSC | bone marrow stromal cells |
| BMP | bone morphogenic protein |
| BOS | bronchiolitis obliterans syndrome |
| bp | base pairs |
| BrdU | 5-bromo-2'-deoxyuridine |
| BSA | bovine serum albumine |

C

| | |
|-----------------------|---------------------------------------|
| °C | degrees Celsius |
| C | cytosine |
| cDNA | complementary DNA |
| CMV | <i>Cytomegalovirus</i> |
| COPD | chronic obstructive pulmonary disease |
| CSE | cigarette smoke extract |
| CT | chiron inhibitor CT99021 |
| CTGF | connective tissue growth factor |
| C _T -value | cycle of threshold value in qPCR |

D

| | |
|--------|---------------------------------------|
| 3D-LTC | 3D <i>ex vivo</i> lung tissue culture |
| d | day(s) |
| Da | dalton |
| Dapi | 4',6-diamidino-2-phenylindole |
| Dkk | dickkopf related protein |
| DMEM | Dulbecco's Modified Eagle's Medium |
| DMF | dimethyl formamide |
| DMSO | dimethyl sulfoxide |
| DNA | deoxyribonucleic acid |
| dNTP | desoxy-nucleotide-tri-phosphate |
| ds | double-stranded |

DTT dithiothreitol
DVL dishevelled

E

E embryonic day
ECL enhanced chemiluminescence
ECM extracellular matrix
EDTA ethylenediaminetetraacetic acid
EGFP enhanced green fluorescent protein
ela elastase
EMT epithelial-to-mesenchymal transition

F

FBS fetal bovine serum
FEV₁ forced expiratory volume within 1 s
FoxM1 forkhead box M1
FVC forced vital capacity
fw Forward
FZD frizzled receptor

G

G guanosine
g gram, standard acceleration
GFP green fluorescent protein
GOLD Global Initiative for Chronic Obstructive Lung Disease
GSK3-beta glycogen synthase kinase 3-beta
gDNA genomic DNA

H

h hour (s)
hs(a) *homo sapiens*
H&E hematoxylin eosin
HRP horse radish peroxidase

I

IgG immunoglobulin protein G
IF immunofluorescence
IL interleukin
IPF idiopathic pulmonary fibrosis
iPS induced pluripotent stem cells
IWP inhibitors of WNT production

K

K kilo
KCl potassium chloride

L

L liter
LCI live cell imaging
LDH lactate dehydrogenase

VI

| | |
|-------------------|---|
| LEF | lymphocyte enhancer factor |
| LGR | leucine-rich repeat containing, G-protein coupled receptors |
| LiCl | lithium chloride |
| LRP | lipoprotein receptor related proteins |
| LSM | laser scanning microscopy |
| M | |
| m | milli |
| M | molar |
| mA | milli Ampere |
| MgCl ₂ | magnesium chloride |
| min | minutes |
| MMLV | Moloney murine leukemia virus |
| MMP | matrix metalloprotease |
| mmu | <i>mus musculus</i> |
| mRNA | messenger RNA |
| μ | micro |
| N | |
| n | nano |
| NaCl | sodium chloride |
| n.d. | not determined |
| nt | nucleotide(s) |
| O | |
| ON | over night |
| P | |
| p | pico |
| p.a. | <i>pro analysis</i> |
| PAGE | polyacrylamide gel electrophoresis |
| PBND | PCR buffer with nonionic detergents |
| PBS | phosphate buffered saline |
| PBST | phosphate buffered saline with Tween® 20 |
| PCLS | precision cut lung slices |
| PCP | planar cell polarity |
| PCR | polymerase chain reaction |
| PDPN | podoplanin = T1alpha |
| PFA | paraformaldehyde |
| poly A | poly adenylation |
| PP1 | protein phosphatase 1 |
| PP2A | protein phosphatase 2A |
| PPE | porcine pancreatic elastase |
| PS | penicillin/streptomycin |
| PY | pack years |
| Q | |
| qPCR | quantitative PCR |

R

| | |
|------|---|
| RAGE | receptor for advanced glycation endproducts |
| RNA | ribonucleic acid |
| rpm | revolutions per minute |
| RT | room temperature |
| rv | reverse |

S

| | |
|---------|-----------------------------------|
| s | second |
| SDS | sodium dodecyl sulfate |
| sFRP | secreted frizzled related protein |
| Sftp | surfactant protein |
| Shh | sonic hedgehog |
| co-SMAD | common-mediator SMAD |
| I-SMAD | inhibitory SMAD |
| R-SMAD | receptor-regulated SMAD |
| smurf | smad ubiquitin regulatory factors |

T

| | |
|-------|---|
| T | thymidine |
| TAE | tris-acetate-EDTA |
| TBS | tri-phosphate buffered saline |
| TBST | tri-phosphate buffered saline with Tween® 20 |
| TCF | T-cell factor |
| TCEP | component of PerfectPure RNA Fibrous Tissue Kit, 5Prime |
| TE | tri-EDTA |
| TEMED | N,N,N',N'-Tetramethylethylenediamin |
| TGF | transforming growth factor |
| TGFbR | TGF-beta-receptor |
| TJP1 | tight junction protein 1 |
| TRIS | tris(hydroxymethyl)-aminomethane |

U

| | |
|---|---------------|
| U | unit, uridine |
|---|---------------|

V

| | |
|---|------|
| V | Volt |
|---|------|

W

| | |
|-------|--|
| w | weight |
| WB | Western Blot |
| Wnt | wingless/integrase-1 |
| Wisp1 | WNT1-inducible signaling pathway protein 1 |
| WST-1 | water soluble tetrazolium salt-1 |

Y

| | |
|---|------|
| y | year |
|---|------|

Z

ZO-1

zona occludens 1

1 ZUSAMMENFASSUNG

Die Chronisch obstruktive pulmonäre Erkrankung (COPD) ist die vierthäufigste Todesursache weltweit. Derzeit gibt es keine kurativen Therapieansätze und eine Lungentransplantation stellt die einzige lebensverlängernde Behandlungsalternative dar. Allerdings führt der Mangel an Spenderorganen dazu, dass die Lungentransplantation nicht für alle Patienten angewendet werden kann. Neue Therapieansätze werden daher dringend benötigt. In der vorliegenden Arbeit wurde eine Methode zur 3D *ex vivo* Kultivierung von Lungengewebe (3D-LTC) murinen und humanen Ursprungs angewendet, um die Regeneration und Wiederherstellung von Lungengewebe in hoher örtlicher und zeitlicher Auflösung zu untersuchen.

In einem ersten Schritt wurde die Herstellung und Kultivierung der 3D-LTC im Vergleich zu bisherigen Methoden verbessert. Zell-Vitalität und -Proliferation konnten bis Tag sieben erhalten werden. Murine sowie humane Proben wurden mittels histologischer und Immunfluoreszenz-Färbungen, orts- und zeit-aufgelöster konfokaler live-cell-Mikroskopie als auch Gen- und Protein-Expressionsanalysen untersucht, um das Model der 3D-LTC hinsichtlich seiner Eignung zur Untersuchung von Signalwegsmodulationen zu charakterisieren. Wie bereits gezeigt, führte die Aktivierung des Wnt/beta-Catenin-Signalweges zur Verminderung des Elastase-induzierten Emphysem im Mausmodell [Kneidinger, et.al., 2011]. TGF-beta ist ein weiterer Signalweg der eine Rolle in der COPD spielt und ein TGF-beta-Mangel kann mit der Entwicklung des Emphysems in Verbindung gebracht werden [Budd, et.al., 2012]. Um weitere Erkenntnis über die mechanistischen Ursachen zu erhalten, wurden die COPD-relevanten Signalwege Wnt/beta-Catenin und TGF-beta in 3D-LTC von COPD Patienten und emphysematösen Mäusen aktiviert. Es konnte gezeigt werden, dass die Aktivierung des Wnt/beta-Catenin Signalweges epitheliale Reparaturmechanismen in den 3D-LTC induziert. Weiterhin korrelierten die Aktivierung des Wnt/beta-Catenin-Signalweges sowie die Aktivierung von alveolären Typ-II-Epithelzellen mit dem Krankheitsschweregrad des Patienten. Diese Ergebnisse weisen darauf hin, dass 3D-LTC von Patienten für die Medikamentenevaluierung hinsichtlich personalisierter Medizin nützlich sein können. Des Weiteren war eine Aktivierung des TGF-beta-Signalweges in 3D-LTC möglich. TGF-beta führte zur Herstellung von Komponenten der extra-zellulären Matrix sowie der Expression von Transkriptionsfaktoren und Genen, die auf eine epitheliale-zu-mesenchymale Transition hinweisen. Es kann daher geschlossen werden, dass das in dieser Arbeit etablierte Model der 3D-LTC die Quantifizierung sowie ort- und zeit-aufgelöste Visualisierung sowohl regenerativer als auch remodulierender Prozesse in der Lunge möglich macht. Die individuelle Reaktion auf eine bestimmte medikamentöse Behandlung kann damit besser prognostiziert werden. Dadurch stellt das in dieser Arbeit etablierte Model der 3D-LTC ein ausgezeichnetes System zur pre-klinischen Medikamententestung dar.

2 SUMMARY

Chronic obstructive pulmonary disease (COPD) is the fourth leading cause of death worldwide. At the moment no curative treatment is available. Thus far, lung transplantation is the only option however donor organ shortage limits its general clinical application. New therapies are desperately needed. Here, 3D *ex vivo* lung tissue cultures (3D-LTC) from diseased murine and human lungs were applied to study repair and remodelling in high spatio-temporal resolution. In a first step, the method of 3D-LTC generation and cultivation was optimized and improved. Cell viability and proliferation was maintained until day seven. Murine and human lung samples were examined by histology, immunofluorescence, spatio-temporal confocal live-cell-imaging, as well as gene and protein expression analyses to fully characterize the suitability of the model for signal pathway modulation. Previous reports demonstrated that Wnt/beta-catenin signal activation led to attenuation of experimental emphysema in mice [Kneidinger, et.al., 2011]. TGF-beta is another pathway involved in COPD and a lack of TGF-beta seems to be related to the emphysematous changes [Budd, et.al., 2012]. To get insight into disease underlying mechanisms the COPD-relevant signalling pathways Wnt/beta-catenin and TGF-beta were activated in 3D-LTC from COPD patients and emphysematous animals. It was demonstrated that Wnt/beta-catenin signal activation initiated epithelial repair in 3D-LTC. Moreover, Wnt/beta-catenin pathway activation and alveolar epithelial type II cell activation significantly correlated with individual disease stage suggesting that 3D-LTC from patients are suitable for individual drug validation and therapy prediction. TGF-beta signalling activation led to the production of extracellular matrix components and induced expression of transcription factors and genes involved in epithelial-to-mesenchymal transition. In conclusion, the model of 3D-LTC established in this thesis allows quantification and spatio-temporal visualization of regenerative processes in the lung. It is suitable to validate and give further mechanistical insight of Wnt/beta-catenin and TGF-beta induced lung repair and remodelling, as well as treatment response prediction to individualized therapy. Thus, the 3D-LTC model presents a superior system for preclinical drug validation.

3 INTRODUCTION

3.1 Lung repair and remodelling

Chronic lung diseases are second leading cause of death worldwide with very limited treatment options. In most diseases such as chronic obstructive pulmonary disease (COPD) and idiopathic pulmonary fibrosis (IPF) no curative treatments are available and even keeping the “status quo” is not possible. Clinicians are seeking new treatment options. Understanding disease onset, development, and progression together with the discovery of markers for early diagnosis is crucial. Several factors are involved in lung repair. A complex interaction of cells, matrix, and the appropriate activation status of various signalling pathways, is required for normal tissue regeneration. Three main components involved in endogenous lung repair are: 1) the endogenous (progenitor) cells (e.g. basal, broncho-alveolar duct junction, Clara, distal progenitor, and ATII cells), 2) signalling pathways (e.g. wingless/integrase-1 (Wnt), sonic hedgehog (Shh), transforming growth factor (TGF) -beta, and Notch), and 3) the extracellular matrix (ECM) (with varying composition and mechanical properties throughout the lung) [Rock, et.al., 2012]. It has been shown that the lung, although known to be an organ of low tissue turnover (with less than 1% of epithelial cells undergoing proliferation in 24 h [Crosby, et.al., 2010]), has the capability of endogenous repair. For example, a cancer patient who had undergone lung resection at age 33 had pronounced compensatory lung growth within 15 years [Butler, et.al., 2012].

3.1.1 Chronic obstructive pulmonary disease

The main focus of this thesis was to study lung repair in the chronic lung disease COPD, which is the fourth leading cause of death worldwide (5% of all deaths globally in 2005) and will most probably increase in prevalence until 2030 [Churg, et.al., 2007, Stockley, et.al., 2009, WHO, Date last updated: October 2013. Date last accessed: June 02 2014]. The main risk factor to develop COPD is tobacco smoke (direct smoking as well as second-hand smoke), while other environmental pollutants and recurring infections of the lower respiratory tract during childhood are also known to be involved in triggering the disease. Patients are most commonly classified using the Global Initiative for Chronic Obstructive Lung Disease (GOLD) stage (I-IV), which is based on lung function data from spirometer measurements [Rabe, et.al., 2007]. The forced expiratory volume in one second (FEV₁) and its ratio to the forced vital capacity (FVC) is a measure for disease severity, is influenced by age, sex, height, and ethnicity, and expressed as percentage of predicted. COPD is mostly diagnosed in patients older than 40 years presenting with shortness of breath and productive cough [Molfinio, et.al., 2007, Rabe, et.al., 2007, Vestbo, et.al., 2013]. While there is currently no curative treatment, disease progression can only be decelerated by pharmacological intervention [Barnes, 2010, WHO, Date last updated: October 2013. Date last accessed: June 02 2014]. Mainly bronchodilators, corticosteroids, phosphodiesterase-4 inhibitors, and combinations thereof are used for therapeutic intervention. While corticosteroids improve quality of life and

reduce exacerbations, there is no uniform decline in lung function but is restricted to a small group of patients [Barnes, 2010, Burge, 2001, Celli, et.al., 2008, Yang, et.al., 2007]. Patients with moderate to severe COPD suffer from progressive decline in lung function, necessitating long-term administration of oxygen (>15 h/d), especially in patients with very severe COPD (stage IV). The only remaining option is lung transplantation, but due to the lack of donor organs, this is only available for a subgroup of patients and further bears the risk of developing a chronic allograft dysfunction, called bronchiolitis obliterans syndrome (BOS). The limitation of therapeutic intervention underlines the need for a better understanding of the disease to develop new therapies.

3.1.2 Pathogenesis of COPD

Smoke, as well as other environmental pollutants, repetitively injures lung epithelial cells, which are lining the airways and alveoli, leading to infiltration of inflammatory cells into the airspaces. This inflammation is not pathogenic in non-susceptible smokers [Hogg, et.al., 2009, Sharafkhaneh, et.al., 2008]. In the subset of patients which are susceptible to develop COPD, pathogenic inflammation is enhanced and leads to chronic bronchitis, small airway obstruction, and peripheral airspace enlargement with alveolar destruction –called emphysema [Chung, et.al., 2008, Hogg, et.al., 2009, Sharafkhaneh, et.al., 2008]. Inflammation is not a singular cause for COPD progression. New paradigms in COPD progression include alveolar epithelial cell senescence and premature aging due to abnormalities in telomere length and expression of senescence-related cell-cycle regulators [Chilosi, et.al., 2012, Shi, et.al., 2012]. Furthermore, “second/additional hits” such as oxidative stress (caused by environmental exposure, such as cigarette smoke), protease/anti-protease imbalances, abnormal healing after injury, aberrant remodelling, and enhanced apoptosis, in addition to the missing ability of the lung to regenerate the injured tissue, are further causes for disease progression [Beasley, 2010, Sharafkhaneh, et.al., 2008].

Small airway obstruction (also known as small airway disease), one of the main features of COPD, occurs due to airway narrowing affecting mainly airways smaller than 2 mm in diameter. Narrowing of the airways primarily occurs due to inflammation and peribronchial fibrotic processes increasing small airway walls thickness [Hogg, et.al., 2004, McDonough, et.al., 2011, Sturton, et.al., 2008]. Airway epithelial cells and the smooth muscle cell layer are the main sites affected. Small airway disease furthermore contributes to progressive airflow limitation and air trapping [Chung, 2005, Stockley, et.al., 2009]. The second main feature of COPD –emphysema– is characterised by airspace enlargement, loss of alveolar structure, and impaired alveolar repair processes. Emphysematous changes typically seen in the lung are shown in Figure 3.1.

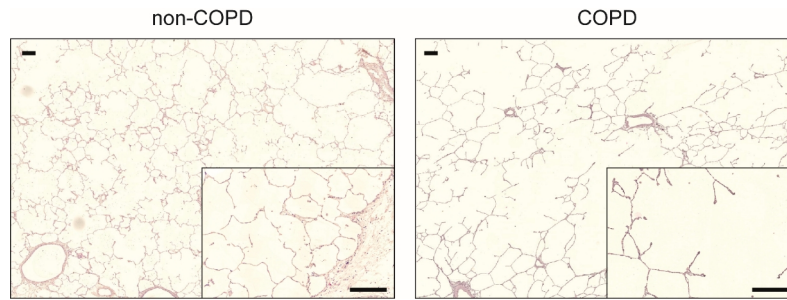


Figure 3.1: Emphysematous changes in patients with COPD showing airspace enlargement and alveolar destruction.

Haematoxylin-Eosin staining of 3D *ex vivo* lung tissue cultures (3D-LTC) from non-COPD and COPD patients. Inserts are showing a higher magnification. Scale bars 100 μm .

An activation of macrophages contributes to the development of emphysema. Macrophages play a central role in recruiting other inflammatory cells, such as neutrophils. Activated macrophages and neutrophils release proteases such as matrix metallo-proteinase (MMP), in particular MMP-9 and MMP-12 as well as neutrophil elastase (ela), leading to enhanced degradation of the alveolar ECM [Shapiro, 2002]. Moreover, activated macrophages and neutrophils secrete chemokines, which further enhances recruitment and infiltration of the tissue by inflammatory cells (Figure 3.2). This vicious cycle is thought to be the driving force behind COPD progression [Sharafkhaneh, et.al., 2008].

In addition, alveolar epithelial type (AT) I and II cells undergo apoptosis in response to cigarette smoke, thereby worsening emphysema. ATI cells are the main cellular component of the alveolus covering 95% of its surface area. The residual area is covered by ATII cells, which are known to be able to differentiate into ATI cells [Barkauskas, et.al., 2013, Rawlins, et.al., 2008]. ATI cells are elongated flat cells and are in close contact to the endothelial cells of the capillary network separated by a basement membrane only. Due to this, the barrier for gas exchange is no thicker than 1-2 μm . This is important as gas exchange is driven by diffusion. Thickening this barrier leads to tremendous reduction in oxygen uptake. Another important component for gas exchange is surfactant (from **surface active agent**), which is produced exclusively by ATII cells. Surfactant proteins help reducing the surface tension and thereby the resistance of the lung during breathing. By this, it is obvious that an abnormal reduction of ATI and/or ATII cells without fast and proper restoration is fatal.

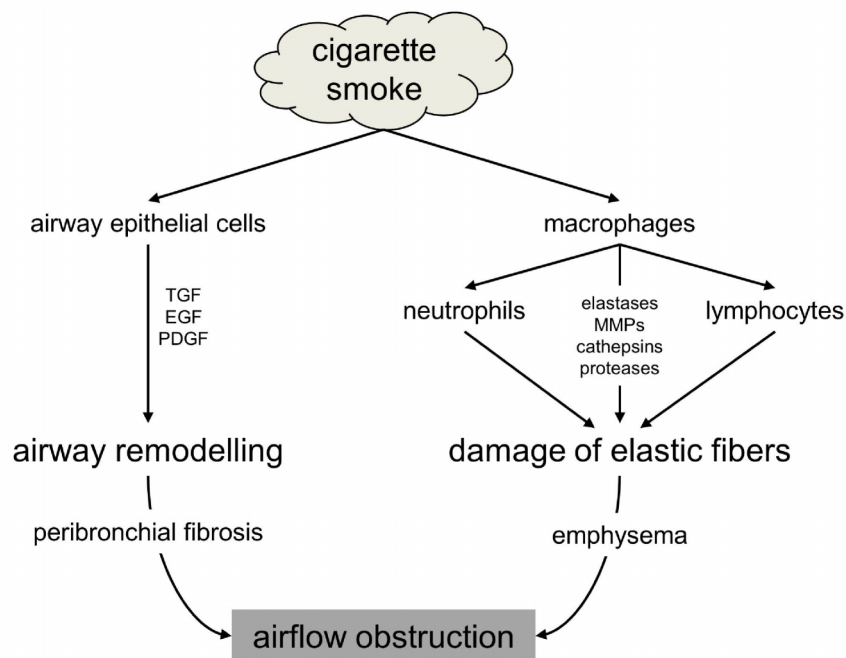


Figure 3.2: Scheme of airflow obstruction development caused by cigarette smoke.

Cigarette smoke induces release of elastolytic enzymes by activated macrophages, neutrophils, and lymphocytes leading to emphysema. The airway epithelial cells release cytokines leading to airway remodelling and peribronchial fibrosis. In total, this leads to the airflow obstruction seen in COPD. Modified from [Sharafkhaneh, et.al., 2008].

3.2 Signalling pathways involved in lung repair

3.2.1 The wingless/integrase-1 (Wnt) signalling pathway

In chronic lung diseases such as COPD and IPF, aberrant activation of Wnt signalling was shown by various groups [Chilosi, et.al., 2003, Ezzie, et.al., 2012, Kneidinger, et.al., 2011, Konigshoff, et.al., 2010, Konigshoff, et.al., 2009, Lam, et.al., 2011, Wang, et.al., 2011]. The Wnt signalling pathway is highly conserved over species and is of importance in embryonic development as well as in postnatal tissue repair and regeneration [Baarsma, et.al., 2013, Konigshoff, et.al., 2010]. The pathway is divided into the canonical (beta-catenin-dependant) and the non-canonical (beta-catenin-independent) signalling axis. Wnt signalling components and modulators involve 19 secreted Wnt ligands, 10 frizzled receptors (FZD), the low-density lipoprotein receptor related proteins (LRP) 5 and 6, and various extracellular modulators (e.g. Dickkopfs (DKK) 1-4). It has been suggested that secreted Wnt ligands can compensate for each other, but Wnt1, 2, 3A, 8, and 10B are known to induce canonical Wnt signalling, while Wnt5A and 11 predominantly mediate non-canonical Wnt signalling [Al Alam, et.al., 2013, Baarsma, et.al., 2013, Niehrs, 2012].

3.2.1.1 Canonical Wnt signalling

In the absence of Wnt ligands, beta-catenin, the key effector of canonical Wnt signalling, is targeted by its destruction complex –consisting of axin, adenomatosis polyposis coli (APC), glycogen

synthase kinase-3 (GSK3), casein kinase-1 (CK-1), and protein phosphatases (PP1, and PP2A). This leads to phosphorylation of beta-catenin, targeting it for proteasomal degradation, and keeping cytoplasmic levels low. When a secreted Wnt ligand is bound to its FZD receptor and co-receptor LRP5/6, the beta-catenin destruction complex is inactivated via phosphorylation of LRP5/6 by GSK3 and CK-1. By this, beta-catenin is no longer phosphorylated, no longer targeted for proteasomal degradation, can enrich in the cytoplasm, and translocate into the nucleus, leading to TCF/LEF-dependent gene transcription. Nuclear translocation seems to be FoxM1-dependent, which can bind to beta-catenin and contains a functional nuclear location signal [Zhang, et.al., 2011]. Target genes of canonical Wnt signalling vary depending on cellular and tissue context. Axin2, a negative feedback regulator, seems to be an exception by being context independent [Grigoryan, et.al., 2008, Nusse, 2012]. Functionally, the canonical Wnt pathway is most predominantly involved in cell proliferation and differentiation [Angers, et.al., 2009, Baarsma, et.al., 2013, Clevers, 2006, Konigshoff, et.al., 2010, Logan, et.al., 2004, Macdonald, et.al., 2007, MacDonald, et.al., 2009, Niehrs, 2012, Nusse, 2012].

3.2.1.2 *Non-canonical Wnt signalling*

Non-canonical Wnt signalling can be divided into the planar cell polarity (PCP) pathway, the Wnt-Ca²⁺-pathway, and several other known pathways (e.g. Wnt-RAP-1, Wnt-ROR2, Wnt-PKA, Wnt-GSK3-MT, Wnt-aPKC, Wnt-RYK, and Wnt-mTOR), which are possibly overlapping with the PCP and Wnt-Ca²⁺-pathway [Niehrs, 2012, Nusse, 2012, Semenov, et.al., 2007]. Following Wnt ligand binding, the PCP pathway acts via the small GTPases Rho and Rac and does not require LRP5/6 for downstream signalling. Thus, the PCP pathway is involved in cytoskeletal rearrangements, polarisation of cell sheets, and cell movements during gastrulation. The PCP and canonical Wnt pathway can antagonize each other. Of particular note, Wnt5A, a ligand well-known for inducing non-canonical Wnt signalling can inhibit Wnt3A-induced canonical Wnt signalling [Bryja, et.al., 2009, Niehrs, 2012].

The Wnt-Ca²⁺-pathway acts via increasing intracellular Ca²⁺-levels which then leads to activation of phospholipase C (PKC), calmodulin-dependent protein kinase II (CAMKII), and nuclear factor of activated T-cells (NFAT), and, similar to the PCP pathway, can antagonize canonical Wnt signalling. The Wnt-Ca²⁺-pathway is known to be involved in development, cancer, inflammation, and neurodegeneration [Baarsma, et.al., 2013, De, 2011, Niehrs, 2012].

3.2.1.3 *Wnt signalling in development*

The Wnt signalling pathway is involved in development and tissue regeneration of different organs and therefore, tight regulation is crucial (see Grigoryan *et al.* for a comprehensive review) [Grigoryan, et.al., 2008]. Different signalling pathways, such as transforming growth factor (TGF) beta, sonic hedgehog (Shh), connective tissue growth factor (CTGF), and Notch, are known to interact with Wnt signalling. For example, FGF and Shh pathways are major downstream targets

of Wnt-regulated Wnt signalling [Ahn, et.al., 2010]. The correct spatio-temporal signalling between the mesenchyme and epithelium is required for organogenesis [Hines, et.al., 2014]. In particular, Wnt signalling is known to be critical in lung development, regeneration and repair, and is deranged in a number of adult lung diseases such as pulmonary fibrosis, lung cancer, and COPD [Chilosi, et.al., 2012, Clevers, 2006, Konigshoff, et.al., 2010, Lam, et.al., 2011, Li, et.al., 2014, Van Scoyk, et.al., 2008].

The lung develops from the endoderm, specifically from the ventral foregut, a process where the correct allocation and expression of FGF9/10, bone morphogenic protein (BMP) 4, Wnt2/7B, and Shh play key roles [Morrisey, et.al., 2010]. First, two buds are formed, which, eventually extend into the left and right lung. This is followed by the pseudoglandular stage whereby “tree-like” branching occurs for several branching generations [Rawlins, 2008]. Wnt, BMP, and FGF play a key role in the pseudoglandular stage by transcriptional activation of Nkx2-1, the earliest marker of the pulmonary lineage.

3.2.1.4 *Wnt signalling in disease and regeneration*

Aberrant activation of canonical Wnt signalling can result in the development of cancers and contributes to various fibroproliferative diseases [Clevers, 2006, Gosens, et.al., 2008, Konigshoff, et.al., 2008, Konigshoff, et.al., 2009, Lam, et.al., 2011]. Furthermore, decreased Wnt/beta-catenin signalling has been demonstrated in human COPD samples and animal models of emphysema. Importantly, activation of Wnt/beta-catenin signalling by inactivation of GSK3 by LiCl led to an attenuation of experimental emphysema [Kneidinger, et.al., 2011, Zhou, et.al., 2012]. Wnt signalling is known to be involved in stem cell proliferation and renewal [Chilosi, et.al., 2012]. In particular, following epithelial injury, Wnt signalling is of major importance for epithelial repair. Mice lacking beta-catenin in alveolar epithelial cells showed increased alveolar epithelial cell death and had more severe fibrosis in a bleomycin induced fibrosis model [Tanjore, et.al., 2013]. Further, knockdown of beta-catenin using a shRNA approach delayed epithelial repair [Zemans, et.al., 2011]. In contrast to other organs like the intestine, the respiratory epithelium has a very slow turnover rate, and it is evident that distortion of Wnt signalling has long-range effects on the functionality of the lung [Rock, et.al., 2011]. As discussed before, the entire process of regeneration and the reasons why some individuals develop lung disease due to improper repair while others are protected is incompletely understood and needs further research to be able to develop new treatments.

3.2.1.5 *Pharmacological modulation of Wnt signalling*

Wnt signalling is involved in the development and progression of various diseases such as cancer, neurologic diseases (e.g. Alzheimer), disorders of bone metabolism (e.g. osteoporosis), inflammatory diseases (e.g. fibrosis), etc. [Niehrs, 2012, Zimmerman, et.al., 2012]. In lung disease, canonical/non-canonical Wnt signalling is aberrantly activated. While it is reactivated in lung

fibrosis, it was shown to be attenuated in COPD [Chilosi, et.al., 2012, Chilosi, et.al., 2003, Ezzie, et.al., 2012, Kneidinger, et.al., 2011, Konigshoff, et.al., 2008, Konigshoff, et.al., 2009, Lam, et.al., 2011, Wang, et.al., 2011]. Wnt signalling modulation is therefore an appealing treatment option for several chronic (lung) diseases. Various chemical compounds can be used to interfere with the Wnt pathway [Baarsma, et.al., 2013, Kahn, 2014].

Inhibition of Wnt signalling can be achieved by interfering with Wnt ligands (e.g. inhibitors of WNT production (IWPs) [Chen, et.al., 2009, Gopalsamy, et.al., 2008, Pelletier, et.al., 2009]), Wnt secretion (LGK974), FZD interaction with DVL [Fujii, et.al., 2007, Grandy, et.al., 2009, Shan, et.al., 2005]), the beta-catenin destruction complex (e.g. inhibitors of Wnt response (IWRs) [Gunaydin, et.al., 2012, Huang, et.al., 2009]), and interference with beta-catenin signalling (e.g. ICG-001 and IQ-1 [Emami, et.al., 2004]). Further examples for Wnt signalling antagonists are 1) Dickkopf proteins and Wise, which each act at the receptor level by binding to LRPs and blocking Wnt ligand binding and 2) sFRPs and WIF-1, which directly bind to Wnt ligands and thereby interfere with receptor binding.

Wnt activation can be achieved by inactivation of the mentioned Wnt antagonists [Gopalsamy, et.al., 2008, Pelletier, et.al., 2009], inhibition of GSK3 (e.g. chiron inhibitor CT99021 (later called CT), LiCl, SB216763, and SB415286 [Bain, et.al., 2007, Murray, et.al., 2004]), or a decrease of beta-catenin breakdown [Baarsma, et.al., 2013]. Most commonly, GSK3 inhibition is used. Bain and colleagues recommended CT because it more specifically inhibits GSK3 as compared to other GSK3 inhibitors [Bain, et.al., 2007]. Recently, LiCl was applied to attenuate emphysema *in vivo* [Kneidinger, et.al., 2011, Zhou, et.al., 2012]. A scheme of canonical Wnt signalling and the inhibition of GSK3 for Wnt pathway modulation are depicted in Figure 3.3. The two pharmacological compounds used in this study (LiCl and CT) are depicted as well.

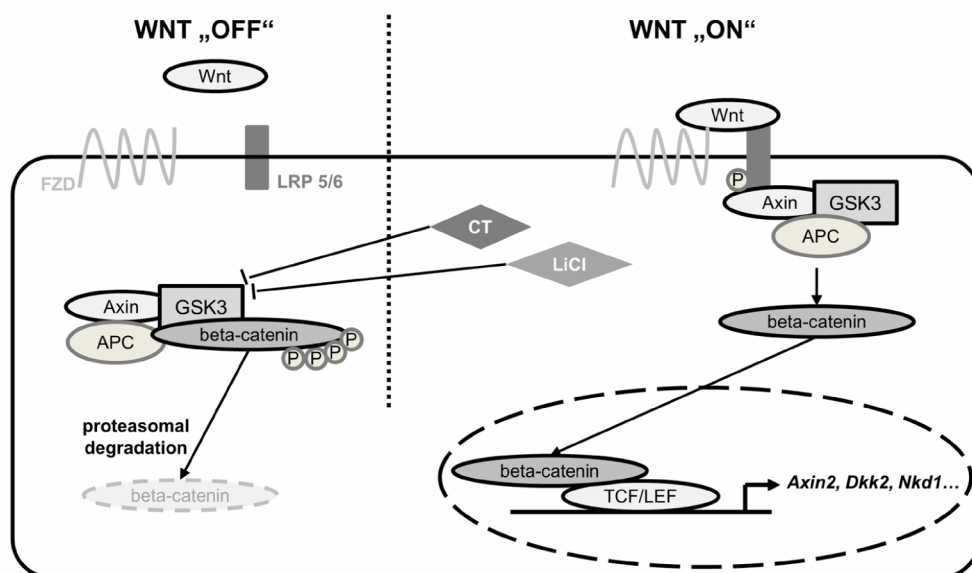


Figure 3.3: Simplified scheme of canonical Wnt/beta-catenin signalling showing its main components.

If no Wnt ligand is bound to its receptors (Frizzled and LRP 5/6) the destruction complex (consisting of APC, Axin, and GSK3) phosphorylates beta-catenin leading to its degradation by the proteasome. When a Wnt ligand is bound to its

receptors the destruction complex is attracted to the cell membrane and cannot phosphorylate beta-catenin anymore making it capable to trans-locate to the nucleus and induce TCF/LEF-dependent gene transcription. LiCl as well as CT inhibit the action of GSK3, thereby leading to pathway activation by prevention of beta-catenin phosphorylation and degradation.

3.2.2 The TGF-beta signalling pathway

In recent studies, a link between TGF-beta and beta-catenin signalling has been shown. Zhou and colleagues confirmed the interaction of beta-catenin with phosphorylated SMAD3 (SMAD, the *Caenorhabditis elegans* protein SMA (from the gene *sma* for small body size) and homolog of both the *Drosophila* protein, mothers against decapentaplegic (MAD)) to form a ternary complex inducing alpha smooth muscle actin (alpha-SMA=Acta2) gene expression in rat lung epithelial cells [Zhou, et.al., 2012]. Furthermore, TGF-beta induced PI3K/Akt2-signalling, leading to inhibition of GSK3 activity in renal tubular epithelial cells [Lan, et.al., 2014]. Additionally, it has been shown that TGF-beta can induce active beta-catenin (ABC, a surrogate marker for active canonical Wnt signalling) via phosphorylation of GSK3 and upregulates beta-catenin mRNA levels [Baarsma, et.al., 2011, Baarsma, et.al., 2011]. This gives evidence, that TGF-beta and Wnt signalling are connected to each other.

The TGF-beta superfamily consists of activins, inhibins, BMP, and growth factors, e.g. TGF-beta1, TGF-beta2, and TGF-beta3 [Massague, 2008, Taylor, et.al., 2008]. TGF-beta is secreted by various cell types and can be integrated into the extracellular matrix in a latent form and released again, by the action of proteases like thrombin, plasmin, and MMPs. Signalling is induced by binding of ligands to TGF-beta-receptor (TGFbR) I and II, which then form a heteromeric complex. This coupling enables the kinase domain of the type II receptor to phosphorylate the type I receptor, leading to activation of small phenotype and mothers against decapentaplegic related protein signalling. There are different classes of SMAD proteins depending on their function, receptor-regulated (R-SMAD: SMAD1, SMAD2, SMAD3, SMAD5, SMAD8/9), common -mediator SMAD (co-SMAD: SMAD4), and antagonistic or inhibitory SMAD (I-SMAD: SMAD6, SMAD7). R-SMADs 2 and 3 bind to the type I receptor, become phosphorylated, and then dissociate from the receptor again. Subsequently, a complex of phosphorylated SMAD2/3 is formed with SMAD4 and this complex interacts with a broad range of DNA-binding partners in the nucleus to regulate gene expression. A simplified scheme of canonical TGF-beta signalling showing its main components is depicted in Figure 3.4. One target gene of canonical smad signalling is SMAD7, which has an inhibitory effect on SMAD2/3 signalling. The SMAD7 protein can act as a negative feedback regulator by recruitment of E3 ubiquitin ligases and smad ubiquitin regulatory factors 1/2 (*smurf1/2*) to mediate receptor turnover, thereby inhibiting TGF-beta signalling [Taylor, et.al., 2008]. Additionally, TGF-beta can induce SMAD-independent signalling leading to activation of several other pathways (e.g. JNK, p38, p42/44 (ERK), and PI-3-kinase pathways) [Budd, et.al., 2012, Zhang, 2009].

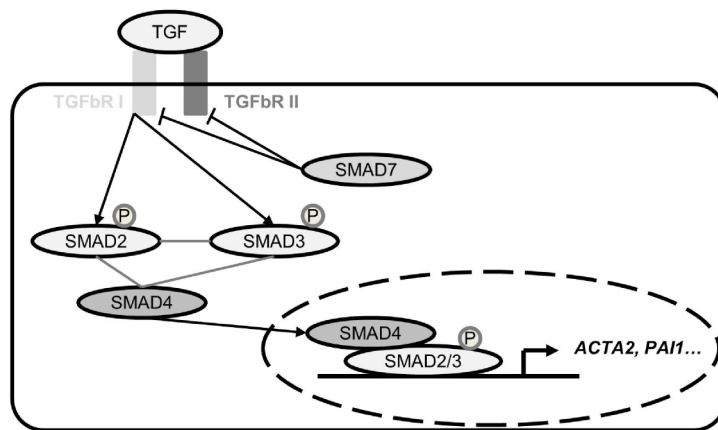


Figure 3.4: Simplified scheme of canonical TGF-beta signalling showing its main components.

When TGF-beta is bound to its receptors (TGF-beta R I, II) SMAD2 and 3 become phosphorylated, form a complex with SMAD4 and translocate to the nucleus leading to target gene expression. SMAD7 inhibits TGF-beta signalling.

3.2.2.1 TGF-beta and epithelial-to-mesenchymal transition

It is well established, that TGF-beta induces epithelial-to-mesenchymal transition (EMT) [Santibanez, et.al., 2011, Willis, et.al., 2007]. EMT is a fundamental process involved in cell differentiation during development and tumour invasion [Bartram, et.al., 2004, Morty, et.al., 2009, Nawshad, et.al., 2005, Thiery, et.al., 2006]. During EMT, epithelial cells differentiate into mesenchymal cells being critical for the development of mesoderm from the endoderm and for organ development in general. This cellular differentiation is characterized by a loss of cellular junctions, mainly E-cadherin and zona occludens-1 (ZO-1), accompanied by increase in alpha-SMA, collagen I, and the transcription factors Snai1 and Snai2 (also known as Snail and Slug) [Crosby, et.al., 2010, Grande, et.al., 2002, Kim, et.al., 2006, Milara, et.al., 2013, Tanjore, et.al., 2011, Thiery, et.al., 2006]. Other mesenchymal markers can be used to determine the progression of EMT as well, e.g. vimentin, connective tissue growth factor, N-cadherin, and MMPs [Willis, et.al., 2007], depending on the context in which EMT occurs. In a fibrotic setting, such as peribronchial remodelling seen in COPD, EMT is characterized by an increase in fibroblasts and myo-fibroblasts. However, not all mesenchymal markers are exclusively expressed by these cells. For this reason, a combination of different markers and readouts is necessary to analyse EMT.

3.2.2.2 TGF-beta in COPD and lung cancer

In COPD, the role of TGF-beta is controversial. On the one hand, peribronchial remodelling with fibrosis, being responsible for airway obstruction, is due to excessive fibrogenic growth factor release, especially TGF-beta [Beasley, 2010, Churg, et.al., 2006]. Furthermore, single nucleotide polymorphisms in the TGF-beta gene are associated with COPD development and smokers as well as COPD patients are reported to have an increased expression of TGF-beta [Chung, 2001, de Boer, et.al., 1998, Kneidinger, et.al., 2011, Takizawa, et.al., 2001, van Diemen, et.al., 2006]. TGF-beta can

be activated in lung fibroblasts and various other pro-fibrotic factors can be secreted from the airways by cigarette smoke [Churg, et.al., 2006, Wang, et.al., 2003]. In addition, fibroblasts derived from COPD patients produced more ECM proteins providing a pro-fibroproliferative environment upon cigarette smoke exposure compared to control cells [Krimmer, et.al., 2012]. This is in accordance to the finding, that TGF-beta expression is increased while the I-SMADs SMAD6 and 7 are reduced in the airway epithelium of patients with COPD [de Boer, et.al., 1998, Santibanez, et.al., 2011]. On the other hand, the emphysematous changes seen in the alveolar regions seem to be related to a lack of TGF-beta [Budd, et.al., 2012, Milara, et.al., 2013]. This shows that TGF-beta effects are highly context and cell-type specific.

Similarly, TGF-beta has differential consequences in the development of cancer, depending on cellular context and the microenvironment. In early stages TGF-beta has been shown to be tumour-suppressive and anti-proliferative, while in later stages TGF-beta becomes pro-oncogenic, inducing proliferation, angiogenesis, immunosuppression, invasion, and metastasis [Adcock, et.al., 2011, Derynck, et.al., 2001, Juarez, et.al., 2011, Massague, 2008, Santibanez, et.al., 2011]. More insight into the role of TGF-beta signalling in cancer and COPD will help to develop therapeutic options for the patients.

3.3 Translational medicine and preclinical models

As already mentioned before, chronic lung diseases are the second leading cause of death worldwide. Many patients die awaiting transplantation since donated organs cannot cover the need. Several approaches have addressed the question how to overcome this shortage: Donor organs are preserved and perfusion pre-treated to make “non-optimal” lungs suitable for transplantation [Bruinsma, et.al., 2014, Butler, et.al., 2002, Cypel, et.al., 2011, op den Dries, et.al., 2013]. Furthermore, the approach of engineering organs *ex vivo* has gained broad scientific interest. For this, donor lungs are decellularized and recellularized with patient specific cells to avoid the need for immunosuppression. Initial studies done in animals are promising but organs are only functional for short periods (hours to days) [Gilpin, et.al., 2014, Ott, et.al., 2010, Petersen, et.al., 2010]. More work needs to be done and will take most probably additional 10-20 years until whole engineered organs will be clinical applicable.

Due to this, new treatment options to treat chronic lung diseases are needed and new models and test systems need to be developed. The problem of translating results from animal models into the clinics are due to small sample size, age and gender differences, different onset and disease progression, and missing of comorbidities in mice compared to humans [Herter-Sprue, et.al., 2013]. Moreover, personalized approaches are needed since patient heterogeneity prevents the usage of a universal applicable treatment. Some progress has already been made in this regard. In cancer research, a new model of “mouse avatars” is used to get insight into disease development and progression to predict individual-specific chemotherapy treatment outcomes [Malaney, et.al., 2014]. Patient derived tumour samples are implanted into mice, which then undergo drug efficacy studies. Dekkers and colleagues described an assay for personalized medicine, using long-term

cultivation of primary intestinal organoids derived from patients with cystic fibrosis, robustly discriminating healthy and diseased patients [Dekkers, et.al., 2013]. With this assay, they propose to facilitate diagnosis and drug development for cystic fibrosis. Moll and colleagues developed a method to model cancer tumours in a 3D environment combining primary human dermal fibroblasts, primary human microvascular endothelial cells, and a tumour cell line in 2D and 3D culture in a decellularized porcine jejunal segment [Moll, et.al., 2013]. This model could possibly be used to analyse pharmaceuticals for clinical application.

All of these approaches use isolated cells or tissue samples to study pharmacological intervention possibly not representing the whole complexity of the tissue present in the patient. The approach of culturing patient tissue *ex vivo* is suggested to be more appropriately mimicking the *in vivo* situation. This can be achieved by cultivation of isolated patient tissues (for example from biopsies or resections). One such method that was already described in the late 1980s is the method of precision cut tissue (e.g. lung) cultures.

3.4 Precision cut tissue slices – 3D *ex vivo* lung tissue cultures

The name “precision cut tissue slices” was established in the mid-eighties, when Smith *et al.* first reported a method to slice liver into 250 µm thin sections with low variation in thickness (<5%) for cultivation and analysis *ex vivo* [Smith, et.al., 1985]. Previously, slices (predominately from liver) were produced by hand with high variability in thickness (one to several mm) and the risk of malnutrition and oxygenation of cells in the middle of slices from high cell density organs limited this approach [Sanderson, 2011]. The development of the Krumdieck tissue slicer helped overcome many of these issues by allowing for precise cutting of slices of less than one mm thickness (in general 25-300 µm) [Liberati, et.al., 2010, Sanderson, 2011].

This *ex vivo* slicing method has been applied to several organs, such as brain [Pilaz, et.al., 2014, Wang, et.al., 2014], heart [Bussek, et.al., 2009, Camelliti, et.al., 2011, Parrish, et.al., 1995], liver [de Graaf, et.al., 2010, De Kanter, et.al., 1999, Hammad, et.al., 2014, Parrish, et.al., 1995, Satoh, et.al., 2005], kidney [De Kanter, et.al., 1999, Parrish, et.al., 1995, Rice, et.al., 2013], organ of Corti [Shim, 2011], and lung [Davidovich, et.al., 2013, De Kanter, et.al., 1999, Delmotte, et.al., 2006, Liberati, et.al., 2010, Martin, et.al., 1996, Morin, et.al., 2013, Parrish, et.al., 1995].

Furthermore, this technique was applied to organs from various species including mice [Delmotte, et.al., 2006, Henjakovic, et.al., 2008, Schleputz, et.al., 2012, Schnorbusch, et.al., 2012], rats [Davidovich, et.al., 2012, de Graaf, et.al., 2010, Martin, et.al., 1996, Moreno, et.al., 2006, Nguyen, et.al., 2013, Schleputz, et.al., 2012], guinea pigs [Bussek, et.al., 2009, Ressemeyer, et.al., 2006, Schleputz, et.al., 2012], sheep [Schleputz, et.al., 2012], dogs [Nguyen, et.al., 2013], ferrets [Nguyen, et.al., 2013], monkeys [Nguyen, et.al., 2013, Schleputz, et.al., 2012], and humans [Camelliti, et.al., 2011, de Graaf, et.al., 2010, De Kanter, et.al., 1999, Schleputz, et.al., 2012, Wohlsen, et.al., 2003]. For the generation of the slices, the lung is perfused with low-melting agarose as a support-material, providing the necessary stiffness. When the tissue slices are placed in culture, the agarose is washed out and an intact 3D lung tissue remains.

Studies using such lung tissue slices have been diverse, including pulmonary physiology, pharmacology, pathogenesis, toxicity, stretch, cytokine release, and viral exacerbations. [Bauer, et.al., 2010, Dassow, et.al., 2010, Davidovich, et.al., 2013, Davidovich, et.al., 2012, Held, et.al., 1999, Henjakovic, et.al., 2008, Liberati, et.al., 2010, Morin, et.al., 2013, Parrish, et.al., 1995, Rausch, et.al., 2011, Schleputz, et.al., 2010, Wright, et.al., 2008, Wyatt, et.al., 2012, Zhou, et.al., 2012]. Typical experimental durations have been reported in the range of 24-72 h, but there has been no extensive characterisation of the cultivation conditions. Most studies use videomicroscopy to analyse the constricting or dilating effect of pharmacological compounds on the bronchi and/or small vessels. Only one pathway modulation study has been performed up to date focusing on cancer samples in general and targeting the PI3K/Akt signalling pathway, which plays a prominent role in cancer [Vaira, et.al., 2010]. This thesis is the first study combining modulation of signalling pathways involved in chronic lung disease (here: Wnt and TGF-beta) with 3D *ex vivo* tissue cultivation.

Even though animal models to study human lung diseases improve, there is still a major lack in translating these results into the clinics. Many pre-clinical and clinical phase studies are still failing. This indicates that there is an urgent need to develop better models or approaches that can be applied in a personalized medicine manner.

3.5 Hypothesis and aims of this thesis

We hypothesised that murine and patient-derived 3D *ex vivo* lung tissue cultures (3D-LTC) represent a suitable tool for signal pathway modulation and preclinical drug testing in COPD.

The first aim of the thesis was to establish the 3D-LTC model as a tool to study lung repair in mice and extensively/comprehensively validate an improved protocol with longer cultivation periods. Further, the 3D-LTC model should be adapted to human tissue biosamples from COPD patients. Comprehensive characterisation of mouse and human lung samples should comprise metabolic and proliferation assessment, morphological examination by histology, immunofluorescence, spatio-temporal confocal live-cell-imaging, as well as gene and protein expression analyses.

The second aim of the thesis was to modulate specific signalling pathways in the 3D-LTC in order to provide proof of concept evidence for the suitability of this technology to study disease-underlying mechanisms and validate novel drugs. In particular, we aimed to investigate the underlying mechanisms of the observed attenuation of emphysema formation upon activation of Wnt/beta-catenin signalling [Kneidinger, et.al., 2011]. This should be achieved by Wnt/beta-catenin activation with two well-known compounds LiCl and CT, respectively. Moreover, we aimed to analyse lung remodelling by the induction of TGF-beta, a well known growth factor activated in lung disease, including COPD.

4 MATERIALS AND METHODS

4.1 Materials

4.1.1 Laboratory equipment and software

Table 4.1: Laboratory equipment

| Product | Manufacturer |
|--|--|
| -80 °C freezer U570 HEF | New Brunswick; Hamburg, Germany |
| -20 °C freezer MediLine LGex 410 | Liebherr; Biberach, Germany |
| Agarose gel running chamber | Biorad; Hercules, CA, USA |
| Analytical scale XS20S Dual Range | Mettler Toledo; Gießen, Germany |
| Autoclave DX-45 | Systec; Wettengel, Germany |
| Autoclave VX-120 | Systec; Wettengel, Germany |
| Bioanalyzer 2100 | Agilent; Böblingen, Germany |
| Cell culture work bench Herasafe KS180 | Thermo Fisher Scientific; Darmstadt, Germany |
| Centrifuge MiniSpin plus | Eppendorf; Hamburg, Germany |
| Centrifuge Rotina 420R | Hettich; Tuttlingen, Germany |
| Centrifuge with cooling, Micro200R | Hettich; Tuttlingen, Germany |
| CO ₂ cell Incubator BBD6620 | Thermo Fisher Scientific; Darmstadt, Germany |
| Demineralized water | Thermo Fisher Scientific; Darmstadt, Germany |
| Dish washer G7893 | Miele & Cie. KG; Gütersloh, Germany |
| Dispenser, Ceramus 2-10ml | Hirschmann Laborgeräte; Eberstadt, Germany |
| Dry ice container Forma 8600 Series, 8701 | Thermo Fisher Scientific; Darmstadt, Germany |
| Electronic pipet filler | Eppendorf; Hamburg, Germany |
| Electrophoretic Transfer Cell, Mini Protean Tetra Cell | Biorad; Hercules, CA, USA |
| Film developer Curix 60 | AGFA; Morsel, Belgium |
| Fridge MediLine LKv 3912 | Liebherr; Biberach, Germany |
| Gel electrophoresis chamber MINIEasy | Carl Roth; Karlsruhe, Germany |
| Gel imaging system ChemiDoc XRS+ | Biorad; Hercules, CA, USA |
| Hyrax M55 (microtome) | Zeiss; Jena, Germany |
| Ice machine ZBE 110-35 | Ziegra; Hannover, Germany |
| Intelli-Mixer RM-2 | Schubert & Weiss Omnilab; Munich, Germany |
| Light Cycler LC480II | Roche Diagnostics; Mannheim, Germany |
| Liquid nitrogen cell tank BioSafe 420SC | Cryotherm; Kirchen/Sieg, Germany |
| Liquid nitrogen tank Apollo 200 | Cryotherm; Kirchen/Sieg, Germany |
| Magnetic stirrer KMO 2 basic | IKA; Staufen, Germany |
| Mastercycler gradient | Eppendorf; Hamburg, Germany |
| Mastercycler Nexus | Eppendorf; Hamburg, Germany |

| | |
|--|--|
| Micro-Dismembrator S | Thermo Fisher Scientific; Darmstadt, Germany |
| Microm EC 350-1 | Thermo Fisher Scientific; Darmstadt, Germany |
| Microm EC 350-2 | Thermo Fisher Scientific; Darmstadt, Germany |
| Microm STP 420D | Thermo Fisher Scientific; Darmstadt, Germany |
| Microscope Axio Imager M2 (fluorescence) | Zeiss; Jena, Germany |
| Microscope Axiovert 40 | Zeiss; Jena, Germany |
| Microscope LSM 710 (confocal) | Zeiss; Jena, Germany |
| Mirax Scan (slide scanner) | Zeiss; Jena, Germany |
| Multipette stream | Eppendorf; Hamburg, Germany |
| NanoDrop 1000 | PeqLab; Erlangen, Germany |
| pH meter InoLab pH 720 | WTW; Weilheim, Germany |
| Pipettes Research Plus | Eppendorf; Hamburg, Germany |
| Plate centrifuge 5430 | Eppendorf; Hamburg, Germany |
| Plate reader Sunrise | Tecan; Crailsheim, Germany |
| Roll mixer | VWR International; Darmstadt, Germany |
| Power Supply Power Pac HC Power Supply | Biorad; Hercules, CA, USA |
| Scale XS400 2S | Mettler Toledo; Gießen, Germany |
| Shaker Duomax 1030 | Heidolph; Schwabach, Germany |
| Syringe pump "aladdin" AL-1000 | World Precision instruments; Sarasota, FL, USA |
| Thermomixer compact | Eppendorf; Hamburg, Germany |
| Ultra pure water supply MilliQ Advantage A10 | Merck, Millipore; Darmstadt, Germany |
| LSM Top table centrifuge MCF-2360 | Schubert & Weiss Omnilab; Munich, Germany |
| Vortex Mixer | IKA; Staufen, Germany |
| Vacuum pump NO22AN.18 with switch 2410 | KNF; Freiburg, Germany |
| Vibratome Hyrax V50 | Zeiss; Jena, Germany |
| Water bath Aqua Line AL 12 | Lauda; Lauda-Königshofen, Germany |

Table 4.2: Software

| Software | Producer |
|---|--|
| Axio Vision LE (AxioVs40 V 8.4.2.0) | Zeiss; Jena, Germany |
| Endnote X7.0.2 | Thomson Reuters; San Francisco, CA, USA |
| GraphPad Prism 5.00 | GraphPad Software; La Jolla, CA, USA |
| IMARISx64 (version 7.6.4) | Bitplane; Zurich, Switzerland |
| Image Lab Version 5.0 | Biorad; Hercules, CA, USA |
| LightCycler® 480 SW 1.5 | Roche Diagnostics; Mannheim, Germany |
| Magelan Software | Tecan; Crailsheim, Germany |
| Microsoft Office Professional Plus 2010 | Microsoft Corporation; Washington, DC, USA |
| Pannoramic Viewer 1.15.2 | 3DHitech Kft; Budapest, Hungary |
| Tristar MicroWin 2000 | Berthold Technologies; Bad Wildbach, Germany |
| Zen 2010 | Zeiss; Jena, Germany |

4.1.2 Chemicals and consumables

Table 4.3: Chemicals and reagents

| Product | Manufacturer |
|--|---|
| 5-bromo-4-chloro-3-indolyl- β -d-galactopyranoside (X-Gal) | Research Product International; Mount Prospect, IL, U.S.A |
| 10x Buffer II | Applied Biosystemes, Life Technologies; Carlsbad, CA, USA |
| 87% Glycerol | AppliChem; Darmstadt, Germany |
| Acetic acid | Merck, Millipore; Darmstadt, Germany |
| Aceton | AppliChem; Darmstadt, Germany |
| Agarose Biozym | Biozym Scientific GmbH; Oldendorf, Germany |
| Agarose, low melting point | Sigma-Aldrich; Taufkirchen, Germany |
| Ammonium peroxodisulfate (APS) | AppliChem; Darmstadt, Germany |
| Amphotericin B solution (250 μ g/ml) | Sigma-Aldrich; Taufkirchen, Germany |
| Biopsy punch (4 mm, 6 mm diameter) | pfm medical; Köln, Germany |
| Bovine serum albumin (BSA) | Sigma-Aldrich; Taufkirchen, Germany |
| Bromphenol blue | AppliChem; Darmstadt, Germany |
| Cell Proliferation Reagent WST-1 | Roche Diagnostics; Mannheim, Germany |
| Complete® Mini without EDTA (Protease-inhibitor) | Roche Diagnostics; Mannheim, Germany |
| Coomassie Brilliant Blue R-250 staining solution | BioRad; Hercules, CA, USA |
| CT | Tocris/R&D; Minneapolis, MN, USA |
| DAPI (4',6-diamidino-2-phenylindole) | Sigma-Aldrich; Taufkirchen, Germany |
| Desoxyribonucleotides mix (dNTPs) | Fermentas; Thermo Fisher Scientific; |
| Dimethyl formamide | Serva; Heidelberg, Germany |
| Dimethyl sulfoxide (DMSO) | Carl Roth; Karlsruhe, Germany |
| Dithiothreitol (DTT) | AppliChem; Darmstadt, Germany |
| D-MEM/F12 | Gibco, Life Technologies; Carlsbad, CA, USA |
| DNase/RNase – free water | Gibco, Life Technologies; Carlsbad, CA, USA |
| Eosin Y (yellowish) | Merck, Millipore; Darmstadt, Germany |
| Ethanol (p.a.) | AppliChem; Darmstadt, Germany |
| Fentanyl | Janssen-Cilag; Neuss, Germany |
| Fetal bovine serum (FBS) "GOLD", heat inactivated | PAA/GE Healthcare; Fairfield, CT, USA |
| Fluorescence mounting medium | Dako; Hamburg, Deutschland |
| Fuchsin acid | Merck, Millipore; Darmstadt, Germany |
| Gelatin | Sigma-Aldrich; Taufkirchen, Germany |
| Glucose | AppliChem; Darmstadt, Germany |
| Glycine, molecular biology grade | AppliChem; Darmstadt, Germany |
| GoTaq G2 Hot Start Green Master Mix, 2x | Promega; Mannheim, Germany |
| Hematoxylin (cryst.) | Merck, Millipore; Darmstadt, Germany |
| HEPES | Life Technologies; Carlsbad, CA, USA |

| | |
|---|--|
| HI-MO Fast drying mounting medium for coverslipping | Bio-Optica; Milan, Italy |
| Hydrochloric acid | AppliChem; Darmstadt, Germany |
| Iron(III) chloride hexahydrate | Merck, Millipore; Darmstadt, Germany |
| Isopropanol, p.a. | AppliChem; Darmstadt, Germany |
| Ketamine | Bela-pharm, Vechta, Germany |
| LiCl | Sigma-Aldrich; Taufkirchen, Germany |
| Light Cycler 480 SybrGreen I Master Mix | Roche Diagnostics; Mannheim, Germany |
| Light green SF yellowish | Merck, Millipore; Darmstadt, Germany |
| Magnesium chloride | AppliChem; Darmstadt, Germany |
| Magnesium chloride hexahydrate | AppliChem; Darmstadt, Germany |
| Medetomidine | Orion Pharma; Hamburg, Germany |
| Methanol, p.a. | AppliChem; Darmstadt, Germany |
| Midazolam | Roche Diagnostics; Mannheim, Germany |
| Molybdato-phosphoric acid hydrate | Merck, Millipore; Darmstadt, Germany |
| Non-fat dried milk powder | AppliChem; Darmstadt, Germany |
| Nonidet P-40 | AppliChem; Darmstadt, Germany |
| Orange G | Merck, Millipore; Darmstadt, Germany |
| Oxalic acid dihydrate | Merck, Millipore; Darmstadt, Germany |
| Paraffin | Richard Allen Scientific; Kalamazoo, MI, USA |
| Penicillin-Streptomycin (10,000 U/ml) | Gibco, Life Technologies; Carlsbad, CA, USA |
| Phosphate buffered saline | Gibco, Life Technologies; Carlsbad, CA, USA |
| PhosSTOP Phosphatase Inhibitor Cocktail Tablets | Roche Diagnostics; Mannheim, Germany |
| Ponceau S solution | Sigma-Aldrich; Taufkirchen, Germany |
| Potassium ferricyanide | Sigma-Aldrich; Taufkirchen, Germany |
| Potassium ferrocyanide | Sigma-Aldrich; Taufkirchen, Germany |
| Potassium permanganate | Merck, Millipore; Darmstadt, Germany |
| Random hexamers | Applied Biosystems, Life Technologies; Carlsbad, CA, USA |
| Recombinant human TGF- β 1protein | R&D Systems; Minneapolis, MN, USA |
| Resorcin-fuchsin | Carl Roth; Darmstadt, Germany |
| Restore Plus Western Blot Stripping Buffer | Pierce, Thermo Fisher Scientific; Schwerte, Germany |
| Rotiphorese Gel 30 (37,5:1) 500 ml | Carl Roth; Darmstadt, Germany |
| Sodium dodecyl sulphate (SDS) pellets | Carl Roth; Darmstadt, Germany |
| Sodium chloride | AppliChem; Darmstadt, Germany |
| Sodium chloride, isotonic (for injection) | B. Braun; Melsungen, Germany |
| Sodium hydroxide | AppliChem; Darmstadt, Germany |
| Sodium phosphate monobasic | Sigma-Aldrich; Taufkirchen, Germany |
| Sodium phosphate dibasic | Sigma-Aldrich; Taufkirchen, Germany |
| SuperSignal West Dura Extended Duration Substrate | Pierce, Thermo Fisher Scientific; Schwerte, Germany |
| SuperSignal West Femto Substrate | Pierce, Thermo Fisher Scientific; Schwerte, Germany |

| | |
|--|---|
| SybrSafe (10,000x in DMSO) | Invitrogen Life Technologies; Carlsbad, CA, USA |
| Tratrazine | Sigma-Aldrich; Taufkirchen, Germany |
| TEMED | AppliChem; Darmstadt, Germany |
| T-PER Tissue Protein Extraction Reagent | Pierce, Thermo Fisher Scientific; Schwerte, Germany |
| Tris base, buffer grade | AppliChem; Darmstadt, Germany |
| Triton X-100 | AppliChem; Darmstadt, Germany |
| Tween 20 | AppliChem; Darmstadt, Germany |
| UltraPure DNase/RNase-Free Distilled Water | Invitrogen, Life Technologies; Carlsbad, CA, USA |
| WST-1 | Roche Diagnostics; Mannheim, Germany |
| Xylene | AppliChem; Darmstadt, Germany |
| Xylazinhydrochloride | cp-pharma; Burgdorf, Germany |

Table 4.4: Consumables

| Product | Manufacturer |
|--|--|
| 96 Well, Black/Clear, Tissue Culture Treated Plate, Flat Bottom with Lid | BD Bioscience, Heidelberg, Germany |
| Cannulas (G20, G21, G26) | B. Braun; Melsungen, Germany |
| Cell culture dishes | Corning, Thermo Fisher Scientific; Schwerte, Germany |
| Cell culture multi well plates | TPP Techno Plastic Products; Trasadingen, Switzerland |
| Cryovials for microdismembrator 1.2 ml | Nalgene, Thermo Fisher Scientific; Schwerte |
| Falcon tubes (15 ml, 50 ml) | BD Bioscience, Heidelberg, Germany |
| Filter tips | Biozym Scientific; Hessisch Oldendorf, Germany |
| Glas Pasteur pipettes | VWR International; Darmstadt, Germany |
| Grinding balls (9 mm, stainless steel) | Neolab; Heidelberg, Germany |
| Hyperfilm® ECL™ Film | Amersham, GE Healthcare; Freiburg, Germany |
| Measuring pipettes sterile, single use (2 ml, 5 ml, 10 ml, 25 ml, 50 ml) | VWR International; Darmstadt, Germany |
| Nitrocellulose membrane | Biozym Scientific; Hessisch Oldendorf, Germany |
| PCR plates | Kisker Biotech; Steinfurt, Germany |
| Reaction tubes (0.5 ml, 1.5 ml, 2 ml) | Eppendorf; Hamburg, Germany Greiner Bio-One; Frickenhausen, Germany |
| Scalpel | B. Braun; Melsungen, Germany |
| Sealing foil for PCR plates | Kisker Biotech; Steinfurt Germany |
| Syringes (1 ml, 10 ml, 20 ml) | B. Braun; Melsungen, Germany Henke-Sass Wolf; Tuttlingen, Germany |
| Tips | Eppendorf; Hamburg, Germany Kisker Biotech; Steinfurt, Germany |
| Whatman blotting paper 3 mm | GE Healthcare; Freiburg, Germany |

4.1.3 Buffers, solutions and media

Table 4.5: Buffers, solutions and media

| Buffer/Solution | Concentration/amount | Substance |
|--|----------------------|-----------------------------------|
| Cultivation medium | 1% | DMEM/F12 |
| | 2.5 µg/ml | PS |
| | 0.1% | Amphotericin B |
| | | FBS |
| HEPES (N-2-hydroxyethylpiperazine-N-2-ethane sulfonic acid) | 1 M | HEPES |
| Laemmli loading buffer (4x) | 8% (w/v) | SDS |
| | 40% (v/v) | Glycerol |
| | traces | Bromophenol blue |
| | 250 mM | Tris/HCl, pH 6.8 |
| | 400 mM | DTT freshly added |
| LacZ-staining solution | 5 mM | Potassium ferricyanide |
| | 5 mM | Potassium ferrocyanide |
| | 2 mM | Magnesium chloride hexahydrate |
| | 65 mM | Sodium phosphate dibasic |
| | 15 mM | Sodium phosphate monobasic |
| PBS pH 7.4 (10x) | 1.37 M | NaCl |
| | 27 mM | KCl |
| | 100 mM | Na ₂ HPO ₄ |
| | 20 mM | KH ₂ PO ₄ |
| PBND-buffer (1x) | 50 mM | KCl |
| | 10 mM | Tris·HCl pH 8,3 |
| | 2.5 mM | MgCl ₂ |
| | 0.1 mg/ml | gelatin |
| | 0.45% v/v | NP40 |
| | 0.45% v/v | Tween-20 |
| Phosphomolybdate solution | 0.2 mg/ml | Proteinase K (20 mg/ml) |
| | 0.4 g/l | Molybdato-phosphoric acid hydrate |
| Ponceau-fuchsin | 0.2 g/l | Orange G |
| | 0.67 g/l | Ponceau S |
| Ponceau-fuchsin | 0.33 g/l | Fuchsin acid |
| | 2 mM | Acetic acid |

| | | |
|---------------------------------------|---|---|
| RIPA protein lysis buffer | 150 mM 10 mM 0.1% (w/v) 1% (v/v) 1% (w/v) 5 mM | NaCl Tris/HCl, pH 7.2 SDS Triton X-100 Sodium deoxy cholate EDTA |
| SDS-PAGE Running Buffer | 250 mM 1.92 M 1% (w/v) | Tris/HCl, pH 7.4 Glycine SDS |
| TAE (50x) | 2 M 5.71% (v/v) 50 mM | Tris/HCl Glacial acetic acid EDTA, pH 8 |
| TBS, pH 7.4 (10x) | 10 mM 150 mM | Tris/HCl pH 7.4 NaCl |
| TBST | | TBS supplemented with 0.05% Tween-20 |
| Transfer Buffer (10x) | 50 mM 400 mM | Tris/HCl Glycine |
| Transfer Buffer (1x) | 10% 200 ml | 10x Transfer Buffer Methanol |
| Weigerts-staining solution | 50% 50% | Weigerts-solution component A Weigerts-solution component B |
| Weigerts-solution component A | 5 g/l in 96% ethanol | Heamatoxylin |
| Weigerts-solution component B | 11.6 g/l 1.5 M | Iron(III) chloride hexahydrate HCl |
| X-Gal solution (light protected) | 40 mg/ml in DMF | 5-bromo-4-chloro-3-indolyl- β -d- galactopyranoside (X-Gal) |
| X-Gal/LacZ solution (light protected) | 250 μ l 9.75 ml | X-Gal solution LacZ-staining solution |

4.1.4 Standards and Kits

Table 4.6: Standards

| Product | Manufacturer |
|--|---------------------------|
| 100 bp DNA ladder | Peqlab; Erlangen, Germany |
| Protein marker V | Peqlab; Erlangen, Germany |
| Quick Start™ Bovine Serum Albumin (BSA) Standard | Biorad; Hercules, CA, USA |

Table 4.7: Kits

| Product | Manufacturer |
|---|---|
| Agilent RNA 6000 Nano Kit | Agilent; Böblingen, Germany |
| BCA Protein Assay Kit | Pierce, Thermo Fisher Scientific; Schwerte, Germany |
| Cell Proliferation ELISA, BrdU (colorimetric) | Roche Diagnostics; Mannheim, Germany |
| LIVE/DEAD® Viability/Cytotoxicity Kit *for mammalian cells* | Invitrogen Life Technologies; Carlsbad, CA, USA |
| PerfectPure RNA Fibrous Tissue Kit | 5Prime; Hilden, Germany |
| RNeasy Mini Kit | Qiagen; Hilden, Germany |
| SFTPC ELISA (mouse and human) | Cusabio; Wuhan, China |

4.1.5 Enzymes

Table 4.8: Enzymes

| Product | Manufacturer |
|------------------------------------|--|
| Porcine pancreatic elastase | Sigma-Aldrich; Taufkirchen, Germany |
| Proteinase K | Pierce, Thermo Fisher Scientific; Schwerte, Germany |
| RNase inhibitor 20 U/μl | Applied Biosystems, Invitrogen, Life Technologies; Carlsbad, USA |
| MuLV Reverse Transcriptase 5,000 U | Applied Biosystems, Invitrogen, Life Technologies; Carlsbad, USA |

4.1.6 Oligonucleotides

Oligonucleotides were purchased from Eurofins MWG Operon; Ebersberg, Germany in a lyophilized, desalted form and reconstituted with DNase/RNase-free water to obtain a concentration of 100 μM. Primers for qPCR were designed with PrimerBLAST from NCBI (<http://www.ncbi.nlm.nih.gov/tools/primer-blast/>). Amplicon size was between 80 and 150 bp with maximal length of 200 bp.

Table 4.9: Primers for genotyping

| Mouse | Gene | Jackson ID | | Sequence 5' - 3' | Size [bp] |
|------------------|------------------|------------|----|---------------------------|-----------|
| BAT-GAL, TOP-GAL | Transgene | oIMR3054 | fw | ATCCTCTGCATGGTCAGGTC | 315 |
| | | oIMR0040 | rv | CGTGGCCTGATTCATTCC | |
| | Internal control | oIMR8744 | fw | CAAATGTTGCTTGTCTGGTG | 210 |
| | | oIMR8745 | rv | GTCAGTCGAGTGCACAGTTT | |
| TCF/LEF-EGFP | Transgene | 11775 | fw | ACAACAAGCGCTCGACCATCAC | ~530 |
| | | 11776 | rv | AGTCGATGCCCTTCAGCTCGAT | |
| | Internal control | oIMR7338 | fw | CTAGGCCACAGAATTGAAAGATCT | 324 |
| | | oIMR7339 | rv | GTAGGTGGAAATTCTAGCATCATCC | |

Table 4.10: Murine quantitative PCR primers

| Gene | | Sequence 5' - 3' |
|--------------|----|---------------------------|
| <i>Aqp5</i> | fw | CCTTATCCATTGGCTTGTCG |
| | rv | CTGAACCGATTCATGACCAC |
| <i>Axin1</i> | fw | CGAAGGGAGATGCAGGAGAGTA |
| | rv | AAGTGCGAGGAATGTGAGGTAGA |
| <i>Axin2</i> | fw | AGCAGAGGGACAGGAACCA |
| | rv | CTGAACCGATTCATGACCAC |
| <i>Dkk2</i> | fw | GAGATCGCAACCATGGTCACT |
| | rv | GGGTCTCCTTCATGTCTTTTATATG |
| <i>Fgfr2</i> | fw | ACACAGATAGCTCCGAAGACGTTGT |
| | rv | CCCAGCCGGACAGCGGAAC |
| <i>Hopx</i> | fw | TCTCCATCCTTAGTCAGACGC |
| | rv | GGGTGCTTGTTGACCTTGTT |
| <i>Hprt</i> | fw | CCTAAGATGAGCGCAAGTTGAA |
| | rv | CCACAGGACTAGAACACCTGCTAA |
| <i>Lef1</i> | fw | GGCGGCGTTGGACAGAT |
| | rv | CACCCGTGATGGGATAAACAG |
| <i>Lgr5</i> | fw | GCGTTCACGGGCCTTCACAG |
| | rv | GGCATCTAGGCGCAGGGATTGA |
| <i>Nkd1</i> | fw | TGTTCTCATCCACGCAATGG |
| | rv | GAGCCCCACTCAGGTTCCA |
| <i>Pdpn</i> | fw | ACAGGTGCTACTGGAGGGCTT |
| | rv | TCCTCTAAGGGAGGCTTCGTC |
| <i>Sfrp2</i> | fw | ATGTCCGCCTTCGGCTTCCC |
| | rv | CCTTGGGAGCTTCTCTGTGGC |
| <i>Sftpc</i> | fw | AGCAAAGAGGTCTGATGGA |
| | rv | GAGCAGAGCCCCTACAATCA |
| <i>Wisp1</i> | fw | GTCCTGAGGGTGGGCAACAT |
| | rv | GGGCGTGTAGTCGTTTCCTCT |
| <i>Wnt2</i> | fw | AGCCCTGATGAACCTTCACAAC |
| | rv | TGACACTTGCATTCTTGTTTCAAG |

Table 4.11: Human quantitative PCR primers

| Gene | | Sequence 5' - 3' |
|---------------|----|------------------------------|
| <i>ACTA2</i> | fw | CGAGATCTCACTGACTACCTCATGA |
| | rv | AGAGCTACATAACACAGTTTCTCCTTGA |
| <i>AQP5</i> | fw | TCACTGGGTTTTCTGGGTAGG |
| | rv | CCTTTGATGATGGCCACACG |
| <i>AXIN2</i> | fw | AGAAATGCATCGCAGTGTGAAG |
| | rv | GGTGGGTTCTCGGGAAATG |
| <i>COL1A1</i> | fw | CAAGAGGAAGGCCAAGTCGAG |
| | rv | TTGTCGCAGACGCAGATCC |
| <i>HOPX</i> | fw | GCCCCACAGAGGACCAGGTG |
| | rv | GCTTGGTTAAGCGGAGGAGAG |
| <i>HPRT</i> | fw | AAGGACCCACGAAGTGTTG |
| | rv | GGCTTTGTATTTTGCTTTTCCA |
| <i>NKD1</i> | fw | CACCCTGTATGACTTTGACAACAAC |
| | rv | CAGAGGAGTCCACCACCTCATAG |
| <i>PAI1</i> | fw | GACATCCTGGAAGTCCCTA |
| | rv | GGTCATGTTGCCTTTCCAGT |
| <i>PDPN</i> | fw | GAGAAAGATGGTTTGTCAACAGTG |
| | rv | GGCGTAACCCTTCAGCTCT |
| <i>SFTPC</i> | fw | GCCCAGTGCACCTGAAACGC |
| | rv | TCTCCAGAACCATCTCCGTGTGT |
| <i>SNAI1</i> | fw | TGTCAGATGAGGACAGTGGGAA |
| | rv | GCCTCCAAGGAAGAGACTGAAGTA |
| <i>SNAI2</i> | fw | TGGCTCAGAAAGCCCCATTAG |
| | rv | TTTCAGCTTCAATGGCATGGGG |

4.1.7 Antibodies

Table 4.12: Primary antibodies for immunofluorescence

| Name | Source | Manufacturer | Order nr. | Dilution |
|-------------------|---------------|---|------------------|-----------------|
| alpha-SMA (ACTA2) | Mouse | Sigma-Aldrich; Taufkirchen, Germany | A5228 | 1:500 |
| Aquaporin 5 | Rabbit | Calbiochem, Millipore; Billerica, MA, USA | 178615 | 1:100 |
| CD45 | Rat | BD; San Jose, CA, USA | 553076 | 1:500 |
| Collagen 1 | Rabbit | Rockland; Gilbertsville, PA, USA | 600-401-103 | 1:100 |
| E-cadherin (CDH1) | Mouse | BD; San Jose, CA, USA | 610181 | 1:100 |
| Hopx | Rabbit | Santa Cruz; Santa Cruz, CA, USA | sc-30216 | 1:100 |
| Podoplanin | Goat | R&D; Minneapolis, MN, USA | AF3244 | 1:100 |
| Podoplanin | Rat | Acris; Herford, Germany | AM01133PU-N | 1:100 |
| SFTPC, pro- | Rabbit | Abcam; Cambridge, UK | ab40879 | 1:500 |
| SFTPC, pro- | Rabbit | Millipore; Billerica, MA, USA | AB3786 | 1:500 |

Table 4.13: Primary antibodies for Western Blot

| Name | Source | Manufacturer | Order nr. | Dilution | Size [kDa] |
|--------------------------------|--------|------------------------------------|-------------|----------|------------|
| β -actin | Mouse | Sigma-Aldrich; Taufkirchen Germany | A3854 | 1:50,000 | 42 |
| β -catenin, active (ABC) | Mouse | Millipore; Billerica, MA, USA | 05-665 | 1:500 | 92 |
| Aquaporin 5 | Rabbit | Abcam; Cambridge, UK | ab78486 | 1:5,000 | 24 |
| Aquaporin 5 | Rabbit | Abcam; Cambridge, UK | ab92320 | 1:1,000 | 24 |
| Hopx | Rabbit | Santa Cruz; Santa Cruz, CA, USA | sc-30216 | 1:1,000 | 13 |
| Podoplanin | Goat | R&D; Minneapolis, MN, USA | AF3244 | 1:1,000 | 40 |
| Podoplanin | Rat | Acris; Herford, Germany | AM01133PU-N | 1:1,000 | 37 |
| SMAD3, phospho | Rabbit | Abcam; Cambridge, UK | Ab52903 | 1:1,000 | 48 |
| SMAD2/3 | Mouse | BD; San Jose, CA, USA | 610843 | 1:1,000 | 58 |

Table 4.14: Secondary antibodies for immunofluorescence

| Antigen | Source | Manufacturer | Order nr. | Dilution |
|--|--------|---|-----------|----------|
| Goat-IgG (H+L), Alexa Fluor 488 conjugated | Donkey | Invitrogen Life Technologies; Carlsbad, CA, USA | A-11055 | 1:1,000 |
| Goat-IgG (H+L), Alexa Fluor 555 conjugated | Donkey | Invitrogen Life Technologies; Carlsbad, CA, USA | A-21432 | 1:1,000 |
| Mouse-IgG, FITC conjugated | Goat | Dako; Hamburg Deutschland | F0479 | 1:500 |
| Mouse-IgG (H+L), Alexa Fluor 555 conjugated | Rabbit | Invitrogen Life Technologies; Carlsbad, CA, USA | A-21424 | 1:1,000 |
| Rabbit-IgG (H-L), Alexa Fluor 488 conjugated | Goat | Invitrogen Life Technologies; Carlsbad, CA, USA | A-11008 | 1:1,000 |
| Rabbit-IgG (H-L), Alexa Fluor 555 conjugated | Goat | Invitrogen Life Technologies; Carlsbad, CA, USA | A-21429 | 1:1,000 |
| Rat IgG (H+L), Alexa Fluor 488 conjugated | Goat | Invitrogen Life Technologies; Carlsbad, CA, USA | A-11006 | 1:1,000 |
| Rat IgG (H+L), Alexa Fluor 555 conjugated | Goat | Invitrogen Life Technologies; Carlsbad, CA, USA | A-21434 | 1:1,000 |

Table 4.15: Secondary antibodies for WB, HRP linked

| Antigen | Source | Manufacturer | Order nr. | Dilution |
|------------|--------|--|-----------|----------|
| Goat IgG | Rabbit | Invitrogen, Life Technologies; Carlsbad, USA | 611620 | 1:15,000 |
| Mouse IgG | Sheep | GE Healthcare; Freiburg, Germany | NA931V | 1:4,000 |
| Rabbit IgG | Donkey | GE Healthcare; Freiburg, Germany | NA934V | 1:10,000 |
| Rat IgG | Goat | GE Healthcare; Freiburg, Germany | NA935V | 1:10,000 |

Table 4.16: Directly HRP conjugated antibodies for WB

| Antigen | Source | Manufacturer | Order nr. | Dilution |
|----------------|--------|-------------------------------------|-----------|----------|
| β -actin | Mouse | Sigma Aldrich; Taufkirchen, Germany | A3854 | 1:50,000 |

4.1.8 Animals

For most of the experiments, and if not stated otherwise, pathogen-free female C57BL/6-N mice (C57BL/6NCrl, Charles River, Germany) in the age of 8-12 weeks were used. Wnt reporter animals were BAT-GAL (B6.Cg-Tg(BAT-lacZ)3Picc/J), and TCF/LEF-GFP (STOCK Tg(TCF/Lef1-HIST1H2BB/EGFP)61Hadj/J), all The Jackson Laboratory, Maine, USA [Ferrer-Vaquer, et.al., 2010, Maretto, et.al., 2003]. Mice were housed with water and food *ad libitum* and could acclimatise for at least one week before used for experiments. All experiments were performed in accordance with the guidelines of the Ethics Committee of the Helmholtz-Center Munich and approved by the Regierungspräsidium Oberbayern, Germany (project number: 55.2-1-54-2532-168-09).

Wnt reporter animals were bred in house with each other, C57BL/6-N, or C57BL/6-J respectively. Tail cuts were used to prepare genomic DNA and normal PCR was run for genotyping. Only positively tested mice in the age of 8-12 weeks were used for the experiments.

4.1.9 Human Tissue

The experiments with human tissue were approved by the Ethics Committee of the Ludwig-Maximillan University Munich, Germany (project-nr. 455-12). The Asklepios Biobank for Lung Diseases, Gauting, Germany (project-nr. 333-10) provided all samples. Written informed consent was obtained from all subjects. Tumour-free tissue from patients that underwent lung tumour resection was used. Patients were either with or without diagnosed COPD. All of them had a smoking history and relevant characteristics are shown in Table 4.17.

Table 4.17: Characteristics of the human patients used for 3D-LTC

| Nr. | Gender | Age [years] | Smoking status | Pack years (PY) | FEV ₁ | FEV ₁ /FVC | GOLD stage |
|-----|--------|-------------|----------------|-----------------------------|------------------|-----------------------|------------|
| 1 | male | 73 | ex-smoker | 80 PY, cessation 12 y | 105 | 86 | no |
| 2 | male | 60 | ex-smoker | n.d. | 122 | 84 | no |
| 3 | male | 51 | active smoker | 40 PY | 106 | 73 | no |
| 4 | male | 68 | smoker | n.d. | 62 | 49 | II |
| 5 | male | 63 | active smoker | 40-60 PY | 85 | 70 | I |
| 6 | male | 73 | ex-smoker | 40 PY, cessation 5-10 y | 81 | 82 | no |
| 7 | female | 72 | ex-smoker | 20-40 PY, cessation 10-20 y | 47 | 51 | III |
| 8 | female | 70 | active smoker | 40-60 PY | 52 | 61 | II |
| 9 | male | 78 | ex-smoker | n.d., cessation > 20 y | 89 | 59 | I |
| 10 | male | 58 | active smoker | 40-60 PY | 60 | 68 | II |
| 11 | female | 64 | active smoker | n.d. | 114 | 89 | no |
| 12 | male | 60 | active smoker | 50 PY | 101 | 71 | no |
| 13 | female | 68 | ex-smoker | 40-60 PY, cessation 1-5 y | 83 | 74 | no |
| 14 | female | 78 | active smoker | 50 PY | 85 | 67 | I |
| 15 | male | 66 | ex-smoker | 70 PY, cessation 12 y | 106 | 86 | no |
| 16 | male | 59 | active smoker | 80 PY | 85 | 67 | I |

4.2 Methods

All microbiology and molecular biology methods were performed according to common good laboratory practice.

4.2.1 Animal model of emphysema induced by elastase instillation

To induce emphysema, mice were anaesthetised with a mixture of medetomidine (0.2 mg/ml), midazolam (2.0 mg/ml), and fentanyl (0.02 mg/ml) (MMF). Porcine pancreatic elastase was dissolved in sterile phosphate-buffered saline and applied *oro tracheally* (80 U/kg body weight). Control mice received 80 μ l sterile phosphate-buffered saline. Animal behaviour and weight were observed every day until day three and every other day afterwards. Mice were breathing heavily and were hardly moving within the first 24 h after elastase instillation. Thereafter, no abnormal behaviour was observed and a difference between control and emphysematous animals was not visible from day two on. Diseased mice significantly lost weight after induction of emphysema over the whole time course (see chapter 3.1, Figure 4.1). Seven days after the instillation, when the inflammatory reaction was gone and emphysema had developed, 3D-LTC were generated. Lungs from healthy (PBS instilled) animals were filled with 1.4 ml while lungs from emphysematous (elastase instilled) animals needed to be filled with approximately 1.7 ml of agarose, due to the emphysema and the resulting increase in lung volume.

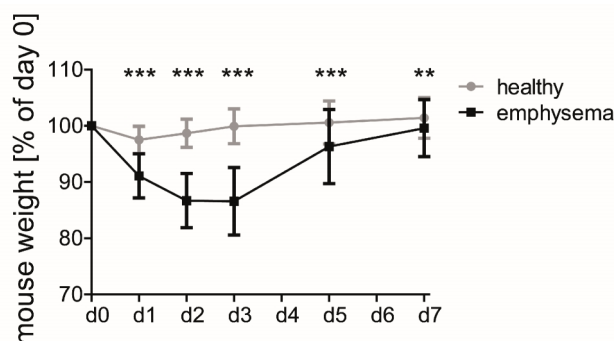


Figure 4.1: Weight of emphysematous mice was significantly decreased at all time points.

Weight of healthy and emphysematous mice at different time points after instillation with PBS or porcine pancreatic elastase. n=75-130. *: p<0.05, **: p<0.01, ***: p<0.001, one way ANOVA with Bonferroni post-test.

4.2.2 Generation of 3D-LTC (PCLS)

An overview of the process of the generation of 3D-LTC, later on also named “slices”, is shown in Figure 4.2. The whole procedure was performed under sterile conditions. Surgical instruments (scissors and forceps) were from Fine Science Tools (Heidelberg, Germany).

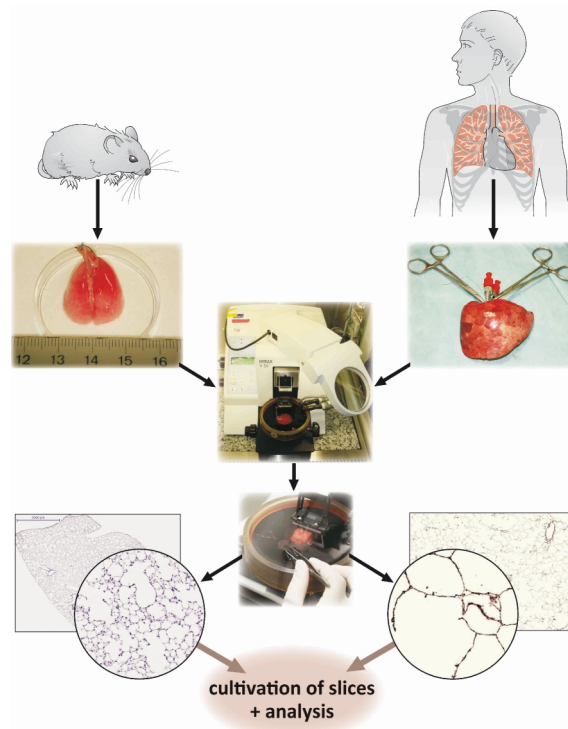


Figure 4.2: Overview of the generation of the 3D-LTC from murine and human samples.

Murine and human lung tissue was filled with low-melting agarose and 3D-LTC were cut using a vibratome. 3D-LTC with intact 3D architecture were cultivated for up to seven days and used for further analysis.

4.2.2.1 Generation of 3D-LTC from murine lungs

For the murine 3D-LTC mice were anaesthetised with a mixture of ketamine and xylazine hydrochloride. After disinfection of the fur by 80% ethanol the skin was opened with scissors from the abdomen to the trachea. Afterwards, the throat was opened with blunt forceps and the surrounding muscles were removed. Two threads were placed below the trachea and a small incision was made for intubation with a cannula. Thereafter, the cannula was fixed with one of the threads and the abdomen was dissected with blunt scissors to expose the inner organs. Mice were killed by exsanguination via the *Vena cava*. After this, the diaphragm was dissected leading to pneumothorax and the thorax was opened. The thymus gland was removed with blunt forceps and the lung was perfused via the right ventricle of the heart with sterile 0.9% NaCl. Broncho-alveolar-lavage (BAL) was taken afterwards with 2x 500 μ l 0.9% NaCl and centrifuged at 5,000 g for 5 min. Supernatant was transferred into a new vial and BAL cells as well as BAL supernatants were snap frozen in liquid nitrogen and stored at -80°C . Thereafter, the lungs were inflated with pre-warmed (37°C) 2% agarose in sterile cultivation medium (4.1.3) without FCS. 1.4 ml agarose was used for healthy animals while 1.7 ml was needed for emphysematous mice. The trachea was closed with the second thread after agarose instillation and lung and heart were excised *en bloc*. After this, the lung was transferred into a tube with cultivation medium and cooled on ice for 10 min, to allow gelling of the agarose. The lobes were separated and cut with a vibratome to a thickness of 300 μ m. The 3D-LTC were cultivated for up to five days under submerged conditions. Only the periphery of

the left lung and the superior and inferior lobe of the right lung were used for slicing. The leftover of these lobes were used for immunohistochemistry. The other two lobes were snap frozen in liquid nitrogen and stored at -80°C. These samples served as “d0” controls for Western blot.

To make sure that the inflation material will not stick to the lung tissue, as it might be the case for the agarose, other materials were used for inflation of the lungs as well. 2% sodium-alginate which was inflated and cross-linked by transferring the whole lung into a 100 mM calcium-chloride solution (in PBS) for 10 min, which was proven by water soluble tetrazolium salt (WST-1) assay to be non-toxic to the cells, turned out to be not suitable. 3D-LTC collapsed during cultivation and permeabilisation for immunofluorescence staining making further imaging impossible. Ultra low melting agarose (tested 2-4%), which has an extreme low melting point and therefore will get dissolve in the cultivation medium and get released from the tissue during cultivation more readily, turned out to be not stiff enough to prepare 3D-LTC.

4.2.2.2 *Generation of 3D-LTC from human lung segments*

For the human 3D-LTC, lung segments without tumours from patients undergoing lung resection due to cancer were cannulised via the remaining bronchus and filled with warm agarose directly after excision. The amount of agarose was adjusted to the size of the tissue and ranged between 20 and 80 ml. The bronchus was closed afterwards with a thread to avoid reflux. Lung segments were cooled on ice for 30 min to allow gelling of the agarose (3%), cut into pieces of an cross sectional area of approximately 2.5 – 4 cm² before they were cut with the vibratome to a thickness of 500 µm, and cultivated for up to 5 days under submerged conditions.

4.2.3 RNA expression analysis

4.2.3.1 *RNA isolation*

For total RNA isolation the Fibrous Tissue Kit was used with slight adaptations of the protocol provided by the manufacturer. Slices were washed twice with PBS, snap frozen in liquid nitrogen and kept at -80 °C until isolation was done. Three to five slices per treatment and time point from different regions of the lung (as suggested by Liberati *et al.* [Liberati, et.al., 2010]) were pooled. Only slices from the periphery of the lung containing no main bronchi were included. Slices were put into a tube with a 9 mm steel ball and put into a Micro-Dismembrator S for 2x 30 s at 3,000 rpm. The device and tubes were cooled with liquid nitrogen in between to avoid sample warming. The powder was lysed with 1 ml lysis buffer containing 12 µl TCEP for 1 h on ice. Afterwards samples were incubated with 25 µl proteinase K for 10 min on ice. For each sample 2 preclear columns were used. 550 µl were put onto the column and centrifuged at 400 g for 60 s. The flow through of the first preclear column was put onto the purification column and centrifuged at 13.000 g for 60 s. This flow through was discarded. The flow through of the second preclear column was put onto the same purification column and centrifuged at 13.000 g for 60 s. Wash step 1 was done twice

with 300 and 100 μl respectively with centrifugation at 13.000 g for 60 s in between. The column was put into a new collection tube and DNase digestion (50 μl of DNase) was done on the column for 20-30 min. Columns were washed twice with 200 μl DNase Wash with centrifugation at 13.000 g for 60 s in between and columns were put afterwards into a new collection tube. Columns were washed twice with 200 μl Wash 2 solution with centrifugation at 13.000 g for 60 s in between and columns were put afterwards into a new collection tube. Columns were centrifuged at 13.000 g for 60 s without solution on top (“dry”) and afterwards put into the elution tube. RNA elution was done with 40 μl elution buffer at 13.000 g for 60 s. After the elution, the flow through was put again onto the column and centrifuged at 13.000 g for 60 s. RNA was kept on ice and concentration was determined with a NanoDrop 1000 spectrophotometer using RNase/DNase free water or elution buffer as blank. For the human samples the quality of the RNA was checked with a Bioanalyzer using the Agilent RNA 6000 Nano Kit according to the protocol provided by the manufacturer. Only samples with a RNA integrity number above 5 (in general 7-8) were used for further analysis.

4.2.3.2 *cDNA synthesis by reverse transcription*

1 μg of RNA in 20 μl RNase/DNase free water was denatured at 72 $^{\circ}\text{C}$ for 10 min then chilled on ice. Transcription was carried out by adding the reagents described in Table 4.18. Incubation at 20 $^{\circ}\text{C}$ for 10 min was followed by 43 $^{\circ}\text{C}$ for 75 min and 99 $^{\circ}\text{C}$ for 5 min in a Mastercycler. cDNA was diluted 1:5 with water and stored at -20 $^{\circ}\text{C}$.

Table 4.18: cDNA synthesis by reverse transcription

| Reagent | Stock Concentration | Final concentration in 40 μl | Volume |
|--|---------------------|---|------------------|
| 10x Buffer II | 100 mM | 10 mM, 1x | 4 μl |
| MgCl ₂ | 25 mM | 5 mM | 8 μl |
| dNTPs | 10 mM | 0.5 mM | 2 μl |
| Random hexamers | 50 μM | 2.5 μM | 2 μl |
| Rnase inhibitor | 5 U/ μl | 0.25 U/ μl | 1 μl |
| MuLV reverse transcriptase | 50 U/ μl | 2.5 U/ μl | 2 μl |
| H ₂ O | | | 1 μl |
| total volume with addition of 1 μg RNA (in 20 μl) | | | 40 μl |

4.2.3.3 *Quantitative PCR (qPCR)*

In general, 12.5 ng/ μl cDNA were used for qPCR. The composition of the qPCR master mix is listed in Table 4.19. All qPCR assays were performed in duplicates with the reaction conditions shown in Table 4.20. For standardization of relative mRNA expression, human and mouse hypoxanthine-guanine phosphoribosyltransferase (HPRT) primers were used. Relative transcript abundance of a gene is expressed in ΔCp values ($\Delta\text{Cp} = \text{Cp}^{\text{reference}} - \text{Cp}^{\text{target}}$). Relative changes of mRNA levels of control/mRNA levels of treatment are presented as $\Delta\Delta\text{Cp}$ values ($\Delta\Delta\text{Cp} = \Delta\text{Cp}^{\text{treated}} - \Delta\text{Cp}^{\text{control}}$).

Table 4.19: Master mix for quantitative PCR

| Reagent | Stock concentration | Final concentration | Volume |
|---|---------------------|---------------------|--------|
| Light Cycler 480 SybrGreen I Master Mix | 2x | 1x | 10 µl |
| Primer mix | 10 µM each | 0.5 µM | 1 µl |
| H ₂ O | | | 4 µl |
| cDNA | 5 ng/µl | 1.25 ng/µl | 5 µl |
| total | | | 20 µl |

Table 4.20: Reaction conditions for quantitative PCR

| Repetitions | Cycle step | Temperature | Time |
|-------------|----------------------|--|---------|
| 1x | Initial denaturation | 95 °C | 5 min |
| | Denaturation | 95 °C | 5 s |
| 45x | Annealing | 59 °C | 5 s |
| | Elongation | 72 °C with single acquisition | 10 s |
| 1x | | 95 °C | 5 s |
| 1x | Melting curve | 60 °C | 1 min |
| 1x | | 60 °C -95 °C with continuous acquisition | |
| | Cooling | 4 °C | on hold |

4.2.4 Genotyping

Tail cuts were used to prepare genomic DNA by lysis with 1x PBNB buffer at 55 °C for 4 h with light shaking. Primer sequences are shown in Table 4.9. Normal PCR was run according to the programs shown in

Table 4.22 and Table 4.23. After the PCR DNA fragments were separated by electrophoresis using a 2 % agarose gel supplemented with 1x SybrSafe. 10 µl of the DNA samples and 5 µl of the 100 bp DNA ladder (Table 4.6) were loaded per pocket. Separation was done in 1x TAE buffer (4.1.3) by applying 80 V for 1 h. The DNA bands were visualized by using the XcitaBlue™ Conversion Screen from the ChemicDoc with illumination at 470 nm.

Table 4.21: PCR reaction mixture for genotyping

| Reagent | Concentration | Volume | Final concentration |
|--|---------------|-------------|---------------------|
| GoTaq G2 Hot Start Green Master Mix | 2x | 10 µl | 1x |
| forward primer transgene | 100 µM | 0.05 µl | 250 nM |
| reverse primer transgene | 100 µM | 0.05 µl | 250 nM |
| forward primer internal control | 100 µM | 0.05 µl | 250 nM |
| reverse primer internal control | 100 µM | 0.05 µl | 250 nM |
| template (genomic DNA) | variable | 0.5 to 2 µl | variable |
| UltraPure DNase/RNase-Free Distilled Water | | up to 20 µl | |

Table 4.22: PCR reaction conditions for genotyping of the TCF-LEF-EGFP mice

| Repetitions | Cycle step | Temperature | Time |
|-------------|----------------------|-------------|---------|
| 1x | Initial denaturation | 94 °C | 3 min |
| | Denaturation | 94 °C | 30 s |
| 35x | Annealing | 60 °C | 30 s |
| | Elongation | 72 °C | 30 s |
| 1x | Final elongation | 72 °C | 2 min |
| | Cooling | 4 °C | on hold |

Table 4.23: PCR reaction conditions for genotyping of the BAT-GAL and TOP-GAL mice

| Repetitions | Cycle step | Temperature | Time |
|-------------|----------------------|-------------------------------|---------|
| 1x | Initial denaturation | 94 °C | 3 min |
| | Denaturation | 94 °C | 20 s |
| 12x | Annealing | 64 °C, with -0.5 °C per cycle | 30 s |
| | Elongation | 72 °C | 35 s |
| | Denaturation | 94 °C | 20 s |
| 25x | Annealing | 58 °C | 30 s |
| | Elongation | 72 °C | 35 s |
| 1x | Final elongation | 72 °C | 2 min |
| | Cooling | 4 °C | on hold |

4.2.5 Viability and proliferation assays

4.2.5.1 Live/Dead assay

Live/Dead staining was performed by using the LIVE/DEAD® Viability/Cytotoxicity Kit *for mammalian cells*. Lung tissue cultures were punched to a diameter of 4 mm using a biopsy punch and incubated with cultivation medium supplemented with 2 µM calcein AM and 4 µM ethidium homodimer-1 for 40 min. Afterwards they were washed twice with PBS, fixed with 4% paraformaldehyde (PFA), and mounted onto glass slides with fluorescent mounting medium. Edges of the cover slips were sealed with nail polish. Calcein AM is converted into the green fluorescent calcein by serum esterases which are only active in viable cells, leading to a green fluorescent cytoplasm. Ethidium homodimer-1 can only enter cells with non-intact cell membranes where it binds to the DNA and leads to a 40 fold increase of red fluorescence in the nucleus. By this, viable cells are identified via the green fluorescent cytoplasm while dead cells are indicated by a red nucleus.

4.2.5.2 *WST-1 assay*

Tissue cultures from the periphery of the lung were punched to a diameter of 4 mm and incubated with 15 µl WST-1 per ml of cultivation medium for mouse slices or 30 µl WST-1 per ml cultivation medium for human slices. WST-1, is a tetrazolium salt, which is converted by the mitochondria of the cells. The conversion of the dye gives a linear measurement for mitochondrial activity. A higher mitochondrial activity can result either from an increased number of cells, and thereby a higher number of dye-converting mitochondria, or from higher metabolic activity. Assuming that the mean number and activity of mitochondria per cell are comparable, this assay can be used as a measure of cellular viability.

After 2 h 150 µl supernatant were measured in a plate reader at 450 nm. Reference measurement at 690 nm was subtracted. For each time point and treatment at least 3 punched slices from different mice, or different lung areas of human slices, were measured. As absorbance measurements for the human slices varied between the different patients, the mean value of the control treatment at d0 was set to 100% for each patient to make comparison possible.

4.2.5.3 *BrdU assay*

Punched lung slices (diameter 4 mm) were incubated with BrdU labelling medium (prepared according to the manual provided by the manufacturer) for 24 h at different time points of the cultivation (d0=labelling of the cells for 24 h from d0 on, d1=labelling of the cells for 24 h from d1 on, d3=labelling of the cells for 24 h from d3 on, d5=labelling of the cells for 24 h from d5 on). By this, the yimidine analog BrdU is incorporated in place of thymidine into the DNA of proliferating cells. With an antibody against BrdU the amount of this incorporation can be quantified based on ELISA technique. The ELISA to determine BrdU incorporation was performed according to the manual provided by the manufacturer. Values were presented relative to d0.

4.2.5.4 *Lactate dehydrogenase (LDH) assay*

LDH is released by the cells into the supernatant. This release is increased when the cells are damaged, as their cell membrane gets leaky. For this reason, the LDH release is normally used as a measurement for toxicity. Punched lung slices (diameter 4 mm) were incubated with 200 µl of fresh cultivation medium 24 h hours before the measurement was done. Cell culture supernatant was taken and cleared from cell debris by centrifugation. Afterwards, 100 µl supernatant was incubated with 100 µl reaction solution (according to protocol provided by the manufacturer: 2.5 µl catalyst mixed with 112.5 µl dye solution per sample) in a 96 well-plate for 15-30 min in the dark at room temperature. Cultivation medium incubated the same time without slices was use as blank. Reaction was stopped with 50 µl of 1 M HCl and absorbance was measured in a plate reader at 490 nm. Reference measurement at 690 nm was substracted.

4.2.6 Proteinbiochemistry

4.2.6.1 Protein isolation and concentration determination

Tissue slices were washed twice in PBS before they were snap frozen in liquid nitrogen and stored at -80 °C. Three to four slices were pooled per treatment and time point and pulverized with a Micro-Dismembrator S the same way as for RNA isolation (4.2.3.1). The powder was lysed with 300-400 µl T-PER-buffer supplemented with phosphatase and protease inhibitors (1 tablet each per 10 ml buffer). Afterwards, samples were frozen at -80 °C and thawed on ice. Thereafter, protein extracts were clarified by centrifugation at 13,000 g at 4 °C and stored at -80 °C. Protein content was measured using the Pierce™ BCA Protein Assay Kit according to the protocol provided by the manufacturer.

4.2.6.2 Protein analysis with Western Blot

15 µg of protein lysate were mixed with Laemmli loading buffer and T-PER buffer for equal volumes. SDS polyacrylamide gel concentration was adjusted to the size of the protein to be detected (ranging from 6 to 15%). Electrophoresis was done with 70 V for 15 min and 120 V for further 60-90 min in SDS-PAGE Running Buffer. Proteins were transferred to nitrocellulose membranes with 300 mA for 90 min at 4 °C using 1x transfer buffer. Unspecific antibody binding was blocked with 5% non-fat milk for 1 h. Blots were incubated with primary antibodies at 4 °C over night or for 1.5 h at RT with light shaking. After three washing steps with TBST at RT blots were incubated with secondary antibodies for 1.5 h at RT. Enhanced chemiluminescence was used to visualize proteins and the signals were measured either using the ChemiDoc or an x-ray film, which was automatically developed with the film developer Curix 60. The used antibodies and concentrations are listed in Table 4.13, Table 4.15, and Table 4.16.

4.2.6.3 Enzyme-linked immunosorbant assay (ELISA)

SFTPC protein concentrations in protein lysates from murine and human 3D-LTC were determined using a mouse/human SFTPC ELISA from Cusabio according to protocol provided by the manufacturer. Samples were measured in triplicates. For murine samples 5 ng and for human samples 2 ng of protein was used. Results were presented as percentage of SFTPC protein to total protein.

4.2.7 Histology

Different stainings were conducted for histological analysis. Samples for staining with Haematoxylin & Eosin, Masson-Trichrome and Elastin (see 4.2.2) were fixed in 4% PFA over night and transferred into paraffin with a Microm STP 420D machine according to the protocol from Table 4.24. Afterwards, samples were embedded into paraffin blocks using the Microm EC350 and

stored at 4°C. 2-3 µm thin sections were cut with a Hyrax M55 microtome and fitted onto glass slides.

Table 4.24: Protocol used for paraffin embedding of tissue samples

| Reagent | Time |
|----------------|-------------|
| 4% PFA | 60 min |
| 4% PFA | 60 min |
| 50% ethanol | 60 min |
| 70% ethanol | 60 min |
| 96% ethanol | 60 min |
| 96% ethanol | 60 min |
| 100% ethanol | 60 min |
| 100% ethanol | 60 min |
| Xylene | 60 min |
| Xylene | 60 min |
| Paraffin | 30 min |
| Paraffin | 45 min |
| Paraffin | 45 min |
| Paraffin | 45 min |

4.2.7.1 *Haematoxylin & Eosin (H&E) staining*

Paraffin sections were deparaffinised and rehydrated before staining according to the following protocol (Table 4.25). After the last step glass slides were covered with coverslips using HI-MO mounting medium.

Table 4.25: Protocol used for H&E staining

| Reagent | Time |
|-----------------------------------|-------------|
| Xylene | 5 min |
| Xylene | 5 min |
| 100% ethanol | 1 min |
| 100% ethanol | 1 min |
| 90% ethanol | 1 min |
| 80% ethanol | 1 min |
| 70% ethanol | 1 min |
| Distilled water | Flushing |
| Heamatoxylin | 5 min |
| Tap water | Flushing |
| HCl-ethanol (0.3% in 70% ethanol) | Up to 1 min |
| Tap water | 10-15 min |
| Distilled water | Flushing |
| Eosin (0.5 g in 70% ethanol) | 8 min |
| Distilled water | Flushing |
| 70% ethanol | Flushing |

| | |
|--------------|----------|
| 80% ethanol | Flushing |
| 90% ethanol | Flushing |
| 100% ethanol | Flushing |
| Xylene | 5 min |
| Xylene | 5 min |

4.2.7.2 Masson-Trichrome (MTC) staining

Masson-Trichrome staining was performed by Maria Neuner according to the protocol shown in Table 4.26.

Table 4.26: Protocol used for Masson-Trichrome staining

| Reagent | Time |
|--|------------------------------|
| Xylene | 5 min |
| Xylene | 5 min |
| 100% ethanol | 1 min |
| 100% ethanol | 1 min |
| 90% ethanol | 1 min |
| 80% ethanol | 1 min |
| 70% ethanol | 1 min |
| Weigerts-staining solution | 10 min |
| Tap water | 3 min, 1x exchange the water |
| HCl-ethanol (0.3% HCl in 70% ethanol) | Up to 1 min |
| Distilled water | Flushing |
| Ponceau-fuchsin | 6 min |
| Distilled water | Flushing |
| 1% acetic acid | Flushing, 1x exchange |
| Distilled water | Flushing |
| Phosphomolybdate solution | 5 min |
| 1% acetic acid | Flushing, 1x exchange |
| Distilled water | Flushing |
| Light green SF (20 mg/l in 0.2% acetic acid) | 8 min |
| 1% acetic acid | Flushing, 1x exchange |
| Distilled water | Flushing |
| 70% ethanol | Flushing |
| 80% ethanol | Flushing |
| 90% ethanol | Flushing |
| 100% ethanol | Flushing |
| Xylene | 5 min |
| Xylene | 5 min |

4.2.7.3 *Elastin staining*

Elastin staining was performed by Maria Neuner with a modified Hart's elastic staining protocol (Table 4.27).

Table 4.27: Protocol used for elastin staining

| Reagent | Time |
|---|------------------------|
| Xylene | 15 min |
| Xylene | 15 min |
| 100% ethanol | 5 min |
| 100% ethanol | 5 min |
| 90% ethanol | 5 min |
| 70% ethanol | 5 min |
| 70% ethanol | 5 min |
| Distilled water (2x) | Flushing |
| 0.25% potassium permanganate | 5 min |
| Distilled water (several) | Flushing |
| 5% oxalic acid dihydrate | 5-10 s |
| Tap water | 5 min with flushing |
| Distilled water | Flushing |
| Resorcsin-fuchsin (1:10 in 70% ethanol with 20 mM HCl) | Over night in the dark |
| Tap water | 15 min with flushing |
| 0.25% tartrazine (in 2.5 mM acetic acid) | 90 s |
| 70% ethanol | Flushing |
| 70% ethanol | Flushing |
| 96% ethanol | Flushing |
| 96% ethanol | Flushing |
| 100% ethanol | 5 min |
| 100% ethanol | 5 min |
| Xylene | 5 min |
| Xylene | 5 min |

4.2.7.4 *LacZ staining*

The tissue cultures were washed twice with PBS and prefixed for 10 min in 4% PFA. After 3 washing steps with PBS the slices were once rinsed with LacZ staining solution to prevent precipitations. Afterwards, the tissue was incubated in X-Gal/LacZ staining solution in the dark at 37°C over night leading to blue staining in the cells in which canonical Wnt signalling was activated. Two further washing steps with PBS were followed by mounting onto glass slides with HI-MO mounting medium. Staining was evaluated via brightfield microscopy.

4.2.7.5 Immunofluorescence

Tissue cultures were washed twice with PBS and fixed with acetone/methanol 50/50 v/v for 20 min. After washing three times with 0.1% BSA in PBS the tissue was punched to a diameter of 4 mm by using a biopsy punch, and incubated with primary antibody over night at 4 °C. Five washing steps with 0.1% BSA in PBS were followed by incubation with secondary antibodies for 1 h. Thereafter, samples were washed three times with 0.1% BSA in PBS and cell nuclei were stained with 0.5 µg/ml DAPI for 5 min. After three washing steps with 0.1% BSA in PBS samples were fixed again with 4% PFA for 30 min and mounted onto microscopy slides with fluorescence mounting medium. Staining was evaluated via confocal microscopy. 3D reconstruction was conducted using the IMARIS software. Antibodies that were used are listed in Table 4.10 and Table 4.12.

4.2.8 Live cell imaging

Confocal time-lapse microscopy was implemented on an LSM710 system (Zeiss) containing an inverted AxioObserver.Z1 stand. 3D-LTC were incubated with primary antibodies in the cultivation medium over night and nuclei were stained with Hoechst for 30 min prior to observation. After punching to a diameter of 6 mm, 3D-LTC were transferred to imaging plates and fixed to avoid movements during imaging. They were kept submerged in DMEM/HAM's F12 medium containing 0.1% FCS and 15 mM HEPES during the whole period of observation. Imaging of the 3D-LTC was performed in a PM S1 incubator chamber (Zeiss) at 37°C. Acquisition of the 3D-LTC started within 30 min after their transfer to the imaging plates. Z-stacks (50-100 µm) were acquired with an EC Plan-Neofluar DICII 20x/ 0.8 NA objective lens (Zeiss) in 30 minutes intervals up to 24 h. The automated time-lapse microscope was operated by ZEN2009 software (Zeiss). The confocal 4D data sets were imported into Imaris 7.4.0 software (Bitplane) and processed by applying a volume rendering algorithm.

4.2.9 Statistical Analysis

All values are shown as mean with standard deviation. For comparison of two groups unpaired t-test with Welch's correction or two tailed, paired t-test (for paired observations) was used. More than two groups were compared with ANOVA and Bonferroni post-test. A p-value lower than 0.05 was considered statistically significant. All statistical analyses were performed with the GraphPad Prism Software.

5 RESULTS

5.1 Characterization of 3D-LTC from healthy/non-COPD tissue over time

In standard 2D cultures, where cells are grown for instance in monolayers, cells normally do not lack oxygen and/or nutrients. This dramatically changes when cells are grown in multilayers and in three dimensional tissues where diffusion gradients may lead to shortage of oxygen and/or nutrients in certain regions of the culture thereby inducing alterations in gene expression due to the adaptation of the cells to the oxygen- and/or nutrient-deprived environment or even cell death by induction of apoptosis or necrosis [Macintosh, et.al., 2013, Poon, et.al., 2010]. To exclude that such oxygen and/or nutrient shortage occurs in the 3D-LTC, their cell viability and proliferation were evaluated. A combination of different methods, such as live cell imaging, Live/Dead staining, WST-1 conversion, and BrdU incorporation, was conducted to confirm cell viability and proliferation over seven days.

First, live cell imaging was applied for analysing cell viability. A time-laps video, depicted as single images, from day seven of the cultivation of a 3D-LTC from a mouse lung showed sustained ciliary beating of a bronchial epithelial cell (Figure 5.1). This gave first evidence that cells inside the tissue culture are viable and remain functional until day seven.

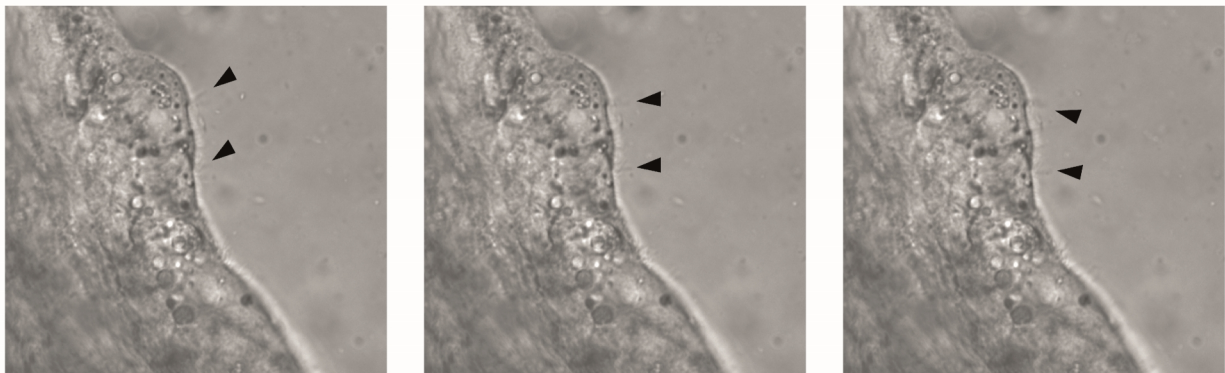


Figure 5.1: Ciliary beating was sustained in 3D-LTC from healthy animals until day seven.

Consecutive live cell imaging pictures of a bronchial epithelial cell in a 3D-LTC from a healthy mouse on day seven of culture. Images were taken with the “maximum speed” method (taken as fast as possible).

Live cell imaging, conducted until day seven showed fast cellular movement of single cells inside the 3D-LTC. These cells seemed to be located on top of the alveolar matrix assuming to be alveolar macrophages/leucocytes. With standard light microscopy, only a low resolution in z-direction (height) could be achieved. To improve resolution, determine cell type specificity, and to evaluate individual cell migration, immunofluorescence labelling of the ECM (collagen I), leucocytes (CD45), and cell nuclei in general (Hoechst) was conducted (Figure 5.2). CD45 labeled and other cells (identified by Hoechst stain only) were moving inside the 3D-LTC during the whole period of observation (12 h starting on day two of the cultivation). This added evidence that the cells inside

the 3D-LTC remained vital over time. To further prove viability Live/Dead staining and mitochondrial activity measurements were conducted, showing positive staining for viable cells during five days of cultivation and increased mitochondrial activity from day one to day three, being stable at day five. The detailed results from 3D-LTC from healthy animals will be shown in Figure 5.5 and Figure 5.6 together with the results from emphysematous animals since no major difference were observed.

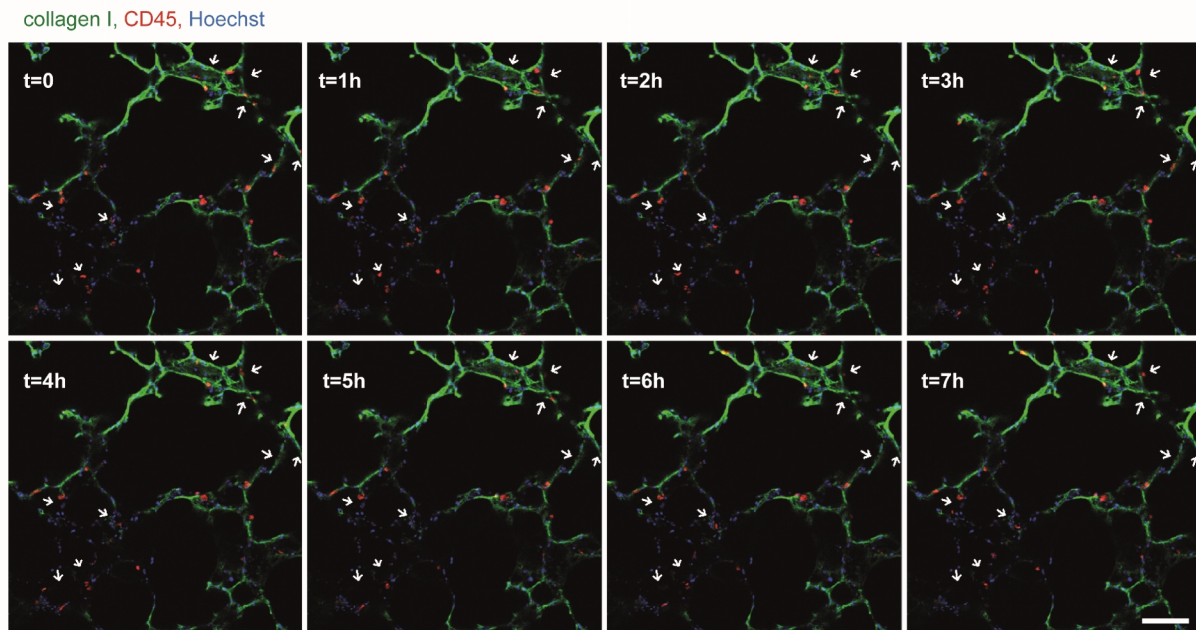


Figure 5.2: Cellular movements in 3D-LTC showing that cells remain viable.

Live cell imaging picture series of a murine 3D-LTC showing migrating cells over time. Images were taken every 15 min on day two for 12 h. Pictures are shown for 0-7 h. The extracellular matrix was stained with collagen I (green), leukocytes with CD45 (red), and nuclei in general with Hoechst (blue). Arrows point to regions where cellular movements occurred. Scale bar 100 μ m.

Next, the proliferative capacity of the cells was analysed by incorporation of BrdU, to get more insight into cellular turnover. Cells were labelled for 24 h at different time points (d0, d1, d3, and d5). Afterwards, an ELISA was conducted and quantitative measurement over the time was evaluated. Proliferation in the 3D-LTC followed the same profile for both 0.1% and 10% FCS cultivation medium showing a significant increase on day three. After that peak, proliferation still occurred but was reduced compared to day three. 10% FCS led to a higher proliferation rate supporting the cell viability data from above (Figure 5.3). Cells inside the 3D-LTC proliferated in the first days of cultivation leading to more viable cells. After this initial peak of proliferation, 3D-LTC stayed stable with ongoing, but reduced proliferation compared to the early time points. In conclusion, 3D-LTC were viable and exhibited proliferative capacity until day five.

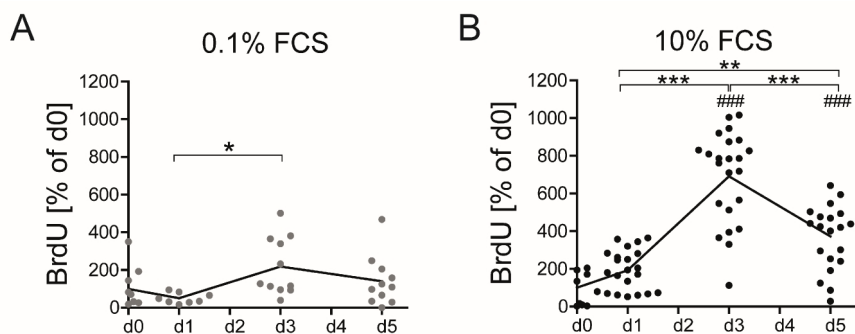


Figure 5.3: Proliferation of the cells in 3D-LTC peaked at day three (=day four) of culture.

Quantitative analysis of the proliferation of cells in murine 3D-LTC cultivated with A) 0.1% FCS and B) 10% FCS cultivation medium. n=11-24. *: p<0.05, **: p<0.01, ***: p<0.001, #: compared to d0, one way ANOVA with Bonferroni post-test.

The next step was to adapt the method of 3D-LTC to human tissue. To characterize viability during cultivation Live/Dead staining and mitochondrial activity were assessed in 3D-LTC from human non-COPD patients. Similar results were obtained compared to the murine 3D-LTC and will be shown in detail in Figure 5.8 and Figure 5.9 together with the results from COPD tissue slices since no major differences were observed.

The sustained ciliary beating, the cellular movements during live cell imaging, the positive Live-staining, and the mitochondrial activity as well as the proliferation data show that 3D-LTC from healthy murine and human non-COPD tissue maintain their viability during cultivation.

5.2 Characterization of 3D-LTC from diseased lung tissue specimen

An animal model for the emphysematous changes seen in COPD is *oro tracheal* instillation of porcine pancreatic elastase (PPE) in the range of 40-120 U/kg mouse. In addition to MMP-2, -9, and -12, elastase is known to be the key elastolytic enzyme contributing to emphysema [Shapiro, 2002]. Peribronchial remodelling, normally seen in COPD, cannot be observed [Antunes, et.al., 2011]. The elastase-induced emphysema model benefits from lower costs and more efficient generation of emphysema compared to other models (e.g. cigarette smoke exposure). The application of elastase *oro tracheally* is very easy and the mortality of the treated animals is low (we observed less than 10% mortality in total). In general, PPE is applied only once, resulting in progressive emphysema development while the applied PPE dose determines emphysema severity [Andersen, et.al., 2012, Inoue, et.al., 2003, Ito, et.al., 2005, Kononov, et.al., 2001, Lucey, et.al., 1998]. In the first few days after administration, a temporary, injury-induced inflammation response occurs with an increase in inflammatory cells in the bronchoalveolar lavage fluid (BALF), which decreases after approximately five days. Even though inflammation is not recurring in this model compared to cigarette smoke exposure, emphysema development increases over time. In this thesis, the elastase-induced emphysema model on day seven after elastase application was used.

5.2.1 Morphology and viability of 3D-LTC after elastase induced emphysema

Next, 3D-LTC from diseased mouse tissue were characterized regarding their morphological characteristics and viability in culture. Cultures of 3D-LTC from healthy and emphysematous mice were imaged after histologic and immunofluorescence staining. Emphysema was clearly visible in the 3D-LTC fabricated seven days after elastase administration. Airspace enlargement and alveolar destruction was also clearly distinguishable. Less elastin (black) was seen in the elastin staining supporting loss of elastin fibres in emphysematous tissue (Figure 5.4A). Immunofluorescence images in Figure 5.4B revealed that specific extra-cellular matrix components like collagen I could be imaged and the antibodies used reached the whole interior of the 3D-LTC, staining the middle of the cultures as well (compare definition of middle plane Figure 5.5A). Single cell types, such as CD45- (leucocytes), pro-SFTPC- (ATII cells), aquaporin5-positive cells (AQP5, ATI cells), as well as positive staining for podoplanin (PDPN, ATI cells), and cellular junctions (shown for E-cadherin, CDH1) was obtained in the 3D-LTC (Figure 5.4C). These data clearly indicate that diseased mouse tissue morphology and structure can be well maintained by 3D-LTC and validate this technology for the use of diseased lung tissue.

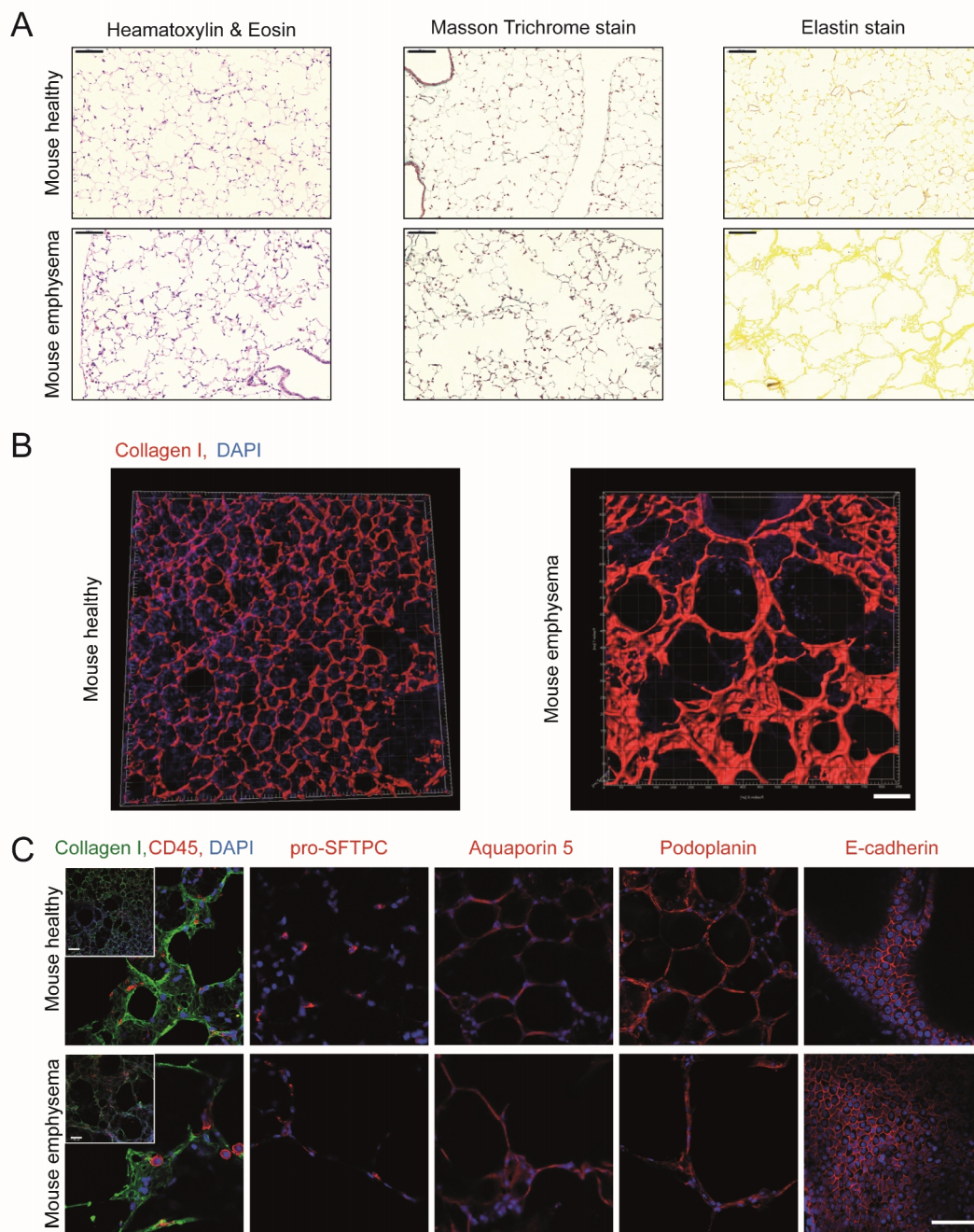


Figure 5.4: Emphysematous changes can be evaluated in the 3D-LTC.

A: H&E, Masson Trichrome, and Elastin staining of 3D-LTC from healthy and emphysematous mice. Scale bar 100 μm .
 B: 3D reconstruction of immunofluorescence staining of collagen I. Scale bar 100 μm . C: Immunofluorescence staining of extracellular matrix with collagen I, specific cell types with CD45 (leucocytes), pro-SFTPC (ATII), aquaporin 5 (ATI), as well as podoplanin (ATI), and cellular junctions with E-cadherin antibodies. Scale bar 50 μm , insert: 100 μm . The nuclei were stained with DAPI.

Live/Dead staining was applied to investigate cell viability in more detail. The whole height (300 μm) of the 3D-LTC was investigated and different regions (top, middle, and bottom plane) were examined (Figure 5.5). Dead cells, indicated by a red nucleus, were nearly absent in the

middle of the 3D-LTC and were mainly seen at slice margins (top and bottom plane). Over the whole period of cultivation, no differences in cell viability, especially no increase in dead cells, was detected, however, a slight decrease in fluorescence intensity of the green dye, indicative for viable cells, from day five on was observed (Figure 5.5B).

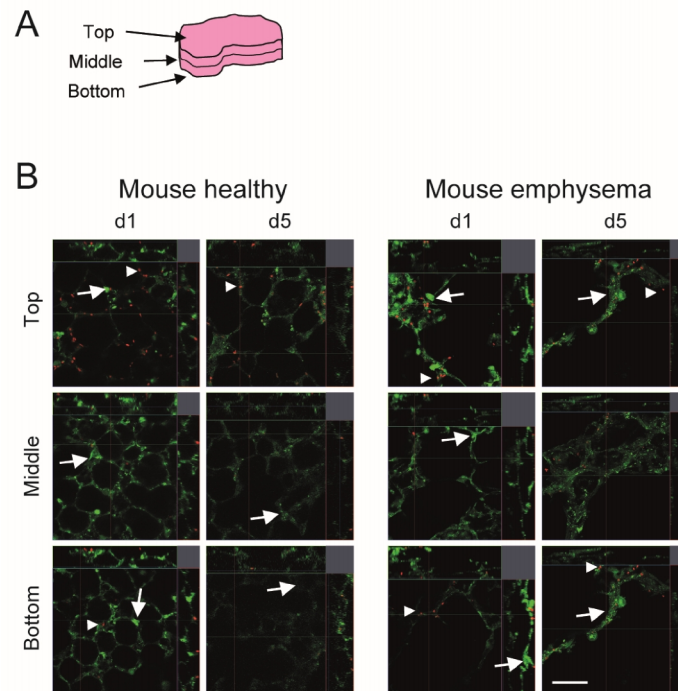


Figure 5.5: 3D-LTC from healthy and emphysematous mice stayed viable over five days of cultivation.

A: Scheme of the different regions of the 3D-LTC referred to as top, middle, and bottom plane. B: Representative Live/Dead confocal images (cut view) of the different planes of the 3D-LTC from healthy and emphysematous mice at the indicated time points. Healthy cells are indicated by green cytoplasm (arrows) and dead cells by red nucleus (arrowheads). Scale bar 50 μm .

The third method to test for cell viability was incubation of 3D-LTC with WST-1 supplemented cultivation medium. Mitochondrial activity was significantly increasing from day one to day three and stayed stable until day five (Figure 5.6). Measurement values from emphysematous mice were slightly lower but exhibited the same kinetics. No significant difference in WST-1 conversion at different time points was observed between 0.1% FCS and 10% FCS medium (data not shown). Furthermore, no significant difference between WST-1 conversion of 3D-LTC from healthy mice (PBS instilled) compared with age matched non-treated mice was seen (data not shown).

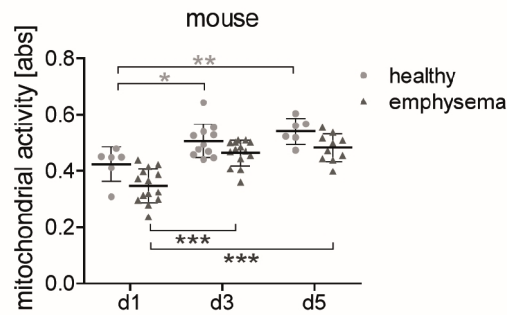


Figure 5.6: WST-1 conversion increased until day three in 3D-LTC from healthy and emphysematous mice. WST-1 conversion of the cells in 3D-LTC from healthy and emphysematous mice cultivated for five days. n=6-11. *: p<0.05, **: p<0.01, one way ANOVA with Bonferroni post-test.

The WST-1 measurement data confirmed the results from the Live/Dead staining and live cell imaging, showing that in 3D-LTC from both healthy and emphysematous mice cells stay viable during the cultivation. Whether cell numbers increased over time, or if the cells simply became activated leading to the increase in WST-1 conversion could not be determined with this method.

5.2.2 Morphology and viability of 3D-LTC from human patients

The major benefit of 3D-LTC is the possibility to generate them from any species. Lung tissue from human patients undergoing lung resection surgery due to lung cancer was used to apply the method as a translational approach and for use as a preclinical testing tool. 3D-LTC were generated from human COPD and non-COPD samples as described in chapter 4.2.2 and analysed regarding morphology and viability, as well. Lung tissue structure, analysed by haematoxylin & eosin staining revealed the emphysematous changes occurring in these lung specimens. Samples from COPD patients had increased alveolar airspaces and showed alveolar destruction (Figure 5.7A). By usage of a collagen I immunofluorescence staining 3D reconstruction of this ECM protein network structure was possible (Figure 5.7B). Similar to the murine samples a broad range of markers was accessible for analysis by immunofluorescence staining, as shown for instance for pro-SFTPC, podoplanin, and E-cadherin (Figure 5.7C).

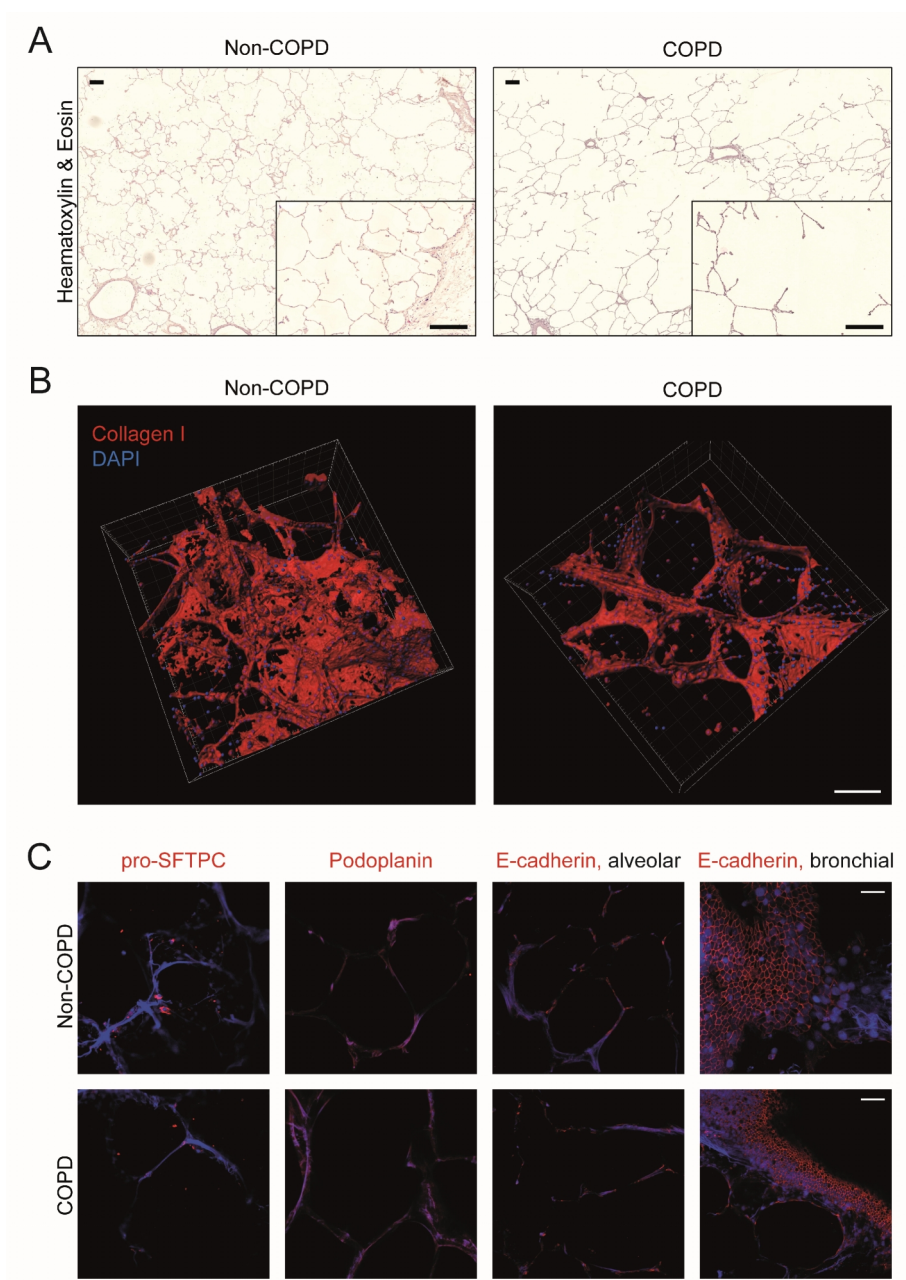


Figure 5.7: Emphysematous changes can be evaluated in 3D-LTC from human patients.

A: H&E staining of 3D-LTC from non-COPD and COPD patients. Inserts are showing a higher magnification. Scale bars 100 μm. B: 3D reconstruction of immunofluorescence staining of collagen I. Scale bar 100 μm. C: Immunofluorescence staining of pro-SFTPC, podoplanin, and E-cadherin. Scale bar 50 μm. The nuclei were stained with DAPI.

Viability of the human 3D-LTC was analysed by Live/Dead staining and WST-1 conversion. Differences in Live/Dead staining between non-COPD and COPD patients was not visible. In the middle plane, only few cells were marked by red staining and therefore considered as dead cells (Figure 5.8).

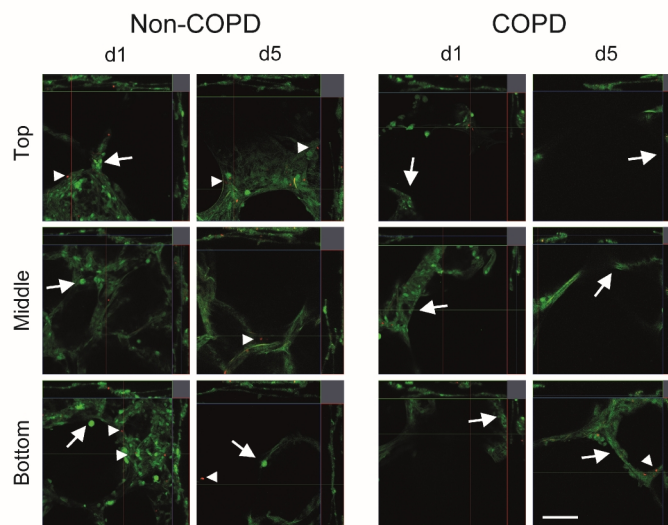


Figure 5.8: 3D-LTC from human patients stayed viable over five days of cultivation.

Live/Dead staining, confocal images (cut view) of the different planes of 3D-LTC from human patients at the indicated time points. Healthy cells are indicated by green cytoplasm (arrows) and dead cells by red nuclei (arrowheads).

Mitochondrial activity of human 3D-LTC showed a similar increase, as seen for the murine samples, being significant until day three and stable afterwards. No significant difference was observed between COPD and non-COPD samples for the analysed time points (Figure 5.9).

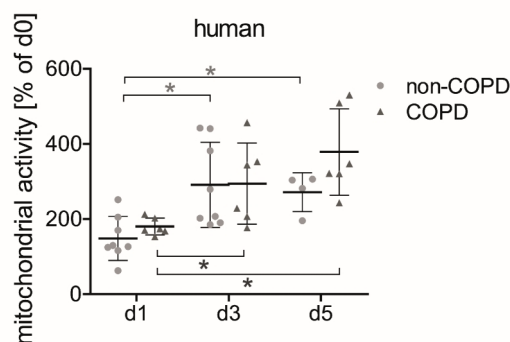


Figure 5.9: WST-1 conversion increases until day three in 3D-LTC from human patients.

WST-1 conversion of the cells in 3D-LTC from non-COPD and COPD patients cultivated for five days. As baseline viability of the 3D-LTC varied between the patients, the measurement values needed to be normalized to the measurement values of d0 for each patient respectively to make comparison possible. n=4-8. *: p<0.05, one way ANOVA with Bonferroni post-test.

Taken together, murine and human 3D-LTC were analysed regarding morphological changes in 3D, specific cell types and their location inside the slice, cellular viability, as well as proliferative capacity. Regarding the kinetic of the metabolic activity, no difference was seen comparing murine versus human 3D-LTC, healthy versus emphysematous, and non-COPD versus COPD, respectively. This gives evidence that 3D-LTC maintain viability over the cultivation of at least five days.

5.3 Characterization of Wnt/beta-catenin signalling in 3D-LTC

As mentioned before, Wnt/beta-catenin signalling is reduced in COPD patients and emphysematous animals [Kneidinger, et.al., 2011, Wang, et.al., 2011, Zhou, et.al., 2012]. Therefore, we analysed whether these known alterations can also be detected in 3D-LTC, which is a prerequisite for using this technology for drug testing and mechanistical studies. The procedure of agarose infiltration and fabrication of the 3D-LTC may have an influence on RNA expression of the cells. Wnt/beta-catenin downregulation may be affected by this. To control for such effects, RNA was isolated and analysed from 3D-LTC directly after vibratome slicing. Wnt target genes, ligands, and receptors were significantly down regulated while Wnt antagonists were upregulated (Figure 5.10). This gives evidence that Wnt signalling downregulation is present in 3D-LTC from emphysematous mice.

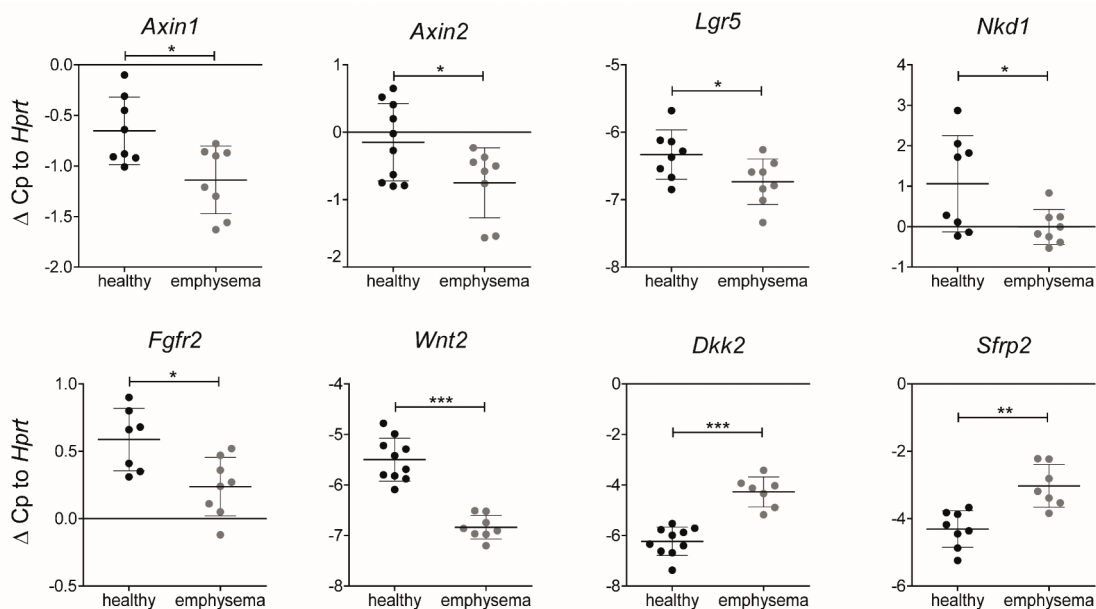


Figure 5.10: Wnt signalling down regulation is retained in 3D-LTC from emphysematous mice.

RNA expression of 3D-LTC from healthy and emphysematous mice was analysed directly after the generation of slices. n=7-10. *: p<0.05, **: p<0.01, ***: p<0.001, unpaired t-test with Welch's correction.

5.4 Wnt/beta-catenin activation in 3D-LTC from emphysematous mice and human patients

It was shown before that Wnt/beta-catenin signalling was downregulated in 3D-LTC from emphysematous tissue and in 3D-LTC from emphysematous mice. Wnt/beta-catenin activation is a possible target to induce repair. Therefore, Wnt/beta-catenin modulation is a target for drug development and testing to gain novel therapeutic options for COPD patients. The effect of pathway activation was further addressed in the present study. For reactivation of Wnt/beta-catenin signalling two different GSK3 inhibitors were used as already mentioned before: LiCl and the chiron inhibitor CHIR99021 (CT), a compound more specific to GSK3 [Bain, et.al., 2007]. For most

experiments, LiCl was applied to analyse the effect of Wnt/beta-catenin activation for lung regeneration, analysed by modulation of ATI and ATII cell markers. CT was used as proof of concept to show that the 3D-LTC model is reactive to other treatments for Wnt/beta-catenin activation as well. With the 3D-LTC model, it is also possible to gain insight into the mechanisms of lung repair due to its 3D structure with allocation of all different cell types residing in the lung and thus benefiting of the perfect mimicking of the *in vivo* situation.

5.4.1 Toxicity of LiCl in 3D-LTC

First, it was evaluated whether GSK3 inhibition with LiCl causes cell toxicity. For this, 3D-LTC were treated with different amounts of LiCl in 0.1% FCS cultivation medium and WST-1 conversion was analysed. No significant toxicity was seen up to a concentration of 10 mM LiCl while treatment with 20 mM LiCl led to significantly reduced mitochondrial activity within 24 h showing that this concentration is toxic to the cells (Figure 5.11).

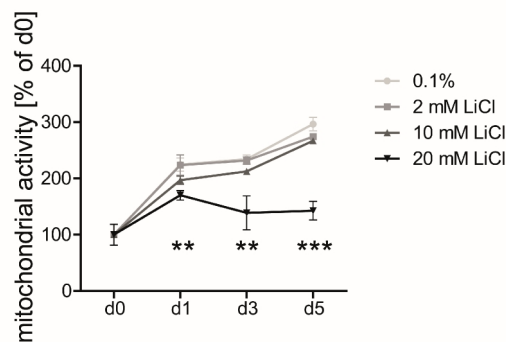


Figure 5.11: LiCl was not toxic to 3D-LTC from healthy mice up to a concentration of 10 mM.

WST-1 conversion of the cells in 3D-LTC from healthy mice cultivated with varying concentrations of LiCl for the indicated time points. n=3. *: p<0.05, **: p<0.01, ***: p<0.001 compared to control treatment (0.1% FCS cultivation medium), one way ANOVA with Bonferroni post-test.

To verify, that 10 mM LiCl is not toxic in the 3D-LTC from emphysematous animals, which might be more susceptible to damage, the WST-1 test was repeated with those 3D-LTC as well. As shown in Figure 5.12, 10 mM LiCl did not induce significant toxicity in 3D-LTC from emphysematous mice. For these reasons, a concentration of 10 mM LiCl was used for all following experiments to activate Wnt/beta-catenin signalling.

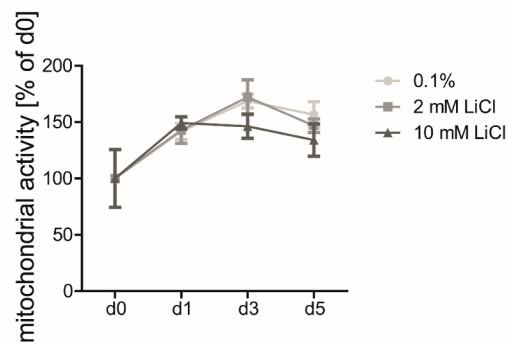


Figure 5.12: LiCl was not toxic to 3D-LTC from emphysematous mice up to a concentration of 10 mM.

WST-1 conversion of the cells in 3D-LTC from emphysematous mice cultivated with varying concentrations of LiCl for the indicated time points. n=3. one way ANOVA with Bonferroni post-test.

5.4.2 Effects of Wnt/beta-catenin activation by LiCl in murine 3D-LTC

First, the activation of Wnt/beta-catenin by LiCl in the emphysematous 3D-LTC was evaluated by analysing Wnt target gene expression. *Axin2* as well as *Dkk2* were significantly upregulated after 6 and 24 h of treatment proving Wnt/beta-catenin activation on transcript level by LiCl (Figure 5.13).

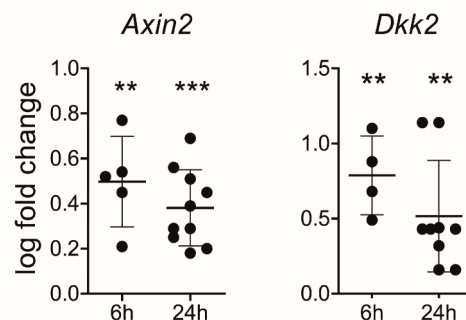


Figure 5.13: Wnt target gene expression was induced in 3D-LTC from emphysematous mice with 10 mM LiCl.

Wnt target gene expression in 3D-LTC from emphysematous mice cultivated with 10 mM LiCl. n=4-10. *: p<0.05, **: p<0.01, ***: p<0.001, one sample t-test.

Second, activation of the Wnt/beta-catenin pathway was determined by expression analysis of ABC protein via Western Blotting. ABC protein expression was significantly increased after 24 h of treatment with 10 mM LiCl in the slices from emphysematous mice giving evidence for the successful activation of Wnt/beta-catenin via LiCl on the protein level as well (Figure 5.14).

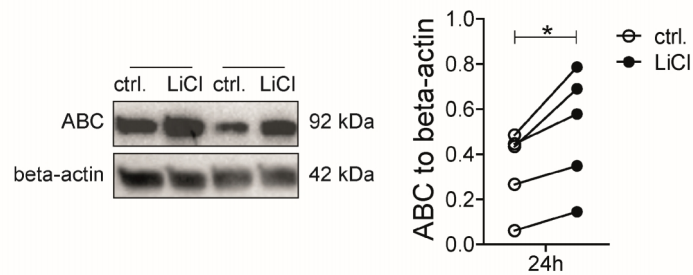


Figure 5.14: Active beta-catenin protein expression was significantly increased in 3D-LTC from emphysematous mice with 10 mM LiCl.

ABC protein expression in 3D-LTC from emphysematous mice treated with 10 mM LiCl for 24 h. left: representative Western Blot from 3D-LTC of two representative emphysematous mice, right: densitometry. n=5. *: p<0.05, paired t-test.

The third method to verify Wnt/beta-catenin activation with LiCl was the treatment of 3D-LTC from emphysematous reporter animals (BAT-GAL and TCF/LEF-GFP [Ferrer-Vaquer, et.al., 2010, Maretto, et.al., 2003]). In 3D-LTC from both reporters LiCl led to an increase in the number of positively stained cells in the lung periphery (Figure 5.15).

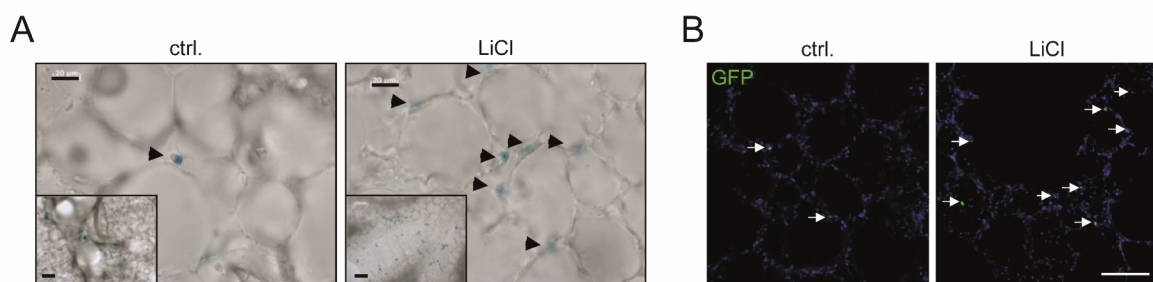


Figure 5.15: LiCl led to an increase in Wnt/beta-catenin activated cells in the periphery 3D-LTC from emphysematous mice.

A: LacZ staining of 3D-LTC from emphysematous BAT-GAL Wnt-reporter animals treated with 10 mM LiCl for 3 h. scale bar 20 μ m, insert 100 μ m. B: Confocal images of the GFP-staining of 3D-LTC from emphysematous TCF/LEF-GFP Wnt-reporter animals treated with 10 mM LiCl for 72 h. Scale bar 50 μ m.

By the usage of live cell imaging of LiCl treated 3D-LTC from emphysematous TCF/LEF-GFP Wnt-reporter mice, the increase in Wnt-activated cells was confirmed by appearance of GFP-positive cells over time. Figure 5.16 shows an imaging time series from a video of the periphery with those cells in the alveolar regions starting to express GFP over time.

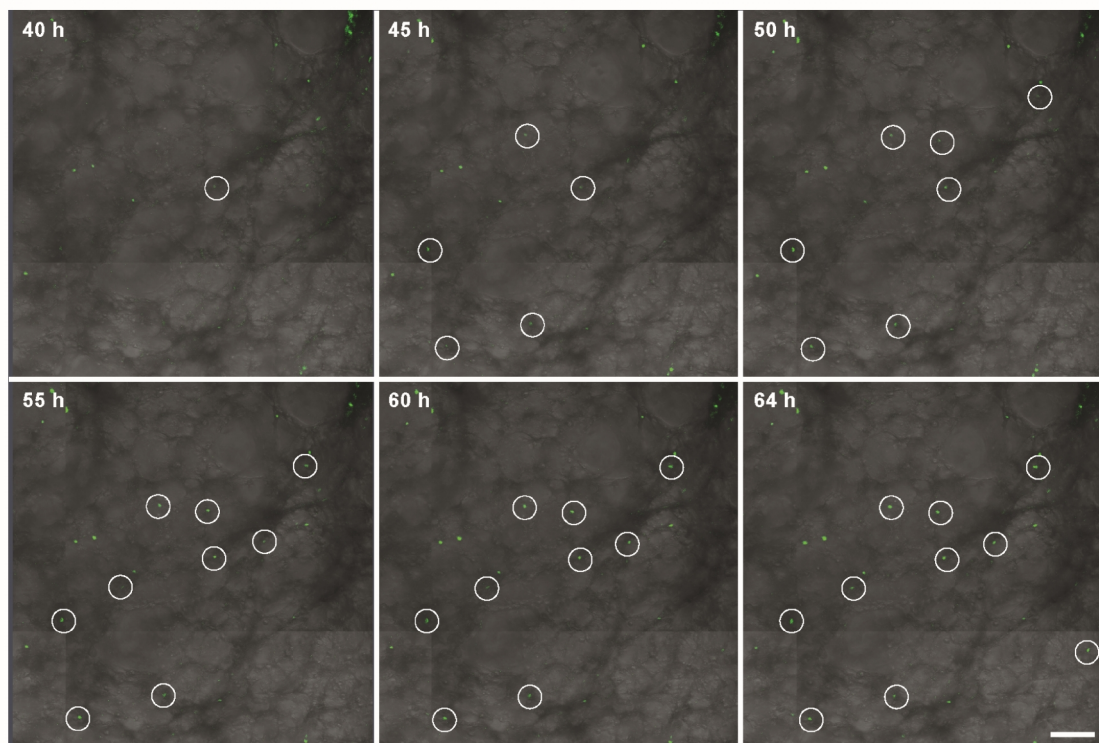


Figure 5.16: Live cell imaging reveals cells in the periphery of 3D-LTC from emphysematous TCF/LEF-GFP Wnt-reporter animals becoming Wnt/beta-catenin activated over time.

Live cell imaging picture series of a 3D-LTC from an emphysematous TCF/LEF-GFP Wnt-reporter animal. Images were taken starting at 40 h of culture for 24 h with imaging every 30 min and are shown for a subset of time points. Circles indicate cells, starting to express GFP due to Wnt/beta-catenin activation. Scale bar 100 μ m.

After proving successful activation of Wnt/beta-catenin signalling by the increased expression of Wnt target genes, the upregulation of ABC, and the increase in Wnt/beta-catenin activated cells, it was important to identify which cells became activated. After LiCl treatment GFP-positive cells in 3D-LTC from emphysematous mice stained positive for the ATII cell marker SFTPC and the ATI cell marker podoplanin (Figure 5.17).

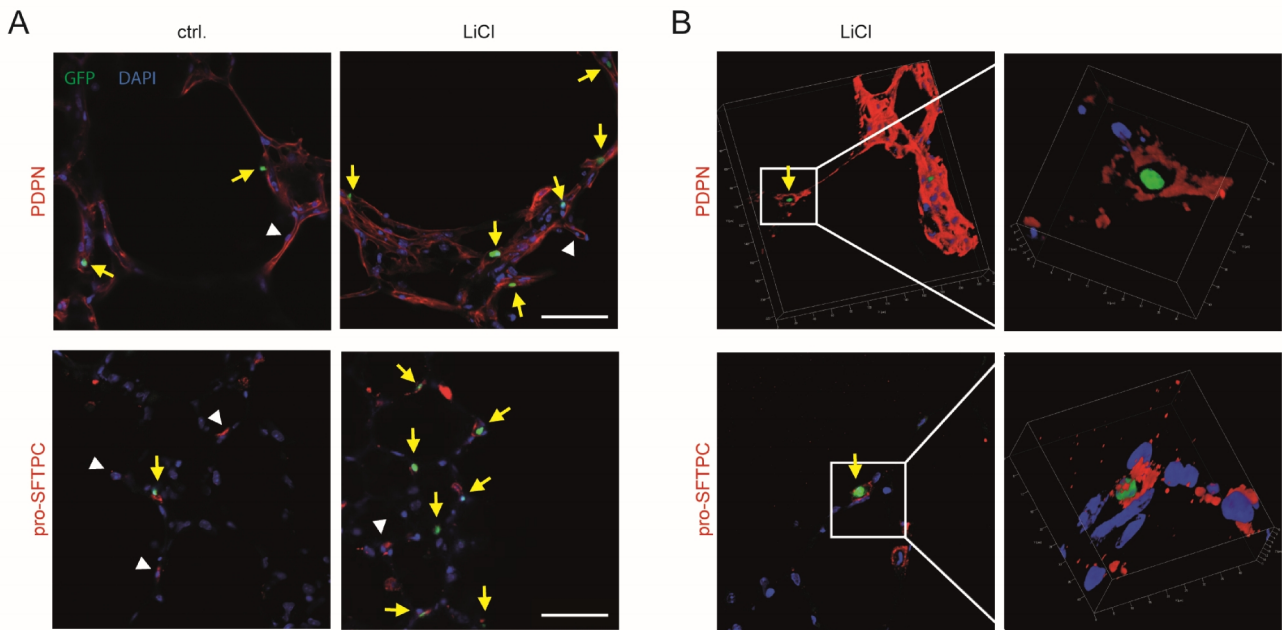


Figure 5.17: Wnt/beta-catenin activated cells expressed markers for ATI as well as ATII cells.

Immunofluorescent labelling of 3D-LTC from emphysematous TCF/LEF-GFP animals for podoplanin (PDPN) and pro-SFTPC after 72 h of treatment with 10 mM LiCl. A) PDPN and pro-SFTPC positive cells are indicated by white arrow heads and double positive (Wnt/beta-catenin activated) cells are indicated by yellow arrows. B) 3D reconstructions of LiCl treated 3D-LTC from emphysematous TCF/LEF-GFP animals. Scale bar 50 μ m.

Further analysis of gene expression of specific markers was conducted to confirm Wnt/beta-catenin activation in ATI as well as ATII cells. LiCl induced no change in the expression of the ATII cell marker *Sftpc* but led to partially differential expression of ATI markers. *Pdpn* was significantly upregulated after 6 and 24 h, *Hopx* was significantly downregulated at 24 h, while *Aqp5* was not significantly changed (Figure 5.18).

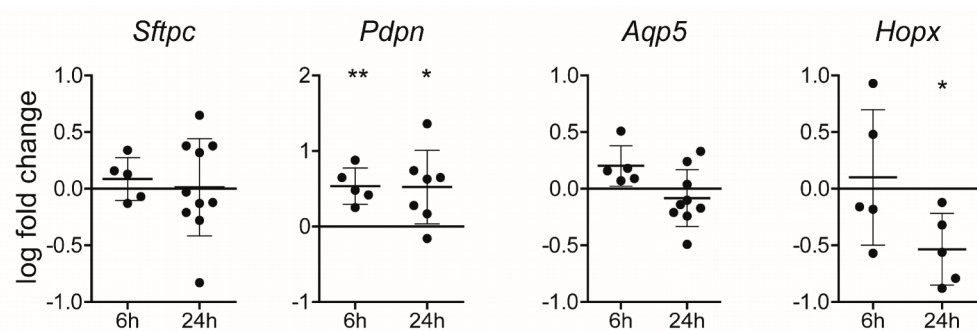


Figure 5.18: Wnt/beta-catenin activation with LiCl did not alter gene expression of the ATII cell marker *Sftpc* while ATI cell markers were differentially expressed in 3D-LTC from emphysematous mice.

Gene expression of ATI and ATII markers in 3D-LTC from emphysematous mice cultivated with 10 mM LiCl. n=5-10.

*: $p < 0.05$, **: $p < 0.01$, one sample t-test compared to hypothetical value 0.

Subsequently, it was analysed whether changes on mRNA level were mirrored on the protein level. For this, a SFPTC ELISA was applied showing no significant alteration in SFPTC expression after LiCl treatment although there was a trend to lower expression (Figure 5.19).

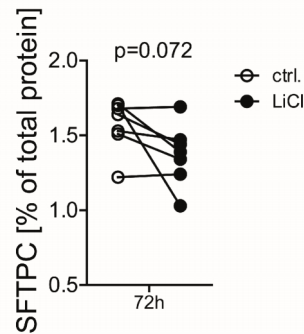


Figure 5.19: Wnt/beta-catenin activation with LiCl did not significantly alter protein expression of SFPTC in 3D-LTC from emphysematous mice.

SFPTC expression in cell lysates of 3D-LTC from emphysematous mice treated for 72 h with 10 mM LiCl was measured via ELISA. n=7. paired t-test.

Protein expression of the ATI markers was analysed via Western Blot. PDPN expression was significantly increased after 72 h of treatment with LiCl while AQP5 and HOPX expression was not significantly altered although HOPX tended to be expressed at lower levels after the treatment which is in accordance to the gene expression data (Figure 5.20).

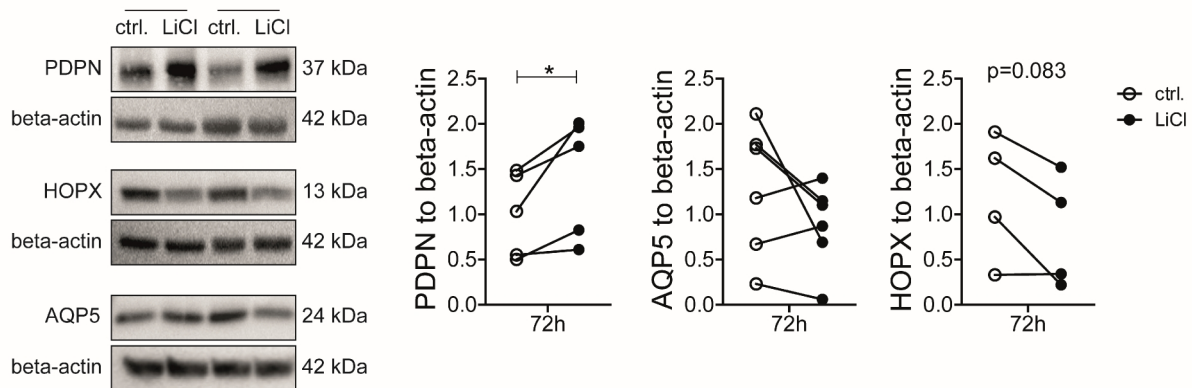


Figure 5.20: Wnt/beta-catenin activation with LiCl leads to differential protein expression of markers for ATI cells 3D-LTC from emphysematous mice.

Podoplanin and HOPX protein expression in 3D-LTC from emphysematous mice treated with 10 mM LiCl for 72 h. left: representative Western Blot, right: densitometry. n=5-6. *: p<0.05, paired t-test.

In summary, the upregulation of Wnt target genes, the increase in ABC protein expression, and the increase in the number of Wnt/beta-catenin-activated cells provide strong evidence, that GSK3 inhibition, using LiCl led to activation of the Wnt/beta-catenin signalling pathway in 3D-LTC from

emphysematous mice. The activated cells were ATI as well as ATII cells and can be tracked with live cell imaging in a spatio-temporal manner.

5.4.3 Effects of Wnt/beta-catenin activation by LiCl in human 3D-LTC

After having proven Wnt/beta-catenin activation in ATI and II cells in 3D-LTC from emphysematous mice, it was further investigated if LiCl can also activate Wnt/beta-catenin signalling in human 3D-LTC and whether there is a difference in the Wnt activation potential of non-COPD and COPD samples. Due to limitation of the available sample material, it was not always possible to have both gene and protein expression data from all patients. Furthermore, there was no significant difference between the protein expression of 3D-LTC from non-COPD and COPD patients. This might be due to the small number of samples (for patient characteristics see Table 4.17). Hence, the results from non-COPD and COPD patients are shown as merged data and no discrimination was conducted, except for the correlation analysis in Figure 5.26.

After analysing Wnt/beta-catenin activation and its effect on epithelial cells in 3D-LTC from emphysematous mice the same experiments were conducted in 3D-LTC from human patients. LiCl treatment led to significant increase of the Wnt target genes *AXIN2* and *NKD1* after 6 and 24 h, respectively, proving Wnt/beta-catenin activation on the transcript level of target genes (Figure 5.21).

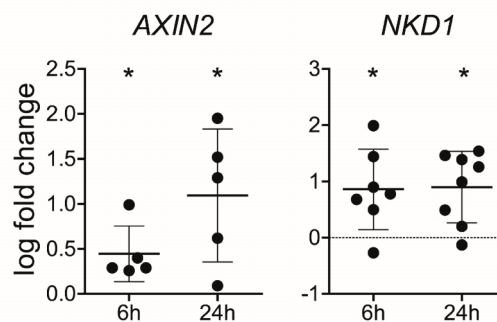


Figure 5.21: Wnt target gene expression is induced in 3D-LTC from human patients with 10 mM LiCl.

Wnt target gene expression in 3D-LTC from human patients cultivated with 10 mM LiCl. n=4-10. *: p<0.05, **: p<0.01, ***: p<0.001, one sample t-test compared to hypothetical value 0.

Next, the activation status of beta-catenin after Wnt pathway modulation was analysed. ABC was significantly upregulated in 3D-LTC from human patients after LiCl treatment for 72 h as well, proving efficient Wnt/beta-catenin activation in these samples by LiCl (Figure 5.22).

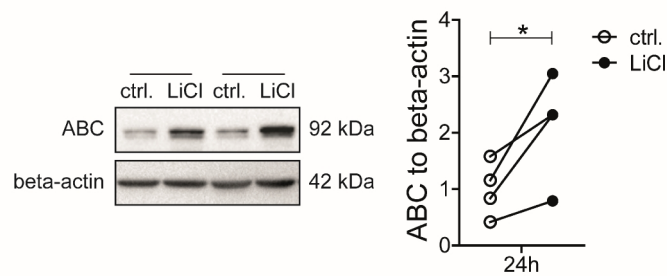


Figure 5.22: Active beta-catenin protein expression is significantly increased in 3D-LTC from human patients with 10 mM LiCl.

ABC protein expression in 3D-LTC from human patients treated with 10 mM LiCl for 24 h. left: representative Western Blot, right: densitometry. n=5. *: p<0.05, paired t-test.

Due to changes of Wnt/beta-catenin signalling in ATI and ATII cells as observed in 3D-LTC from emphysematous animals, it was evaluated if these cell types are also activated in the human 3D-LTC. The effects of Wnt/beta-catenin activation on the transcript level markers for ATI and ATII cells were analysed and are shown in Figure 5.23. Wnt/beta-catenin activation led to a significant increase of the ATII cell marker *SFTPC* which was in contrast to the murine cultures, in which no alteration was seen. The ATI cell markers followed the same expression pattern already shown in the murine cultures. *PDPN* was significantly upregulated over time while *AQP5* expression was not altered. *HOPX* expression was significantly downregulated after 72 h which was seen already earliest after 24 h in the murine samples.

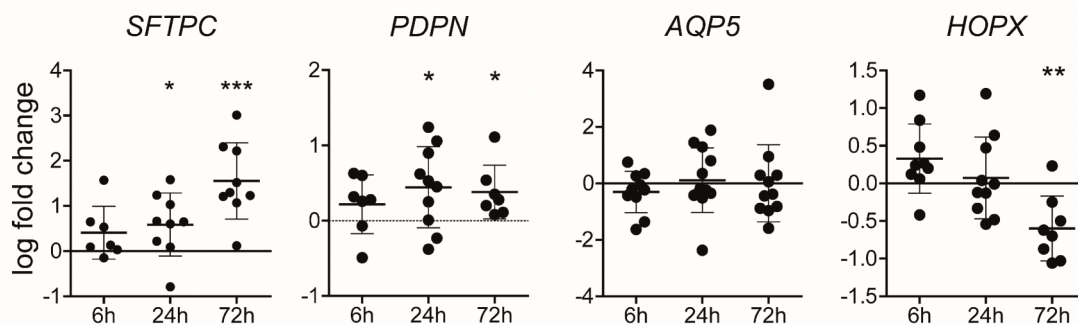


Figure 5.23: Wnt/beta-catenin activation led to differential RNA expression of ATI and ATII cell markers in 3D-LTC from human patients.

Gene expression of ATI and ATII markers in 3D-LTC from human patients cultivated with 10 mM LiCl. n=5-10. *: p<0.05, **: p<0.01, ***: p<0.001 one sample t-test compared to hypothetical value 0.

Expression of ATI and ATII markers was confirmed on protein level. LiCl led to a significant upregulation of *SFTPC* protein expression as analysed by ELISA (Figure 5.24) which is in accordance to its increase on transcript level.

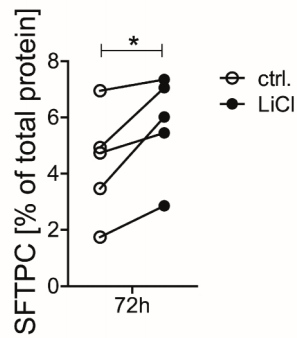


Figure 5.24: SFTPC protein expression was significantly increased by Wnt/beta-catenin activation with LiCl in 3D-LTC from human patients.

SFTPC expression in cell lysate of 3D-LTC from human patients treated for 72 h with 10 mM LiCl was measured via ELISA. n=5. *: p<0.05, paired t-test.

Similar as in 3D-LTC from emphysematous mice, PDPN protein levels were significantly increased while HOPX expression was not significantly altered, but again, showed a trend for downregulation. In contrast to the 3D-LTC from emphysematous mice, AQP5 was significantly downregulated which was contrary to its transcript level suggesting posttranscriptional regulation of AQP5 (Figure 5.25).

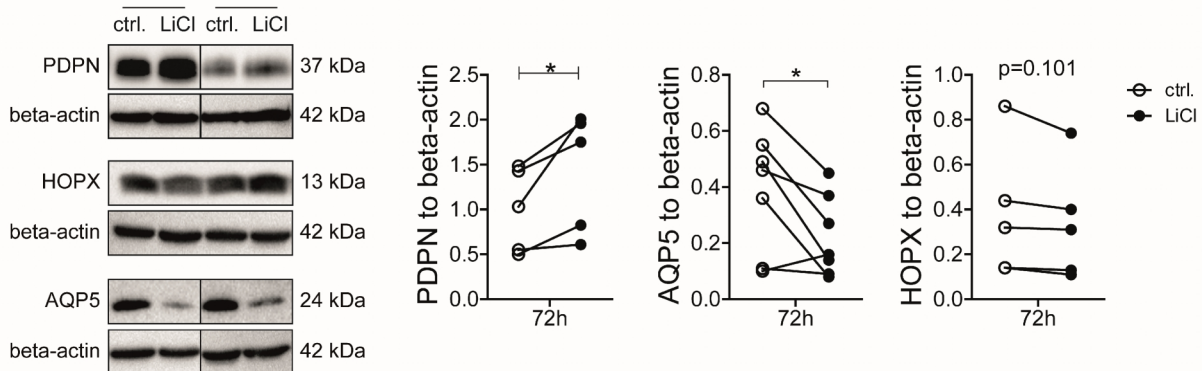


Figure 5.25: Wnt/beta-catenin activation with LiCl led to differential protein expression of markers for ATI cells in 3D-LTC from human patients.

Podoplanin and HOPX protein expression in 3D-LTC from human patients treated with 10 mM LiCl for 72 h. left: representative Western Blot, from 3D-LTC of two representative patients. right: densitometry. n=5-6. *: p<0.05, paired t-test.

Next, *AXIN2* and *SFTPC* gene expression in the 3D-LTC was correlated with disease severity of the respective patients, revealing a significant negative correlation: Inducibility of *AXIN2* and *SFTPC* gene expression was higher in patients with low FEV1/FVC value, as indicative for more severe COPD (Figure 5.26).

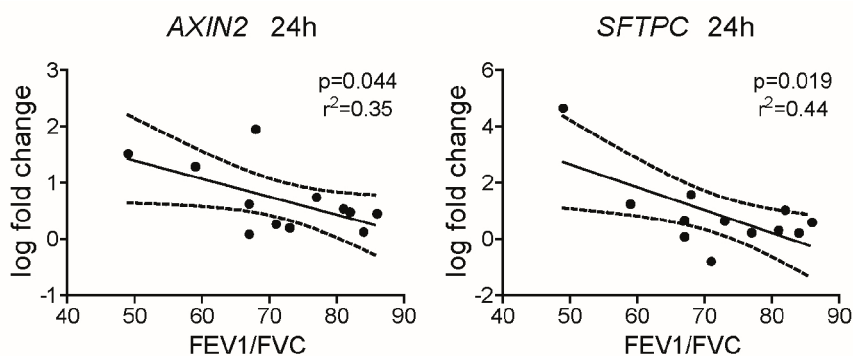


Figure 5.26: *AXIN2* and *SFTPC* induction by LiCl in 3D-LTC from human patients correlates with disease severity.

RNA expression of *AXIN2* and *SFTPC* after LiCl treatment for 24 h was correlated with FEV₁/FVC value of individual patients. n=12. Linear regression. The dashed lines indicate the 95% confidence interval.

Taken together, Wnt/beta-catenin signalling by LiCl was efficiently activated in 3D-LTC from both emphysematous mice and human patients as determined by increased target gene expression, ABC protein expression, and increased number of Wnt/beta-catenin activated cells in 3D-LTC from emphysematous Wnt reporter animals. LiCl treatment led to differential expression of ATI and ATII markers on transcript and protein level. Specific differences were observed in mice compared to human tissues for *SFTPC* expression, which was inducible in the human samples but not altered in the murine ones, and *AQP5*, which was downregulated in the human samples but not altered in the murine ones. Correlation analysis demonstrates the potential of the 3D-LTC from human patients as a predictive tool linking induction of gene expression with disease severity.

5.4.4 Wnt/beta-catenin activation by CT in 3D-LTC

As already mentioned before, Wnt/beta-catenin activation was additionally analysed with a different GSK3 activator, i.e. CT, as a proof of concept study to test novel drugs for therapeutic efficacy using 3D-LTC. First, the non-toxicity of the treatment with 2 μ M CT was determined by WST-1 conversion of 3D-LTC from healthy mice. 10 mM LiCl and 20 mM LiCl were used as additional control treatments. 20 mM LiCl, but not 10 mM LiCl, induced significant differences in WST-1 conversion by day three, proving once again, that 10 mM LiCl was not toxic. Neither 2 μ M CT nor the respective DMSO control led to a reduction in WST-1 conversion giving evidence that both treatments (LiCl and CT) applied to the 3D-LTC used for Wnt/beta-catenin activation were not toxic (Figure 5.27).

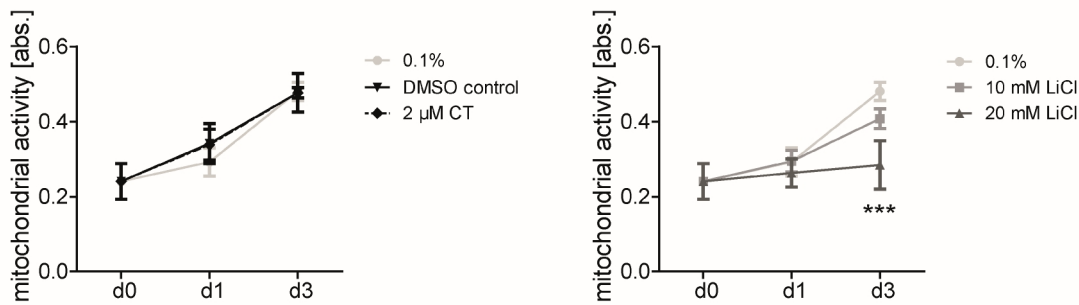


Figure 5.27: 2 μ M CT is not toxic to 3D-LTC from healthy mice.

WST-1 conversion of the cells in 3D-LTC from healthy mice cultivated with 10 mM LiCl, 20 mM LiCl, 2 μ M CT, and DMSO control. For better visualisation, the treatments were depicted in separate graphs. $n=4$. *: $p<0.05$, **: $p<0.01$, ***: $p<0.001$ compared to control treatment (0.1% FCS cultivation medium), one way ANOVA with Bonferroni post-test.

After excluding toxicity of the treatment, the small molecule CT was used in 3D-LTC from both emphysematous mice and human patients for proof of concept experiments of Wnt/beta-catenin activation. *Axin2* was significantly upregulated after CT treatment in the murine as well as human cultures after 6 and 24 h while *Dkk2* and *NKD1* were significantly upregulated after 24 h (Figure 5.28, Figure 5.29). These results confirmed that Wnt/beta-catenin activation can be induced in 3D-LTC from emphysematous mice as well as human patients on transcript level by CT treatment.

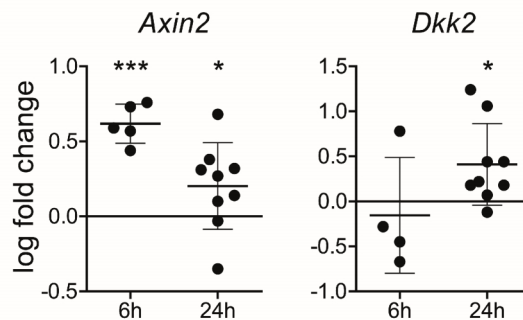


Figure 5.28: Wnt target gene expression was induced in 3D-LTC from emphysematous mice with 2 μ M CT.

Wnt target gene expression in 3D-LTC from emphysematous mice cultivated with 2 μ M CT. $n=4-9$. *: $p<0.05$, **: $p<0.01$, ***: $p<0.001$, one sample t-test.

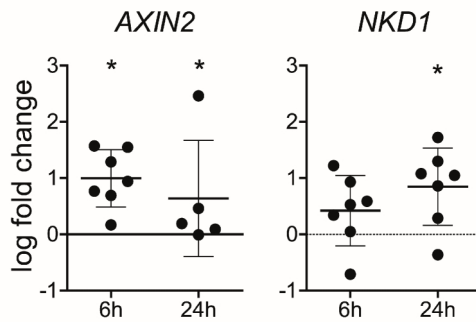


Figure 5.29: Wnt target gene expression was induced in 3D-LTC from human patients with 2 μ M CT.

Wnt target gene expression in 3D-LTC from human patients cultivated with 2 μ M CT. n=5-7. *: p<0.05, one sample t-test compared.

As shown in Figure 5.30 and Figure 5.31 ABC protein levels were significantly upregulated in both species after CT treatment for 24 h. Both the upregulation of Wnt target genes and increased expression of ABC provided evidence, that CT is able to induce Wnt/beta-catenin signalling in 3D-LTC similar to LiCl and can be applied as alternative drug in the model.

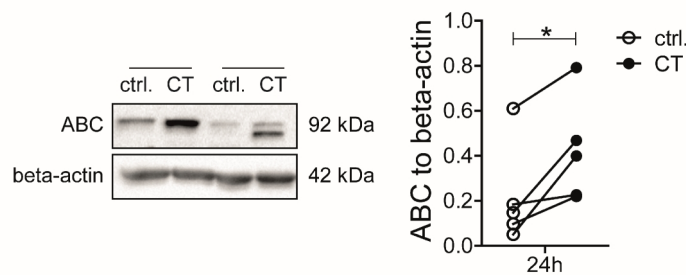


Figure 5.30: Active beta-catenin protein expression was significantly increased in the 3D-LTC from emphysematous mice with 2 μ M CT.

ABC protein expression in 3D-LTC from emphysematous mice treated with 2 μ M CT for 24 h. left: representative Western Blot from lung slices of two representative emphysematous mice. right: densitometry. n=5. *: p<0.05, paired t-test.

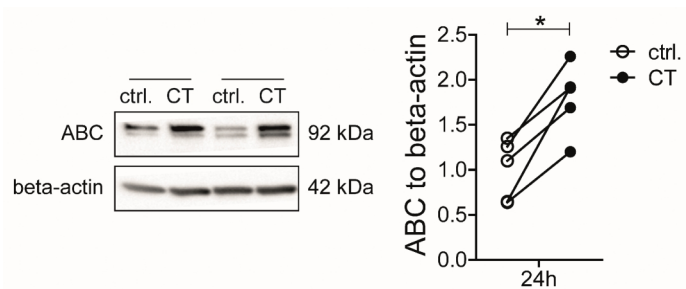


Figure 5.31: Active beta-catenin protein expression was significantly increased in the 3D-LTC from human patients with 2 μ M CT.

ABC protein expression in 3D-LTC from human patients treated with 2 μ M CT for 24 h. left: representative Western Blot from lung slices of two representative human patients. right: densitometry. n=5. *: p<0.05, paired t-test.

5.5 TGF-beta activation in 3D-LTC

TGF-beta is known to be involved in the development and progression of various diseases including COPD and lung cancer [Massague, 2008]. TGF-beta has been shown to be oncogenic and induce epithelial-to-mesenchymal transition (EMT) [Massague, 2008, Thiery, et.al., 2006]. For this, TGF-beta treatment was used as a further proof of concept study in order to evaluate the potential of 3D-LTC that different signalling pathways can be modulated in 3D-LTC. As done before, 10 mM LiCl, 2 μ M CT, and the DMSO-control were included into the WST-1 assay, to prove assay functionality and reliability (see Figure 5.27). TGF-beta did not induce cellular toxicity in 3D-LTC (Figure 5.32).

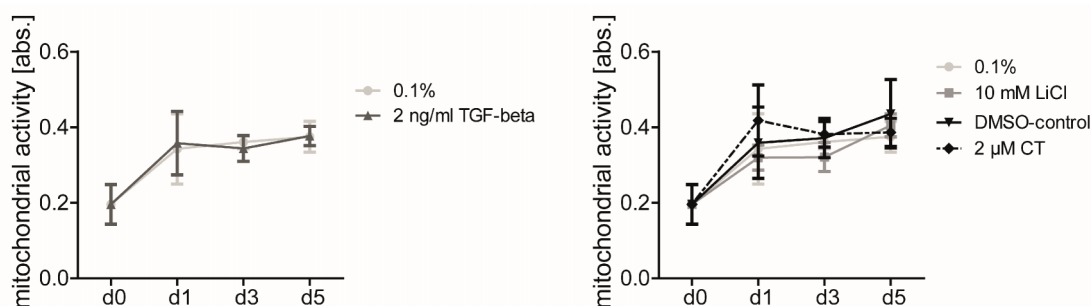


Figure 5.32: TGF-beta is not toxic to 3D-LTC from healthy mice.

WST-1 conversion of the cells in 3D-LTC from healthy mice cultivated with 10 mM LiCl, 2 ng/ml TGF-beta, 2 μ M CT, and DMSO-control. For better visualisation, the treatments are depicted in separate graphs. n=4. One way ANOVA with Bonferroni post-test.

Next, TGF-beta activation was analysed by detecting phosphorylated SMAD3 using Western Blot analysis. Indeed, TGF-beta treatment induced SMAD3 phosphorylation in 3D-LTC from human patients as shown by an increase in the ratio of phosphorylated SMAD3 to total SMAD2/3 (Figure 5.33).

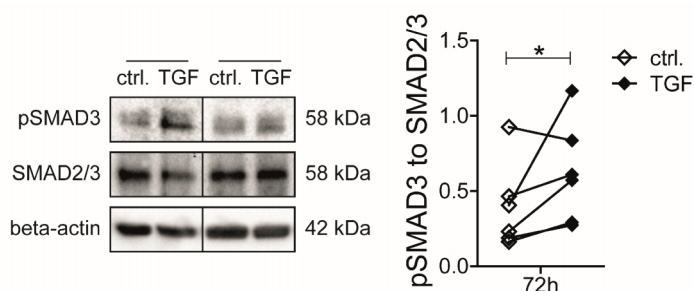


Figure 5.33: TGF-beta treatment leads to induction of SMAD3 phosphorylation in 3D-LTC from human patients.

Phosphorylated SMAD3 (pSMAD3) and total SMAD2/3 protein expression in 3D-LTC from human patients after 72 h of treatment with 2 ng/ml TGF-beta. left: representative Western Blot, right: densitometry. n=6. *: p<0.05, paired t-test.

In addition, several TGF-beta target genes were upregulated by TGF-beta treatment of human 3D-LTC such as *PAI1* and smooth muscle actin (*ACTA2*), a (myo)-fibroblast marker, as well as the ECM

protein *COL1A1* after 24 and 72 h respectively, giving further evidence of TGF-beta pathway activation. In addition, the transcription factors *SNAI1* and *SNAI2*, which have been implicated in EMT, were significantly increased in the human 3D-LTC (Figure 5.34).

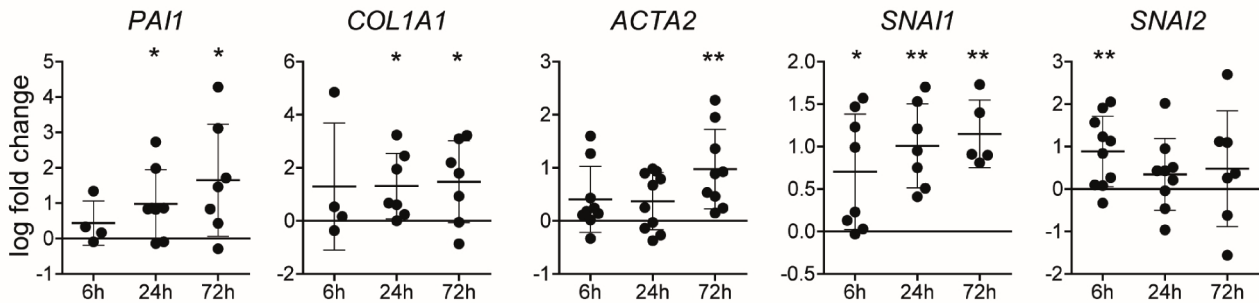


Figure 5.34: TGF-beta treatments leads to increased expression of target genes, (myo)-fibroblast markers, and transcription factor involved in EMT in 3D-LTC from human patients.

Gene expression in 3D-LTC from human patients after different times of treatment with 2 ng/ml TGF-beta. n=4-10. *: p<0.05, **: p<0.01, paired t-test.

Immunofluorescence staining of smooth muscle actin and collagen I of 3D-LTC from both healthy mice and human patients showed increased staining in alveolar epithelial cell regions (Figure 5.35).

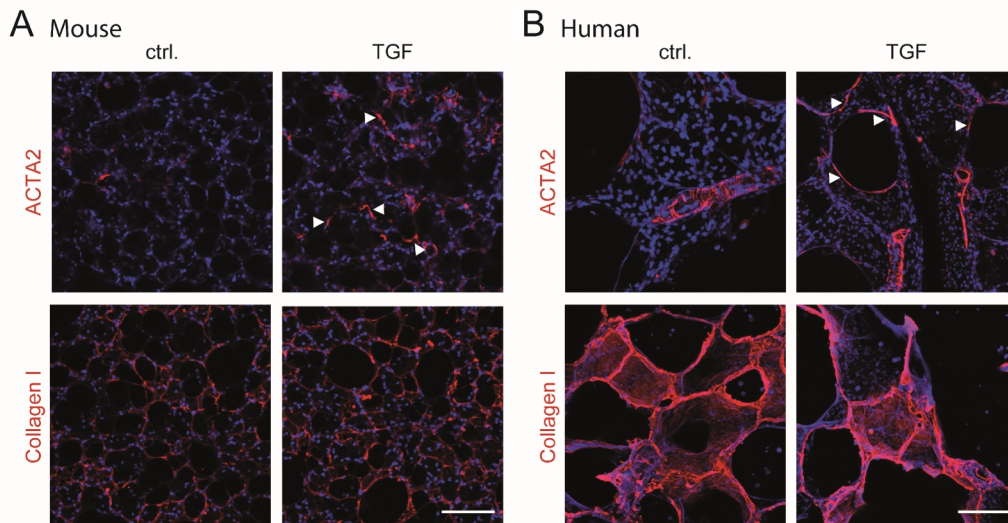


Figure 5.35: Alveolar expression of smooth muscle actin (ACTA2) is induced by TGF beta treatment in 3D-LTC from healthy mice and human patients.

Immunofluorescence staining of smooth muscle actin (ACTA2) and collagen I in 3D-LTC from A) healthy animals and B) human patients after different times of treatment with 5 ng/ml TGF-beta. Arrow heads point to smooth muscle actin stained cells in alveolar regions due to TGF-beta treatment. Scale bars 100 μ m.

Taken together, the increase in target gene expression and factors involved in EMT demonstrate successful modulation of TGF-beta signalling and induction of disease relevant alterations in 3D-LTC from both healthy animals and human patients.

6 DISCUSSION

COPD is a progressive disease with no curative treatment options for aging patients (>50 y). Wnt/beta-catenin signalling is known to be downregulated in COPD and re-activation of this pathway has been shown to attenuate experimental emphysema in a mouse model of elastase-induced emphysema [Kneidinger, et.al., 2011, Wang, et.al., 2011]. The exact mechanism(s) underlying this disease are currently unknown. Furthermore, pharmacological interventions shown to be effective in animal models still bear a high risk of failure in clinical trials [Malaney, et.al., 2014, Miller, et.al., 2011]. This makes the development of novel test systems and animal models for preclinical drug testing and pathway modulation studies important. In this work, the application of a 3D-LTC model for preclinical testing and analysis of molecular mechanisms was established and validated.

In the literature, precision cut lung slices (PCLS), are mainly used for pharmacological studies and only short periods of time (24-72 h) [Liberati, et.al., 2010, Sanderson, 2011]. Up to now, a detailed characterization of this model has not been conducted. This is a significant difference to the method of 3D-LTC presented in this work, in which cultivation was prolonged to seven days. By successful adaptation of the 3D-LTC to human samples, clinically more relevant results were obtained. Reactivation of the signalling pathways Wnt/beta-catenin and TGF-beta provided proof of evidence for translational application and suitability of this model for preclinical drug testing and personalized medicine.

6.1 Characterisation of 3D-LTC

6.1.1 Influence of the process of slice generation

3D-LTC from murine and human lung tissue had sustained ciliary beating and leucocytes maintained motility in the tissue during cultivation. Cells remained viable, as assessed by Live/Dead assay and mitochondrial activity, significantly increased from day one to three, and remained stable thereafter. Proliferation peaked at day three and was enhanced by usage of a higher amount of FCS (10%). Thereby, 3D-LTC remained viable for a cultivation period of at least seven days (see 5.1). This is a significant improvement to the cultivation of lung slices reported by Henjakovic *et al.* who showed major cell death and nuclear degeneration in PCLS from rat tissue by 72 h [Henjakovic, et.al., 2008]. The main differences between their study and this work were: 1) the method of slice fabrication (Krumdieck tissue slicer vs. vibratome), 2) the agarose concentration for the infiltration (1.5 vs. 2%), 3) slice thickness (200 vs. 300 μm), 4) immersion medium utilized during slice generation (Earl's balanced salt solution vs. cultivation medium DMEM/F12 without FCS), 5) an additional washing step for 2 h in DMEM before cultivation done by Henjakovic *et al.*, and 6) the medium during experimental cultivation (no FCS vs. 0.1%/10% FCS). The thickness and concentration of agarose was more or less comparable between the previous and current method —being 200 vs. 300 μm and 1.5 vs. 2%, respectively— therefore,

differences in diffusion limitations can be excluded as a reason for the observed differences in the early onset of cell death. One significant methodological difference is that while Henjakovic and co-workers used the rather harsh method of tissue slicing with the Krumdieck device, a more delicate method of cutting using a vibratome was applied for the generation of the 3D-LTC in this work. While slices were not washed before cultivation in this thesis, the additional washing step does not seem to influence cell viability, since the slices from Henjakovic contained hardly any dead cells at early time points. They commented on addition of FCS in concentrations of 1%, 3%, and 10%, which led to increased cellular survival. Unfortunately, this data was not included into the manuscript, thus making it difficult to draw a conclusion regarding the length of this increased cellular survival. Even though a rather low concentration of 0.1% FCS was used for 3D-LTC in this work, it possibly explains the difference in viability seen. Lastly, the method of slice generation used by Henjakovic may have induced cellular damage, which materialized at a later time point. Slicing with the Krumdieck device requires applying pressure on top of the tissue cores during slicing. This may induce pressure-induced injury, which is lacking in the case of the vibratome where the tissue is glued onto a holder without compressing and further injuring the tissue.

6.1.2 Influence of the slice thickness and tissue density

The most similar study in comparison to the current work is from Vaira and colleagues [Vaira, et.al., 2010]. Slices (300-500 μm) were generated from human cancer tissues (colon, prostate, and lung) using a vibratome as well, and cultivated with Ham's F12 medium supplemented with 20% FCS and kanamycin. The MTT assay (a similar assay to WST-1 also utilizing a tetrazolium salt for measuring mitochondrial activity) was used to determine cell viability. Although it did not reach statistical significance, Vaira *et al.* observed a decrease in cell viability (~40-50%) on day three, five, and seven [Vaira, et.al., 2010]. These results are in contrast to the sustained and even increasing WST-1 conversion seen over the seven days of cultivation in the 3D-LTC described in this thesis. A possible explanation for this is the tissue composition itself. As cancer tissue is more dense than healthy tissue, the thickness of the slices (300-500 μm) may have led to limitations in nutrient supply and oxygenation, especially in the middle of the tissue. Cells inside the human body are not more than 100-200 μm apart from a capillary due to diffusion limits [Jain, et.al., 2005, Lovett, et.al., 2009, Rouwkema, et.al., 2008]. Furthermore, in tissue grown *in vitro* and re-implanted into the body, cells inside the re-implanted piece of tissue only survive within this same distance range from capillaries [Jain, et.al., 2005, Lovett, et.al., 2009, Rouwkema, et.al., 2008]. Cells farther away die within a short time frame and lead to inflammation which may have been the case in the cancer slices described by Vaira and colleagues [Vaira, et.al., 2010]. Liver slices of the same thickness described by Vaira (500 μm) showed severe necrosis in the central area [Olinga, et.al., 1997]. Vaira and colleagues showed a non-significant but decreasing trend in proliferation with quantification of Ki67 staining being ~60% on day seven [Vaira, et.al., 2010]. Cells in the later time points staining positive for Ki67 were mostly restricted to the marginal areas of the slices and absent in the middle. This is in agreement with the hypothesis, that cells in the middle are facing

sub-optimal nutritional supply and oxygenation due to slice thickness and do not proliferate anymore. Interestingly, no significant increase in TUNEL staining was described suggesting that cells did not become apoptotic/necrotic. In general the data is difficult to interpret as the results varied between the different organs (colon, prostate, and lung) and patients, with some of them showing opposite kinetics for both Ki67 staining and TUNEL assay [Vaira, et.al., 2010]. In stark contrast, the 3D-LTC generated in this thesis do not exceed the passive diffusion limit since lung tissue has a lower tissue density per volume compared to cancer and cells never face a distance of more than a few micro meters to the next open airspace or alveoli where fresh, oxygenated medium is available. This suggests that limitations were not of concern in the 3D-LTC.

A variety of methods have been utilized to assess slice viability. Umachandran *et al.* reported a time-dependant increase in LDH release (~ 50%) from rat lung slices within the first 24 h which remained unchanged at later time points (48 and 72 h) [Umachandran, et.al., 2004]. Histological assessment using H&E staining of paraffin-embedded slices did not show correlative loss of tissue architecture or nuclear degeneration within the first 12 h but for incubations of 24 h and longer [Umachandran, et.al., 2004]. In this study the authors analysed the effects of slice thickness on metabolic activity (exemplified by the metabolism of 7-ethoxycoumarin). Optimal thickness was determined to be 600 µm (tested 420-700 µm) and thus thicker than the 3D-LTC used in this work. Slices were metabolic active for only 8 h compared to the prolonged mitochondrial activity until day seven shown in this study. Usage of the Krumdieck tissue slicer additional to the higher thickness might explain this short period of metabolic activity.

Next to metabolic activity, slice thickness is influencing cell viability. Due to the slicing of the tissue, cells at the margins are injured and die as indicated by Live/Dead staining (Figure 5.5 and Figure 5.8). As dying cells secrete cytokines and cellular debris is left behind, this will possibly influence the intact tissue function in 3D-LTC. The thicker the slice, the lower this influence will be. Optimisation of slice thickness in this regard was not conducted and not an aim of this thesis. A future study should determine the optimal thickness of the slices comparing the reduced negative effects of the dead cells at slice margins and their paracrine signalling (thick slices beneficial) with the diffusion limitations for oxygen and nutrients (thin slices beneficial) [Liberati, et.al., 2010, Sanderson, 2011, Umachandran, et.al., 2004]. Nonetheless, it was assumed that cellular death at the tissue margins did not have a major effect on the subsequent cultivation of the 3D-LTC in this thesis, because the medium was changed before the pharmacological treatments started, thereby removing dead cells, cellular debris, and cytokines secreted from dying cells.

In summary, the generation of 3D-LTC by the method of vibratome sectioning led to viable cultures for up to seven days, thereby showing improvement as compared to slice cultivation protocols reported by other groups [Henjakovic, et.al., 2008, Umachandran, et.al., 2004, Vaira, et.al., 2010]. Significantly increased proliferation was observed on day three by using 10% FCS cultivation medium (see Figure 5.3), an effect, that was not reported up to now since most studies showed a rather decreasing cell proliferation over time. The adaptations of the method for slice generation by using a vibratome in this thesis and the subsequent gentle handling of the delicate slices

prolonged cell viability up to seven days. Nonetheless, cultivation of the 3D-LTC for longer periods and analysis at late time points (day seven and later) might not lead to reliable results anymore. The drop in proliferation after day three may be due to the inability of the cells to maintain their activation status, which is supported by the decrease in intensity of the Live staining on day five and the stable and not further increasing WST-1 conversion. Cells might switch to a state, where cellular function is just maintained but no tissue repair can be induced anymore. Sanderson stated: “In general, lung slice viability appears to be excellent for 1 to 3 days” [Sanderson, 2011]. The results from the viability and proliferation analysis in this work are in accordance with this notion. All pathway modulation studies were conducted only up to three days to assure reliability of cellular responses in the 3D-LTC. This issue should be addressed in further studies starting treatments at a later time point after slice generation to gain knowledge if cells are still responsive after pre-cultivation of the 3D-LTC.

6.1.3 Influence of the cultivation medium and culture conditions

Different cultivation media and variations in FCS concentrations influence cellular behaviour regarding viability and proliferation (see 5.1). Moreover, medium composition alters cellular metabolism, growth rate, and can favour the selective growth of certain cell types [Geys, et.al., 2007, Rehberg, et.al., 2014]. Liberati *et al.* reported on the different cell cultivation media used for slice cultivation [Liberati, et.al., 2010]. The medium used in this work (DMEM/F12) was described previously to support cell viability [Liberati, et.al., 2010].

It was stated by Liberati and colleagues that no FCS in the cultivation medium avoids “potential confounding influence of serum components on tissue reactions” [Liberati, et.al., 2010]. Furthermore, Sanderson claimed that only sustaining cultivation media are needed and FCS supplementation is not required to maintain slices viable [Sanderson, 2011]. This is in accordance with the finding, that proliferation could be increased with higher amounts of FCS. A comparison to media containing no FCS was not conducted in this thesis. The study from Delmotte *et al.*, who also observed ciliary beating, revealed no differences when the experiments were conducted in serum-free cultivation medium or medium supplemented with 10% FCS [Delmotte, et.al., 2006]. Accordingly, it was shown here that regarding mitochondrial activity the FCS content is not relevant, while a higher FCS content in the cultivation medium is beneficial for the rate of cell proliferation (see 5.1). A detailed comparative study for optimising medium formulations to cultivate 3D-LTC has not yet been performed and will be critical in a future study. A standardized medium formulation for 3D-LTC may be idealised as supporting viability and non-selective growth in all cell types. The aspect of oxygen concentration should be addressed in such a comparative study as well. This might overcome limitations of oxygenation in the middle of dense tissue cultures but needs to be carefully evaluated, since high oxygen concentration are potentially harmful.

Taken together, the medium used for cultivation of the 3D-LTC and the FCS content of 0.1% was suitable to keep cells viable. Cells in the middle of 3D-LTC were able to proliferate and react to pathway specific treatments.

6.1.4 Influence of the cultivation technique

In this work, 3D-LTC were cultivated under submerged conditions in well plates. Nonetheless, there are other cultivation systems available as well. Some groups cultivate the slices on Transwell inserts to apply an air-liquid interface to them [Vaira, et.al., 2010]. One group compared five different incubation systems for rat liver slice cultivation over 24 h: a shaken flask (an Erlenmeyer in a shaking water bath), a stirred-well (24-well culture plate equipped with grids and magnetic stirrers), a rocker platform (6-well culture plate with Netwell insert rocked on a platform), a roller system (dynamic organ culture rolled on an insert in a glass vial), and a 6-well shaker (6-well culture plate in a shaking water bath) [Olinga, et.al., 1997]. While they observed no difference during short time cultivation, after 24 h the shaken flask, the rocker platform, and the 6-well shaker incubation systems were superior to the others regarding morphology, viability, LDH leakage, restoration of testosterone metabolism, Phase I metabolism, and restoration and maintenance of energy charge. Slices kept in the stirred-well cultivation system performed badly and were not able to sustain cell viability up to 24 h. The authors suggested, that alternating exposure of the slices to air and medium are beneficial as was shown before [Smith, et.al., 1985]. Direct comparisons are limited, since in this thesis no stirring was applied to the 3D-LTC. Further, liver tissue is more dense than lung tissue and is more susceptible to nutrient and oxygen shortage. According to Sanderson however, the immersion of the slices in cultivation medium is sufficient to maintain cell viability [Sanderson, 2011]. For this reason, no stirring of the medium or perfusion of the 3D-LTC was necessary to maintain viability. In a study by Ghaedi and colleagues, ATII cells generated from induced pluripotent stem cells (iPS) were cultivated in a rotating bioreactor system exposing the cells to air/liquid conditions. This cultivation was shown to be beneficial regarding ATII to ATI trans-differentiation making the application of small molecules to inhibit the Wnt/beta-catenin pathway unnecessary [Ghaedi, et.al., 2014].

In conclusion, an optimized cultivation technique (e.g. perfusion cultivation or inclusion of alternating air-liquid contact) may additionally enhance cell viability and long-term cultivation of 3D-LTC. Future studies are needed to clarify the experimental parameters, which can be controlled to maximize the potential of 3D-LTC and are beneficial to induce specific cellular differentiation.

6.1.5 Benefits and limitations of the 3D-LTC

The benefits of the method of 3D-LTC established in this thesis are: the viability and capability of the cells to proliferate during cultivation (due to the freshness and quality of the starting material), the reduction of animal numbers and human sample material needed to conduct studies, the

similarity to the *in vivo* environment, the broad range of applications, and the translation to other tissues/organs and diseases.

6.1.5.1 *Biosample preparation*

The “quality” of an organ influences its suitability for the 3D-LTC technique [Vickers, et.al., 2005]. The shorter the time after explantation until experiments are conducted, the more reliable the results will be. It is already known from organ transplantation that a short ischemia time is beneficial [Souidi, et.al., 2013, Weyker, et.al., 2013]. In this work, the slices were generated from fresh tissue. Mice were sacrificed and slices generated directly afterwards, being available for treatments within one hour. The human 3D-LTC were similar. Due to the more complex procedure and the longer gelling-time, these were available for treatments after three to four hours after explantation. Therefore, it is supposed that the quality of the tissue was excellent and variations between different batches of 3D-LTC were small. This was crucial for the prolongation of cellular viability and proliferative capacity over the cultivation period.

6.1.5.2 *Reduction in sample material*

With the optimized protocol of 3D-LTC described here, cells stayed proliferative and were kept in their natural environment, making a broad range of preclinical applications possible, such as live cell imaging, cell tracking, pathway modulation, and mechanistic studies. For gene expression analysis over time, a comparison of the different lobes (different regions) of the lung, from which the slices were generated, was conducted. Slices were pooled from different regions of one lobe (to obtain enough material for RNA isolation) and gene expression was compared to the other lobes. No inter-lobar differences were seen in 3D-LTC from healthy animals (data not shown). It was suggested by Sanderson, that slices should be taken from different lung regions, in order to not bias the final findings [Sanderson, 2011]. This may not be necessary in non-treated, healthy animals, where less regional differences are observed. The composition of the tissue, regarding the amount of alveoli was heterogeneous for both emphysematous animals and human samples depending on the region that was used for slicing. To not bias findings due to emphysema heterogeneity, serial slices were used for the different treatments. By this, it was assured that control and treated slices originated from a similar region and differences observed were due to the specific treatment. This is another benefit from the technique of 3D-LTC. Slices from one sample can be used for control and treatment, overcoming the issue of inter-individual variances. Furthermore, different methods, such as viability testing, morphological analysis, gene and protein expression, and live cell imaging can be conducted from one sample, thereby again reducing inter-individual variances and making results more robust and reliable. Consequently, the amount of samples necessary for a study is reduced as well. Less animals and patient material is required, decreasing the number of animals needed and making repetitive sampling unnecessary.

6.1.5.3 *Natural environment and cellular composition in 3D*

There are distinct and striking advantages for using 3D-LTC. The three-dimensional structure of the tissue and the cells generally remain intact whereas cell isolation procedures and subsequent culture likely influences cellular behaviour. Physical contact and paracrine signalling with various different neighbour cell types is retained leaving the cells in a more physiological environment similar to the *in vivo* situation. For that reason, it is possible to conduct cellular interaction studies, which is limited in normal *in vitro* single cell cultivation settings.

Cellular composition, meaning the ratio of different cell types to each other, is the same as *in vivo*, which is almost impossible to recapitulate *in vitro* by co-cultivation systems. Every additional cell type adds complexity for interpretation. This is why co-culture systems are normally restricted to two or three different cell types resembling the main components of the organ/site of tissue studied. For the lung for example, an application called “lung on a chip” was established using human alveolar epithelial cells and microvascular endothelial cells to reconstruct the alveolar-capillary barrier on an artificial, thin, porous, and flexible PDMS membrane [Huh, et.al., 2010]. In theory more complex cell compositions can be used as well but one of the benefits of the 3D-LTC is the aforementioned natural environment, i.e. cellular matrix, the cells are facing. If cells are placed in tissue culture wells or plates, the composition and mechanical properties of the matrix they are confronted with are dramatically different from their *in vivo* microenvironment. Tissue culture plastic is very stiff (~3GPa), and even if coated with extra cellular matrix (ECM) components, it does not reflect the natural tissue stiffness (~1kPa for the alveolus) [Discher, et.al., 2005, Yang, et.al., 2014]. An alternative current approach to generate *in vivo*-like three-dimensional environments utilizes decellularising tissue with retaining ECM composition and recellularising with one or more cell types. Cellular behavior and in particular the role of the ECM for cellular function and cell fate decisions could be investigated by this [Bonvillain, et.al., 2012, Booth, et.al., 2012, Ghaedi, et.al., 2013, Gilpin, et.al., 2014, Sokocevic, et.al., 2013, Wagner, et.al., 2014].

6.1.5.4 *Applications of 3D-LTC*

3D-LTC can furthermore be used for various applications such as high-resolution 4D live imaging. Internal organs are usually not easily accessible for imaging due to imaging artefacts produced by the surrounding tissue. 3D-LTC are overcoming this problem, being directly accessible. Therefore, cellular behaviour and cellular pathways can be studied by *ex vivo* cultivation of 3D-LTC in real-time. This provides a permissible experimental setup to analyse all the components involved in endogenous tissue repair (discussed in 3.2.1.4) and was shown in this work (Figure 5.1, Figure 5.2, and Figure 5.16). Live cell imaging of 3D-LTC has not been used extensively in prior studies. Most researchers studying broncho-dilation/-constriction used standard transmission light microscopy, owing to the fact that high resolution in the z-direction and labelling of specific cell types is not necessary for determination of changes in bronchial diameter [Khan, et.al., 2007, Martin, et.al., 1996, Seehase, et.al., 2011, Sturton, et.al., 2008]. Live cell imaging using

immunofluorescence staining was previously applied successfully to lung slices by de Proost *et al.* who imaged neuroepithelial bodies and their accompanying Clara cells after stimulation with 50 mM potassium ions. Their experiments were only carried out until 12 h after animal sacrifice, since this was the longest time point without significant cell death [De Proost, et.al., 2008]. Imaging mainly focused on Ca²⁺-signalling, but did not include cell tracking. Ca²⁺-signalling is a fast process and is imaged within minutes, making long-term cultivation and prolonged cellular viability not a main prerequisite for the analysis. Another study successfully applied live cell imaging to study ciliary beat function [Delmotte, et.al., 2006]. In this study, cells were imaged for only short periods (on the scale of minutes) as well. The first published work on confocal imaging in lung slices was conducted by Zhou and colleagues who induced local epithelial cell damage by a laser beam and imaged Ca²⁺-signalling and airway contractions [Zhou, et.al., 2012]. The extension of the live cell imaging to periods of up to 48 h described in this work is an improvement to the studies done so far and gives evidence that cells can be tracked in 3D over time. With this, the method of 3D-LTC is applicable to the whole range of genetically modified and lineage tracing/reporter animals illustrating the remarkable value for the scientific community.

Additional applications described in the literature include the use of vibratome slices from rat lung tissue to apply the patch clamp technique on single ATI cells to study their implication in ion and fluid balance over a period of 8 h [Bourke, et.al., 2005]. This study proves that the patch clamp technique in combination with live cell imaging can be applied to 3D-LTC. Furthermore, distention studies combined with live cell imaging were conducted [Dassow, et.al., 2010, Davidovich, et.al., 2013] giving evidence, that 3D-LTC can be used to analyse ventilator induced injury and by this proving its applicability to study various diseases. This further shows the broad range of applications the 3D-LTC can be used for.

6.1.5.5 *Translation to other animal models, organs, and diseases*

Similarly, animals from other disease models can be used to generate 3D-LTC. To alternatively model COPD for instance, cigarette smoke can be applied to mice as main stream as well as side stream smoke to simulate not only active but also passive smoking [John, et.al., 2014]. In contrast to the instillation of elastase, the cigarette smoke exposure animal model recapitulates both main features of COPD seen in humans, including airway remodelling as well [Antunes, et.al., 2011]. Although it takes several months (approximately three to six months) of smoke exposure to develop emphysema and the severity of the disease can only be compared to GOLD stage I and II in humans [Churg, et.al., 2007] it would be of interest to include 3D-LTC from cigarette smoke exposed mice to validate the findings described in this work with another animal model.

As mentioned before, the technique of 3D-LTC is already applied to various organs, such as brain, heart, liver, kidney, and lung [Liberati, et.al., 2010, Sanderson, 2011]. This is beneficial for preclinical testing. A candidate drug, shown to be effective in a certain organ can be tested for toxicity of its application route, without the need for testing it directly in the whole animal. Drugs are usually applied *intra venous* or ingested and thereby enter the blood circulation. The first

organs affected are the liver and kidneys. 3D-LTC from both organs, tested in parallel to the candidate drug, can give hints for the anticipated pharmacologic/toxic *in vivo* response. For the lung, this may be of minor importance since the accessibility of the injured areas via inhalation in part overcomes drug delivery via the circulation.

Furthermore, not only COPD and cancer can be studied by using the method of 3D *ex vivo* tissue cultivation. With slight adaptations, it can be applied to study any other lung disease, such as fibrosis, as well.

6.1.5.6 Limitations

A drawback of precision cut tissue slices may be the lack of the immune system and stem cell supply after explantation and generation of the 3D-LTC. There is no connection to the blood system anymore, therefore, no inflammatory or progenitor cells can migrate from the body into the slice. Effects studied with the model of 3D-LTC may therefore not exactly resemble the *in vivo* situation. Nevertheless, this may also be an advantage for studies where the effect of specific exogenous added stem/progenitor or inflammatory cells is analysed.

A further limitation is the lack of the air liquid interface inside the alveoli by usage of a submerged cultivation. Although some groups use tissue culture inserts to keep the slices at an air liquid interface, a benefit from that is not proven up to now and needs further evaluation [Olinga, et.al., 1997, Vaira, et.al., 2010].

The benefit of complexity of the tissue composition in 3D-LTC adds another drawback. Due to this, interpretation of results is difficult since different cell types may react opposite to a certain treatment.

The lung is constantly stretched and recoiled by the action of breathing. The natural occurring mechanical stimulation of the cells thereby is difficult to recapitulate within the 3D-LTC *in vitro*. One group developed a bioreactor to bi-axially stretch the slices [Dassow, et.al., 2010]. Stretching the 3D-LTC might be important for surfactant production, since ATII cells react to mechanical stress with upregulation and increased expression of SFTPC [Dietl, et.al., 2010, Douville, et.al., 2011, Majumdar, et.al., 2012]. This is significant since SFTPC reduces surface tension and helps to prevent alveolar collapse and cellular damage [Lutz, et.al., 2015, Malacrida, et.al., 2014]. *In vivo* it was shown that patients with COPD benefit from physical activity [Benton, 2014, Incorvaia, et.al., 2014]. The right amount of stretch is crucial because prolonged mechanical ventilation is known to induce apoptosis of alveolar type II cells [Kroon, et.al., 2013]. Furthermore, oxygen supply needs to be carefully investigated and controlled. It was shown that hyperoxia (80-90% O₂) increased cell stiffness by actin cytoskeleton rearrangement and led to cell detachment during stretch [Wilhelm, et.al., 2014]. Taken together, stretch and the right amount of oxygen critically influence cell survival and differentiation, and thereby, the regeneration of the injured or diseased lung tissue and may be necessary components yet to determine.

Even though, there are still limitations to overcome, the benefits of the method of 3D-LTC are predominant over the disadvantages. The method is laborious but opens an avenue between animal studies and clinical trials by the inclusion of patient material. As more companies provide tissue slicers and vibratomes it is likely, that it will become a standard procedure in research laboratories in the near future.

6.2 Pathway modulation studies with 3D-LTC

As shown before, both signalling pathways studied in this work (Wnt/beta-catenin and TGF-beta) could be activated successfully without inducing significant cellular toxicity (see 5.4.1, 5.4.4, and 5.5). For Wnt/beta-catenin activation two different GSK3 inhibitors (10 mM LiCl and 2 μ M CT) were applied and showed similar strength in pathway activation. Both compounds have been previously used in both *in vivo* and *ex vivo* models. LiCl was shown to attenuate experimental emphysema by activating Wnt/beta-catenin signalling (predominantly in ATII cells) [Kneidinger, et.al., 2011]. Similarly, human fetal lung explants treated with 5 μ M CT, showed an upregulation of ABC at the protein level [Zhang, 2012 #336]. These results are in accordance with the results presented in this thesis (5.4.4). Furthermore, the upregulation of different Wnt/beta-catenin target genes (*TCF4*, *LEF1*, *MMP7*, *CYCD1*) were also observed [Zhang, et.al., 2012]. This shows that both compounds are capable of Wnt/beta-catenin activation.

6.2.1 Wnt/beta-catenin activation

Wnt/beta-catenin signalling has been reported to be reduced in emphysematous animals and COPD patients [Kneidinger, et.al., 2011, Zhou, et.al., 2012]. Slice generation did not change the dysregulation of the Wnt/beta-catenin pathway and its downregulation was still detectable at the onset of cultivation of 3D-LTC from emphysematous animals (see Figure 5.10). From this it can be assumed, that differences seen *ex vivo* still reflect the *in vivo* situation and results from the *ex vivo* model may be extrapolated *in vivo*.

With the use of live cell imaging and BAT-GAL and TCF/LEF-GFP Wnt-reporter animals [Ferrer-Vaquer, et.al., 2010, Maretto, et.al., 2003] Wnt/beta-catenin activated cells could be identified and traced (see Figure 5.16 and Figure 5.17). These studies could possibly be extended for studying Wnt/beta-catenin activation kinetics by quantification of the increase in activated cells over time. Activated cells were located in the periphery of the lung, staining positive for ATI and ATII markers (such as podoplanin and surfactant protein C). The identification of these cells, expressing markers of ATII cells was already shown before [Kneidinger, et.al., 2011], while the expression of ATI markers was not described up to now.

Slight differences in the expression pattern of ATI and ATII markers were seen comparing the 3D-LTC from murine and human tissue. In both, murine and human 3D-LTC, LiCl led to an increased expression of podoplanin and a decrease in Hopx. Aqp5 was significantly downregulated at the protein level in the 3D-LTC from human patients, where in contrast, no regulation by LiCl was detected in 3D-LTC from emphysematous mice. While the ATII marker SFTPC was not altered after

LiCl treatment in 3D-LTC from emphysematous mice, its expression was significantly increased in human 3D-LTC stimulated with LiCl. This led to the speculation that AII to AI trans-differentiation was influenced by Wnt/beta-catenin pathway modulation.

The exact role of Wnt/beta-catenin in AII to AI trans-differentiation is not yet known. It has been suggested, that Wnt/beta-catenin activation during lung injury promotes differentiation to AI-like cells [Flozak, et.al., 2010]. Flozak and colleagues showed that inhibition of beta-catenin/T-cell factor signalling in primary rat AII cells led to reduced expression of AI markers (podoplanin and receptor for advanced glycation endproducts (RAGE)) and a decrease in cell survival. In direct contrast, Ghaedi and colleagues used a Wnt inhibitor (IWR-1) on AII cells, generated from iPS. Wnt inhibition led to the induction of an AI phenotype in these AII cells [Ghaedi, et.al., 2013]. Wang and colleagues observed that adenoviral overexpression of miR-375 in primary rat AII cells inhibited the Wnt/beta-catenin pathway and trans-differentiation to AI cells [Wang, et.al., 2013]. Marconett and colleagues used an integrated transcriptomic and epigenomic analysis of *in vitro* differentiated primary human alveolar epithelial cells to AI cells and confirmed the activation of the Wnt pathway in this process [Marconett, et.al., 2013]. Taken together Wnt inhibition in primary rat AII led to trans-differentiation to AI cells. The opposite results from Ghaedi may be explained by the fact that the AII cells were generated from iPS having an "AII-like phenotype" [Ghaedi, et.al., 2013] and due to this could be different from primary AII cells. Thereby it may be assumed that Wnt activation will lead to increased AII to AI trans-differentiation in the 3D-LTC, which the increase in podoplanin and SFTPC in the human 3D-LTC was in accordance with.

Thus far, it is believed that AI cells arise from a pool of mature AII cells which trans-differentiate into AI cells. This was seen for *in vitro* cultivation of isolated primary AII cells several times by different groups [Fehrenbach, 2001, Flozak, et.al., 2010, Ghaedi, et.al., 2013, Marconett, et.al., 2013]. However, recent evidence by Treutlein and colleagues suggests the existence of bipotent alveolar epithelial cells during murine lung development giving rise to AI and AII cells and expressing markers of both lineages [Treutlein, et.al., 2014]. AI cells might therefore stem from trans-differentiating AII cells or this bipotent alveolar epithelial progenitor as a second source.

Treutlein and colleagues showed that Hopx is a marker of AI cells and was not detectable in fully differentiated AII cells anymore [Treutlein, et.al., 2014]. A reduction of Hopx expression would be indicative of either, a reduced amount of AI cells or (assuming a non-changing amount of AI cells) an increased differentiation of AII progenitor cells (still expressing Hopx) to mature AII cells (lacking Hopx expression). Thereby an overall decrease in Hopx expression would be detected.

Podoplanin, another marker of AI cells was showing increased expression in 3D-LTC from both species but is not exclusively expressed by AI cells, but for example endothelial cells [Herzog, et.al., 2013, Kunita, et.al., 2011] and fibroblasts [Inoue, et.al., 2014]. Even though slices were carefully chosen to include mainly alveolar regions, small bronchi and vessels could not be excluded to be located in the slices. Treatments affected all residing cells of the 3D-LTC, including endothelial cells and fibroblasts, thereby complicating interpretation of the results, since these cells may react with opposite regulation of podoplanin. The increase in podoplanin expression

nonetheless is in accordance to the finding, that WNT3A treatment, a ligand activating Wnt/beta-catenin signalling, led to increased podoplanin expression in RLE-6TN cells (a cell line derived from rat lung ATII cells) [Fujiwara, et.al., 2007]. By this, it was not unexpected that Wnt/beta-catenin activation may lead to an increase in podoplanin expression. The provider of the cells quotes that these cells exhibit characteristics of ATII cells but did not comment on SFTPC expression as marker for these cells. These cells might either be similar to the bipotent alveolar progenitors stated by Treutlein *et al.* or already started to trans-differentiate into ATI cells, which is known to happen fast during *in vitro* cultivation of ATII cells [Fehrenbach, 2001, Flozak, et.al., 2010, Ghaedi, et.al., 2013, Marconett, et.al., 2013].

The ATI marker AQP5 is not exclusively expressed by ATI cells but bronchial acinar and ciliated duct columnar cells as well [Borok, et.al., 2002]. The decrease in Hopx in 3D-LTC from both emphysematous mice and human patients after LiCl treatment suggests a decrease in ATI cells. Aqp5 might decrease due to the fact that there are less ATI cells but its expression was not altered in the murine 3D-LTC. This suggests that the bronchial acinar and ciliated duct columnar cells might have increased their AQP5 expression, leading to a non-altered overall expression. The increase in podoplanin might be explained by an increased expression in other cells, such as endothelial cells, compensating for the decrease due to less ATI cells. SFTPC expression was stable in 3D-LTC from emphysematous mice after LiCl treatment, suggesting that the ATII cell population was staying stable either by proliferation of ATII cells or differentiation of bipotent alveolar epithelial cells to mature ATII cells. Taken together this might indicate that in the murine slices the amount of ATI cells was decreasing while the ATII cell population stayed stable.

In human 3D-LTC, an increased expression of the ATII marker SFTPC was detected due to LiCl treatment. This supposes a stabilisation or even increase of the ATII cell population. HOPX as well as AQP5 expression were reduced, while podoplanin expression was increased leading to the assumption that the ATI cell population was decreasing in the human samples due to Wnt/beta-catenin activation, while the ATII cell population increased.

The bipotent alveolar epithelial cells described by Treutlein *et al.* might still reside in the adult lung and may be located in the 3D-LTC as well, which has not been analysed thus far. If so, this pool of cells could be a replenishing source for the trans-differentiating ATII cells and mature ATI cells. The study by Treutlein and colleagues was conducted with murine samples [Treutlein, et.al., 2014]. For this reason, it is not known whether this bipotent progenitor population exists in human lung tissue as well, potentially leading to a different process of cellular turnover, in which only ATII to ATI trans-differentiation in combination with proliferation of ATII cells is involved. For better visualisation, the concept proposed for the differentiation and cellular turnover in both species is depicted in Figure 6.1. The exact mechanism of cellular differentiation was not addressed in this work. For this, cell tracking experiments, tracking the ATII cells and staining for ATI markers should be conducted. Furthermore, it needs to be clarified whether a bipotential progenitor cell exists in the human lung, and if these cells reside in adult human tissue as well.

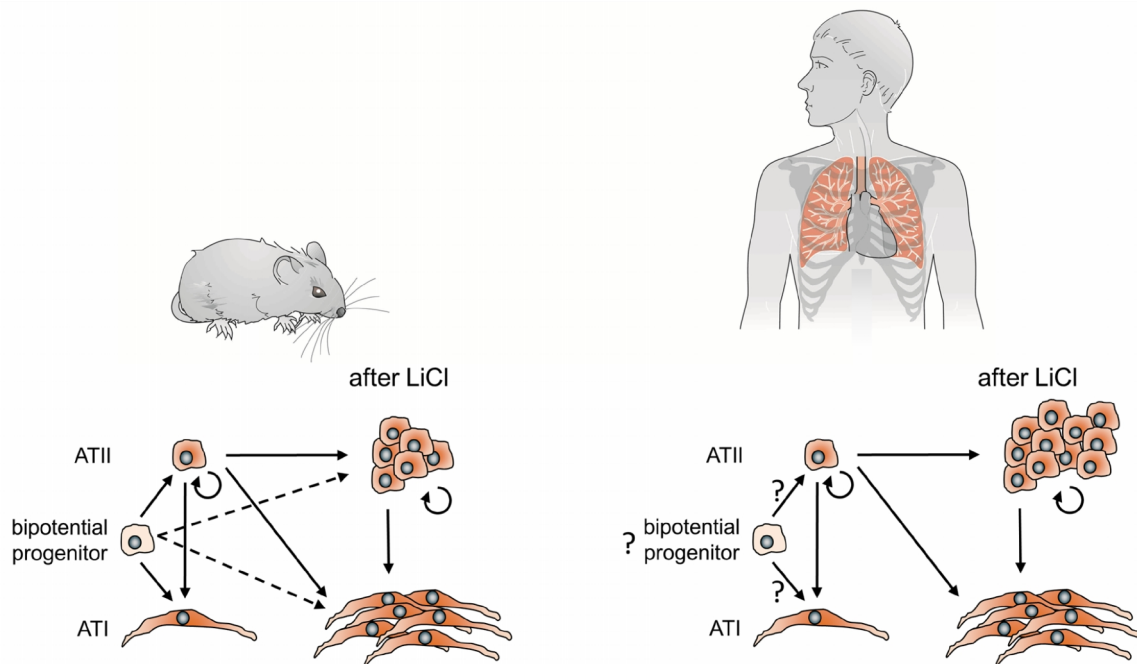


Figure 6.1: Proposed differentiation of progenitor cells into ATI and AII cells in the 3D-LTC after Wnt/beta-catenin activation by 10 mM LiCl.

Proposed differentiation in 3D-LTC from emphysematous mice (left) and human patients (right). The existence of a bipotential progenitor cell in humans was not shown up to now.

Wnt signalling is known to be essential for lung development and stem cell maintenance [Angers, et.al., 2009, Baarsma, et.al., 2013, Niehrs, 2012, Nusse, 2012]. Thus, future studies using the technique of 3D-LTC will be helpful to analyse whether Wnt pathway re-activation might lead to lung epithelial cell regeneration by specifically targeting the bipotent alveolar epithelial progenitors (and thereby, leading to direct activation of the AII and ATI cell population) or whether Wnt signalling induces AII to ATI trans-differentiation in human diseased lung tissue.

6.2.2 TGF-beta activation

The human lung specimen studied in this work originated from non-COPD and COPD patients undergoing lung resection due to cancer. TGF-beta signalling is involved in COPD as well as cancer and shown to be lacking in emphysema, which is one of the main pathological features of COPD. Due to this, TGF-beta treatment was applied to the human samples to gain insight, if this pathway could be reactivated and potentially initiate lung repair.

TGF-beta signaling is involved in chronic lung disease like fibrosis, COPD and cancer with different levels of activation. In fibrosis and the sites of peribronchial remodeling in COPD TGF-beta is upregulated [Beasley 2010, Churg 2006], while in the alveolar regions a lack of TGF-beta seems to be causative for emphysema [Budd 2012, Milara 2013]. TGF-beta is also known to induce epithelial-to-mesenchymal transition (EMT) marked by loss of E-cadherin and an increase in expression of alpha-SMA, collagen I, and the transcription factor genes SNAI1 and SNAI2 [Crosby 2010, Grande 2002, Kim 2006, Milara 2013, Tanjore, H. 2011, Thiery 2006]. Induction of TGF-beta

signalling in human 3D-LTC by recombinant TGF-beta treatment resulted in induction of SMAD3 protein phosphorylation and target gene upregulation (*PAI1*, *COL1A1*, and *ACTA2*) proving successful pathway activation. Additionally, an increased expression of alpha-SMA protein in alveolar epithelial regions in both murine and human 3D-LTC was shown by IF. This strongly suggests that distal epithelial cells may have undergone EMT in 3D-LTC, since the increased expression of alpha-SMA protein was seen primarily in alveolar epithelial regions. Moreover, the transcription factors *SNAI1* and *SNAI2* were expressed at increased levels in human 3D-LTC treated with recombinant TGF-beta.

A number of *in vitro* studies have investigated the role of TGF-beta on specific lung cell types. Xi and colleagues treated A549 cells (human epithelial cells) with TGF-beta, and observed increased SMAD2 and SMAD3 phosphorylation [Xi, et.al., 2014]. Furthermore, alpha-SMA, collagen I and SNAI1 protein expression were also found to be increased in the treated A549 cells [Xi, et.al., 2014]. In a similar study, Câmara and colleagues found that TGF-beta-treated human bronchial epithelial cells (HBE) had increased expression of vimentin, alpha-SMA, phosphorylated SMAD2, and N-cadherin, while E-cadherin was decreased [Camara, et.al., 2010]. TGF-beta has also been shown to affect alpha-SMA expression in lung fibroblasts. Treatment of primary human lung fibroblasts with TGF-beta induced up-regulation of alpha-SMA protein expression [Berschneider 2014, Kasabova 2014].

The increased expression of alpha-SMA that was observed in this work may be due to activation of epithelial cells, undergoing EMT or alveolar-residing fibroblasts gaining a more myo-fibroblast-like phenotype. The exact cell type which stained positive for alpha-SMA in the alveolar regions was not determined in this thesis. It would also be of interest whether TGF-beta treatment induced ATII to ATI differentiation in 3D-LTC, since it has been previously shown that TGF-beta treatment promoted trans-differentiation of murine primary ATII cells [Zhao, et.al., 2013]. Further analysis needs to be done regarding which cell types are activated and whether this repair can occur in diseased tissue. Future studies utilizing slices from lineage tracing mice would also be helpful in elucidating which cell type most significantly obtains a myo-fibroblast phenotype.

In summary, TGF-beta activation led to induction of EMT-related gene and protein expression in 3D-LTC. As a lack of TGF-beta is related to emphysema [Budd, et.al., 2012, Milara, et.al., 2013] it is reasonable to assume that TGF-beta addition may lead to cellular reactivation and could possibly lead to lung repair.

6.3 3D-LTC as a tool for preclinical testing

In general, animal models are used to study human diseases. They are developed to mimic the disease as close as possible. Nonetheless, animal models can only partially recapitulate human diseases and usually lack the heterogeneity seen in patients. This may be one of the reasons why only 5% of anti-cancer drugs that succeeded in preclinical testing get approved by the Food and Drug Administration [Malaney, et.al., 2014]. “Mouse avatars”, a model in which pieces of the

patients' tumour are implanted into immunodeficient mice, is one approach for personalized drug testing helping to find the suitable treatment for individual patients. Due to high costs and duration, this is not applicable to all patients why alternatives are needed. Directly studying the patients' tissue therefore is appealing. This can be achieved by the usage of 3D-LTC from human patients having the possibility for drug testing in a personalized medicine manner. Due to the high similarity of the human tissue and the 3D-LTC, the approach used in this thesis has the potential to bridge the gap between animal studies and clinical trials.

As previously discussed, murine and human samples expressed similar levels of podoplanin and HOPX but exhibited differences regarding SFTPC and AQP5 expression. While both markers were not altered in murine 3D-LTC in response to LiCl treatment, gene and protein expression of SFTPC was upregulated, while AQP5 was downregulated at the protein level in the human samples. There are a number of variables, which could explain the discrepancies observed between mouse and human samples. First, mice were young (age 8-12 weeks), while the samples from the humans were from elderly patients (mean age 66 ± 8 years). According to the findings from Zhou and colleagues, there was no difference in emphysema development when they compared young and old mice exposed to cigarette smoke [Zhou, et.al., 2013]. This suggests that results from the animal experiments might not have varied by using animals being in a comparable period of life matched to the humans but needs further investigation to come to a definite conclusion.

Second, the mouse model of elastase-induced emphysema is different from cigarette smoke induced emphysema, one of the main features of COPD. Inflammation due to repeated cigarette smoke-induced injury was absent in the elastase induced emphysema. In contrast to the mouse models, human tissue came from patients, which all had cancer and a smoking history with a median value of 51 ± 18 pack years and lifetime exposure to environmental pollutants (see Table 4.17). The missing inflammation, missing exposure to environmental pollutants, and missing cancer co-morbidity in the case of the emphysematous mice may have contributed to the differences seen between the 3D-LTC from both species.

Although the mouse models are easy to handle, easily accessible, and a relatively cheap way to study diseases, human samples need to be studied in parallel to improve the probability that results that can be successfully transferred into clinical practice [Liberati, et.al., 2010, Vickers, et.al., 2005].

The value of the 3D-LTC established in this work towards this aim is apparent. As already discussed, samples from a specific patient can be used in a personalized medicine manner. It is possible to test the effects of a certain treatment for each specimen individually in a semi-high throughput fashion. Furthermore, by using 3D-LTC from both mice and humans, we can further our understanding of the similarities and differences between the two species in lung disease. Most probably, this will help to predict, which findings are transferable and where dissimilarities would lead to non-transferable conclusions if experiments would be conducted *in vitro* or with animals, only.

In this work, it was shown, that *AXIN2* and *SFTPC* gene expression correlated with disease severity (see Figure 5.26) which was not shown in human 3D-LTC before. This gives evidence that 3D-LTC from human patients could be used as a predictive tool for drug testing in a personalized medicine manner, tailoring treatments to the individual requirements of the patient. This might be one potential avenue to anticipate adverse effects in patients and make drug testing safer before clinical studies are conducted. These results also suggest that even patients with more severe COPD (e.g. GOLD stage IV, which were not included in this study) might benefit from the Wnt/beta-catenin activation. A further study could contain a comparative evaluation of the treatment effects in 3D-LTC and functional outcomes in the corresponding patient to further validate this model. This would help to predict the reaction of the patient to a certain pharmacological intervention in a fast and relatively easy accessible fashion.

6.4 Conclusion

This study characterised 3D-LTC from murine and human samples over a cultivation period of seven days. Cellular viability, proliferation, and functionality was proven by various assays. Moreover, 3D-LTC were studied in a spatio-temporal manner using live cell imaging. This is an improvement compared to the studies performed until now, where long-term viability was a major limiting factor. In this work, it was demonstrated that different signalling pathways could be activated in the 3D-LTC, shown specifically for Wnt/beta-catenin and TGF-beta. TGF-beta activation resulted in an increased expression of transcription factors implicated in epithelial-to-mesenchymal transition in human 3D-LTC. Furthermore, a more unrestricted alpha-SMA protein expression in the alveolar epithelial cell region was observed suggesting that epithelial cells express mesenchymal markers upon TGF-beta activation. Wnt/beta-catenin activation revealed activation of ATI as well as ATII cells as shown by the use of Wnt reporter animals. Furthermore, markers for ATI and ATII cells were differentially regulated in response to Wnt/beta-catenin activation indicating potential differentiation of ATII to ATI cells and thereby induction of repair mechanisms. This provides evidence that the Wnt signalling pathway is a potential target for pharmacological intervention in COPD management. The exact mechanism of activation was not determined in this study. Differences in response to treatments were observed between the murine and human 3D-LTC, highlighting the importance of studying human tissue for preclinical testing. Correlation analysis revealed a negative correlation of Wnt/beta-catenin activation with disease severity on gene expression level, demonstrating that the 3D-LTC provide a valid tool to analyse human tissue responses for preclinical drug testing and personalized medicine.

In summary, it was shown, that different signalling pathways – the Wnt/beta-catenin as well as the TGF-beta pathway – can be activated in 3D-LTC. Wnt/beta-catenin activation was confirmed with two different pharmacological GSK3 inhibitors, and resulted in differential expression of ATI and ATII markers in 3D-LTC from both emphysematous animals and human patients. Matrix alterations and cellular movements can be imaged with high spatio-temporal resolution in 3D

providing evidence for the suitability of the 3D-LTC for cell tracking and analysis of ECM repair mechanisms. Furthermore, inducibility of *AXIN2* expression, as well as *SFTPC*, indicating ATII cell activation after Wnt/beta-catenin activation with LiCl, can be correlated with disease severity of the patients. It is proposed that any signalling pathway can be activated in 3D-LTC. At least for the PI3K/AKT signalling pathway, successful modulation in tissue slices has already been shown [Vaira, et.al., 2010]. In this work, essential proof of concept for pathway modulation and drug validation in human 3D-LTC was provided, which we believe will open new avenues for superior clinical translation and personalized medicine.

7 REFERENCES

- Adcock I.M., et al. (2011): "Chronic obstructive pulmonary disease and lung cancer: new molecular insights". *Respiration; international review of thoracic diseases* 81, 265.
- Ahn Y., et al. (2010): "Inhibition of Wnt signaling by Wise (Sostdc1) and negative feedback from Shh controls tooth number and patterning". *Development* 137, 3221.
- Al Alam D., et al. (2013): "Wingless: developmentally important genes that respond adversely to smoking". *Thorax* 68, 703.
- Andersen M.P., et al. (2012): "Alveolar fractal box dimension inversely correlates with mean linear intercept in mice with elastase-induced emphysema". *Int J Chron Obstruct Pulmon Dis* 7, 235.
- Angers S., et al. (2009): "Proximal events in Wnt signal transduction". *Nature reviews Molecular cell biology* 10, 468.
- Antunes M.A., et al. (2011): "Elastase-induced pulmonary emphysema: insights from experimental models". *Anais da Academia Brasileira de Ciencias* 83, 1385.
- Baarsma H.A., et al. (2013): "The WNT signaling pathway from ligand secretion to gene transcription: molecular mechanisms and pharmacological targets". *Pharmacol Ther* 138, 66.
- Baarsma H.A., et al. (2011): "{beta}-Catenin signaling is required for TGF- β 1-induced extracellular matrix production by airway smooth muscle cells". *Am J Physiol Lung Cell Mol Physiol* 301, 956.
- Baarsma H.A., et al. (2011): "Activation of WNT/beta-catenin signaling in pulmonary fibroblasts by TGF-beta is increased in chronic obstructive pulmonary disease". *PLoS One* 6, e25450.
- Bain J., et al. (2007): "The selectivity of protein kinase inhibitors: a further update". *The Biochemical journal* 408, 297.
- Barkauskas C.E., et al. (2013): "Type 2 alveolar cells are stem cells in adult lung". *J Clin Invest* 123, 3025.
- Barnes P.J. (2010): "Inhaled corticosteroids in COPD: a controversy". *Respiration; international review of thoracic diseases* 80, 89.
- Barnes P.J. (2010): "New therapies for chronic obstructive pulmonary disease". *Medical principles and practice : international journal of the Kuwait University, Health Science Centre* 19, 330.
- Bartram U., et al. (2004): "The role of transforming growth factor beta in lung development and disease". *Chest* 125, 754.
- Bauer C.M., et al. (2010): "Treating Viral Exacerbations of Chronic Obstructive Pulmonary Disease: Insights from a Mouse Model of Cigarette Smoke and H1N1 Influenza Infection". *PLoS One* 5, e13251.

- Beasley M.B. (2010): "Smoking-related Small airway disease--a review and update". *Advances in anatomic pathology* 17, 270.
- Benton M.J. (2014): "Physical activity in chronic obstructive pulmonary disease: Is it a process or an outcome?". *Respirology* 19, 298.
- Bonvillain R.W., et al. (2012): "A nonhuman primate model of lung regeneration: detergent-mediated decellularization and initial in vitro recellularization with mesenchymal stem cells". *Tissue Eng Part A* 18, 2437.
- Booth A.J., et al. (2012): "Acellular normal and fibrotic human lung matrices as a culture system for in vitro investigation". *Am J Respir Crit Care Med* 186, 866.
- Borok Z., et al. (2002): "Lung edema clearance: 20 years of progress: invited review: role of aquaporin water channels in fluid transport in lung and airways". *Journal of applied physiology* 93, 2199.
- Bourke S., et al. (2005): "Development of a lung slice preparation for recording ion channel activity in alveolar epithelial type I cells". *Respir Res* 6, 40.
- Bruinsma B.G., et al. (2014): "Organomatics and organometrics: Novel platforms for long-term whole-organ culture". *Technology* 2, 13.
- Bryja V., et al. (2009): "The extracellular domain of Lrp5/6 inhibits noncanonical Wnt signaling in vivo". *Molecular biology of the cell* 20, 924.
- Budd D.C., et al. (2012): "Targeting TGFbeta superfamily ligand accessory proteins as novel therapeutics for chronic lung disorders". *Pharmacol Ther* 135, 279.
- Burge S. (2001): "Should inhaled corticosteroids be used in the long term treatment of chronic obstructive pulmonary disease?". *Drugs* 61, 1535.
- Bussek A., et al. (2009): "Tissue slices from adult mammalian hearts as a model for pharmacological drug testing". *Cell Physiol Biochem* 24, 527.
- Butler A.J., et al. (2002): "Successful extracorporeal porcine liver perfusion for 72 hr". *Transplantation* 73, 1212.
- Butler J.P., et al. (2012): "Evidence for adult lung growth in humans". *N Engl J Med* 367, 244.
- Camara J., et al. (2010): "Epithelial-mesenchymal transition in primary human bronchial epithelial cells is Smad-dependent and enhanced by fibronectin and TNF-alpha". *Fibrogenesis & tissue repair* 3, 2.
- Camelliti P., et al. (2011): "Adult human heart slices are a multicellular system suitable for electrophysiological and pharmacological studies". *Journal of molecular and cellular cardiology* 51, 390.
- Celli B.R., et al. (2008): "Effect of pharmacotherapy on rate of decline of lung function in chronic obstructive pulmonary disease: results from the TORCH study". *Am J Respir Crit Care Med* 178, 332.

- Chen B., et al. (2009): "Small molecule-mediated disruption of Wnt-dependent signaling in tissue regeneration and cancer". *Nature chemical biology* 5, 100.
- Chilosi M., et al. (2012): "The pathogenesis of COPD and IPF: distinct horns of the same devil?". *Respir Res* 13, 3.
- Chilosi M., et al. (2003): "Aberrant Wnt/beta-catenin pathway activation in idiopathic pulmonary fibrosis". *The American journal of pathology* 162, 1495.
- Chung K.F. (2001): "Cytokines in chronic obstructive pulmonary disease". *The European respiratory journal Supplement* 34, 50s.
- Chung K.F. (2005): "The role of airway smooth muscle in the pathogenesis of airway wall remodeling in chronic obstructive pulmonary disease". *Proc Am Thorac Soc* 2, 347.
- Chung K.F., et al. (2008): "Multifaceted mechanisms in COPD: inflammation, immunity, and tissue repair and destruction". *Eur Respir J* 31, 1334.
- Churg A., et al. (2006): "Cigarette smoke drives small airway remodeling by induction of growth factors in the airway wall". *Am J Respir Crit Care Med* 174, 1327.
- Churg A., et al. (2007): "Animal models of cigarette smoke-induced chronic obstructive lung disease". *Contrib Microbiol* 14, 113.
- Clevers H. (2006): "Wnt/beta-catenin signaling in development and disease". *Cell* 127, 469.
- Crosby L.M., et al. (2010): "Epithelial repair mechanisms in the lung". *Am J Physiol Lung Cell Mol Physiol* 298, L715.
- Cypel M., et al. (2011): "Normothermic ex vivo lung perfusion in clinical lung transplantation". *N Engl J Med* 364, 1431.
- Dassow C., et al. (2010): "Biaxial distension of precision-cut lung slices". *J Appl Physiol* 108, 713.
- Davidovich N., et al. (2013): "Uses of Remnant Human Lung Tissue for Mechanical Stretch Studies". *Cellular and molecular bioengineering* 6, 175.
- Davidovich N., et al. (2012): "Reproducible Uniform Equibiaxial Stretch of Precision-Cut Lung Slices". *Am J Physiol Lung Cell Mol Physiol* 304, L210.
- De A. (2011): "Wnt/Ca²⁺ signaling pathway: a brief overview". *Acta biochimica et biophysica Sinica* 43, 745.
- de Boer W.I., et al. (1998): "Transforming growth factor beta1 and recruitment of macrophages and mast cells in airways in chronic obstructive pulmonary disease". *Am J Respir Crit Care Med* 158, 1951.
- de Graaf I.A., et al. (2010): "Preparation and incubation of precision-cut liver and intestinal slices for application in drug metabolism and toxicity studies". *Nature protocols* 5, 1540.

- De Kanter R., et al. (1999): "Organ slices as an in vitro test system for drug metabolism in human liver, lung and kidney". *Toxicol In Vitro* 13, 737.
- De Proost I., et al. (2008): "Functional live cell imaging of the pulmonary neuroepithelial body microenvironment". *Am J Respir Cell Mol Biol* 39, 180.
- Dekkers J.F., et al. (2013): "A functional CFTR assay using primary cystic fibrosis intestinal organoids". *Nat Med* 19, 939.
- Delmotte P., et al. (2006): "Ciliary beat frequency is maintained at a maximal rate in the small airways of mouse lung slices". *Am J Respir Cell Mol Biol* 35, 110.
- Derynck R., et al. (2001): "TGF-beta signaling in tumor suppression and cancer progression". *Nat Genet* 29, 117.
- Dietl P., et al. (2010): "Lamellar body exocytosis by cell stretch or purinergic stimulation: possible physiological roles, messengers and mechanisms". *Cell Physiol Biochem* 25, 1.
- Discher D.E., et al. (2005): "Tissue cells feel and respond to the stiffness of their substrate". *Science* 310, 1139.
- Douville N.J., et al. (2011): "Combination of fluid and solid mechanical stresses contribute to cell death and detachment in a microfluidic alveolar model". *Lab Chip* 11, 609.
- Emami K.H., et al. (2004): "A small molecule inhibitor of beta-catenin/CREB-binding protein transcription [corrected]". *Proc Natl Acad Sci U S A* 101, 12682.
- Ezzie M.E., et al. (2012): "Gene expression networks in COPD: microRNA and mRNA regulation". *Thorax* 67, 122.
- Fehrenbach H. (2001): "Alveolar epithelial type II cell: defender of the alveolus revisited". *Respir Res* 2, 33.
- Ferrer-Vaquer A., et al. (2010): "A sensitive and bright single-cell resolution live imaging reporter of Wnt/ss-catenin signaling in the mouse". *BMC developmental biology* 10, 121.
- Flozak A.S., et al. (2010): "Beta-catenin/T-cell factor signaling is activated during lung injury and promotes the survival and migration of alveolar epithelial cells". *J Biol Chem* 285, 3157.
- Fujii N., et al. (2007): "An antagonist of dishevelled protein-protein interaction suppresses beta-catenin-dependent tumor cell growth". *Cancer research* 67, 573.
- Fujiwara N., et al. (2007): "Monoclonal antibody 7F9 recognizes rat protein homologous to human carboxypeptidase-M in developing and adult rat lung". *Respirology* 12, 54.
- Geys J., et al. (2007): "Optimisation of culture conditions to develop an in vitro pulmonary permeability model". *Toxicol In Vitro* 21, 1215.
- Ghaedi M., et al. (2013): "Human iPS cell-derived alveolar epithelium repopulates lung extracellular matrix". *J Clin Invest* 123, 4950.

- Ghaedi M., et al. (2014): "Alveolar epithelial differentiation of human induced pluripotent stem cells in a rotating bioreactor". *Biomaterials* 35, 699.
- Gilpin S.E., et al. (2014): "Enhanced Lung Epithelial Specification of Human Induced Pluripotent Stem Cells on Decellularized Lung Matrix". *Ann Thorac Surg* 98, 1721.
- Gopalsamy A., et al. (2008): "Identification of diarylsulfone sulfonamides as secreted frizzled related protein-1 (sFRP-1) inhibitors". *Journal of medicinal chemistry* 51, 7670.
- Gosens R., et al. (2008): "The GSK-3/beta-catenin-signalling axis in smooth muscle and its relationship with remodelling". *Naunyn-Schmiedeberg's archives of pharmacology* 378, 185.
- Grande M., et al. (2002): "Transforming growth factor-beta and epidermal growth factor synergistically stimulate epithelial to mesenchymal transition (EMT) through a MEK-dependent mechanism in primary cultured pig thyrocytes". *J Cell Sci* 115, 4227.
- Grandy D., et al. (2009): "Discovery and characterization of a small molecule inhibitor of the PDZ domain of dishevelled". *J Biol Chem* 284, 16256.
- Grigoryan T., et al. (2008): "Deciphering the function of canonical Wnt signals in development and disease: conditional loss- and gain-of-function mutations of beta-catenin in mice". *Genes & development* 22, 2308.
- Gunaydin H., et al. (2012): "Novel binding mode of a potent and selective tankyrase inhibitor". *PLoS One* 7, e33740.
- Hammad S., et al. (2014): "Protocols for staining of bile canalicular and sinusoidal networks of human, mouse and pig livers, three-dimensional reconstruction and quantification of tissue microarchitecture by image processing and analysis". *Archives of toxicology* 88, 1161.
- Held H.D., et al. (1999): "Characterization of airway and vascular responses in murine lungs". *Br J Pharmacol* 126, 1191.
- Henjakovic M., et al. (2008): "Ex vivo lung function measurements in precision-cut lung slices (PCLS) from chemical allergen-sensitized mice represent a suitable alternative to in vivo studies". *Toxicol Sci* 106, 444.
- Henjakovic M., et al. (2008): "Ex vivo testing of immune responses in precision-cut lung slices". *Toxicol Appl Pharmacol* 231, 68.
- Herter-Sprie G.S., et al. (2013): "New cast for a new era: preclinical cancer drug development revisited". *J Clin Invest* 123, 3639.
- Herzog B.H., et al. (2013): "Podoplanin maintains high endothelial venule integrity by interacting with platelet CLEC-2". *Nature* 502, 105.
- Hines E.A., et al. (2014): "Tissue Crosstalk in Lung Development". *Journal of cellular biochemistry* 115, 1469.

- Hogg J.C., et al. (2004): "The nature of small-airway obstruction in chronic obstructive pulmonary disease". *N Engl J Med* 350, 2645.
- Hogg J.C., et al. (2009): "The pathology of chronic obstructive pulmonary disease". *Annu Rev Pathol* 4, 435.
- Huang S.M., et al. (2009): "Tankyrase inhibition stabilizes axin and antagonizes Wnt signalling". *Nature* 461, 614.
- Huh D., et al. (2010): "Reconstituting organ-level lung functions on a chip". *Science* 328, 1662.
- Incorvaia C., et al. (2014): "Effects of pulmonary rehabilitation on lung function in chronic obstructive pulmonary disease: the FIRST study". *European journal of physical and rehabilitation medicine* 50, 419.
- Inoue H., et al. (2014): "Podoplanin expressing cancer-associated fibroblasts in oral cancer". *Tumour biology : the journal of the International Society for Oncodevelopmental Biology and Medicine* 35, 11345.
- Inoue S., et al. (2003): "Impaired pulmonary inflammatory responses are a prominent feature of streptococcal pneumonia in mice with experimental emphysema". *Am J Respir Crit Care Med* 167, 764.
- Ito S., et al. (2005): "Mechanics, nonlinearity, and failure strength of lung tissue in a mouse model of emphysema: possible role of collagen remodeling". *Journal of applied physiology* 98, 503.
- Jain R.K., et al. (2005): "Engineering vascularized tissue". *Nature biotechnology* 23, 821.
- John G., et al. (2014): "The composition of cigarette smoke determines inflammatory cell recruitment to the lung in COPD mouse models". *Clinical science* 126, 207.
- Juarez P., et al. (2011): "TGF-beta in cancer and bone: implications for treatment of bone metastases". *Bone* 48, 23.
- Kahn M. (2014): "Can we safely target the WNT pathway?". *Nature reviews Drug discovery* 13, 513.
- Khan M.A., et al. (2007): "Kinetics of in vitro bronchoconstriction in an elastolytic mouse model of emphysema". *Eur Respir J* 30, 691.
- Kim K.K., et al. (2006): "Alveolar epithelial cell mesenchymal transition develops in vivo during pulmonary fibrosis and is regulated by the extracellular matrix". *Proc Natl Acad Sci U S A* 103, 13180.
- Kneidinger N., et al. (2011): "Activation of the WNT/ β -Catenin Pathway Attenuates Experimental Emphysema". *Am J Respir Crit Care Med* 183, 723.
- Konigshoff M., et al. (2008): "Functional Wnt signaling is increased in idiopathic pulmonary fibrosis". *PLoS One* 3, e2142.

- Konigshoff M., et al. (2010): "WNT signaling in lung disease: a failure or a regeneration signal?". *Am J Respir Cell Mol Biol* 42, 21.
- Konigshoff M., et al. (2009): "WNT1-inducible signaling protein-1 mediates pulmonary fibrosis in mice and is upregulated in humans with idiopathic pulmonary fibrosis". *J Clin Invest* 119, 772.
- Kononov S., et al. (2001): "Roles of mechanical forces and collagen failure in the development of elastase-induced emphysema". *Am J Respir Crit Care Med* 164, 1920.
- Krimmer D.I., et al. (2012): "Matrix proteins from smoke-exposed fibroblasts are pro-proliferative". *Am J Respir Cell Mol Biol* 46, 34.
- Kroon A.A., et al. (2013): "Mechanical ventilation-induced apoptosis in newborn rat lung is mediated via FasL/Fas pathway". *Am J Physiol Lung Cell Mol Physiol* 305, L795.
- Kunita A., et al. (2011): "Podoplanin is regulated by AP-1 and promotes platelet aggregation and cell migration in osteosarcoma". *The American journal of pathology* 179, 1041.
- Lam A.P., et al. (2011): "beta-catenin signaling: a novel mediator of fibrosis and potential therapeutic target". *Current opinion in rheumatology* 23, 562.
- Lan A., et al. (2014): "Akt2 Mediates TGF-beta1-Induced Epithelial to Mesenchymal Transition by Deactivating GSK3beta/Snail Signaling Pathway in Renal Tubular Epithelial Cells". *Cell Physiol Biochem* 34, 368.
- Li D., et al. (2014): "Myeloid cell RelA/p65 promotes lung cancer proliferation through Wnt/beta-catenin signaling in murine and human tumor cells". *Oncogene* 33, 1239.
- Liberati T.A., et al. (2010): "In vitro lung slices: a powerful approach for assessment of lung pathophysiology". *Expert Rev Mol Diagn* 10, 501.
- Logan C.Y., et al. (2004): "The Wnt signaling pathway in development and disease". *Annual review of cell and developmental biology* 20, 781.
- Lovett M., et al. (2009): "Vascularization strategies for tissue engineering". *Tissue Eng Part B Rev* 15, 353.
- Lucey E.C., et al. (1998): "Remodeling of alveolar walls after elastase treatment of hamsters - Results of elastin and collagen mRNA in situ hybridization". *American Journal of Respiratory and Critical Care Medicine* 158, 555.
- Lutz D., et al. (2015): "Alveolar Derecruitment and Collapse Induration as Crucial Mechanisms in Lung Injury and Fibrosis". *Am J Respir Cell Mol Biol* 52, 232.
- Macdonald B.T., et al. (2007): "SnapShot: Wnt/beta-catenin signaling". *Cell* 131, 1204.
- MacDonald B.T., et al. (2009): "Wnt/beta-catenin signaling: components, mechanisms, and diseases". *Developmental cell* 17, 9.
- Macintosh R.L., et al. (2013): "Autophagy in tumour cell death". *Seminars in cancer biology* 23, 344.

- Majumdar A., et al. (2012): "Jamming dynamics of stretch-induced surfactant release by alveolar type II cells". *Journal of applied physiology* 112, 824.
- Malacrida L., et al. (2014): "Sevoflurane anesthesia deteriorates pulmonary surfactant promoting alveolar collapse in male Sprague-Dawley rats". *Pulm Pharmacol Ther* 28, 122.
- Malaney P., et al. (2014): "One mouse, one patient paradigm: New avatars of personalized cancer therapy". *Cancer letters* 344, 1.
- Marconett C.N., et al. (2013): "Integrated transcriptomic and epigenomic analysis of primary human lung epithelial cell differentiation". *PLoS genetics* 9, e1003513.
- Maretto S., et al. (2003): "Mapping Wnt/beta-catenin signaling during mouse development and in colorectal tumors". *Proc Natl Acad Sci U S A* 100, 3299.
- Martin C., et al. (1996): "Videomicroscopy of methacholine-induced contraction of individual airways in precision-cut lung slices". *Eur Respir J* 9, 2479.
- Massague J. (2008): "TGFbeta in Cancer". *Cell* 134, 215.
- McDonough J.E., et al. (2011): "Small-airway obstruction and emphysema in chronic obstructive pulmonary disease". *N Engl J Med* 365, 1567.
- Milara J., et al. (2013): "Epithelial to mesenchymal transition is increased in patients with COPD and induced by cigarette smoke". *Thorax* 68, 410.
- Miller W.R., et al. (2011): "Bridging the gap between translational research and clinical application". *Journal of the National Cancer Institute Monographs* 2011, 134.
- Molfini N.A., et al. (2007): "Chronic obstructive pulmonary disease: histopathology, inflammation and potential therapies". *Pulm Pharmacol Ther* 20, 462.
- Moll C., et al. (2013): "Tissue engineering of a human 3D in vitro tumor test system". *Journal of visualized experiments : JoVE*
- Moreno L., et al. (2006): "Pharmacology of airways and vessels in lung slices in situ: role of endogenous dilator hormones". *Respir Res* 7, 111.
- Morin J.P., et al. (2013): "Precision cut lung slices as an efficient tool for in vitro lung physio-pharmacotoxicology studies". *Xenobiotica* 43, 63.
- Morrissey E.E., et al. (2010): "Preparing for the first breath: genetic and cellular mechanisms in lung development". *Developmental cell* 18, 8.
- Morty R.E., et al. (2009): "Transforming growth factor-beta signaling across ages: from distorted lung development to chronic obstructive pulmonary disease". *Proc Am Thorac Soc* 6, 607.
- Murray J.T., et al. (2004): "Exploitation of KESTREL to identify NDRG family members as physiological substrates for SGK1 and GSK3". *The Biochemical journal* 384, 477.

- Nawshad A., et al. (2005): "Transforming growth factor-beta signaling during epithelial-mesenchymal transformation: implications for embryogenesis and tumor metastasis". *Cells Tissues Organs* 179, 11.
- Nguyen D.T., et al. (2013): "Paramyxovirus infections in ex vivo lung slice cultures of different host species". *Journal of virological methods* 193, 159.
- Niehrs C. (2012): "The complex world of WNT receptor signalling". *Nature reviews Molecular cell biology* 13, 767.
- Nusse R. (2012): "Wnt signaling". *Cold Spring Harbor perspectives in biology* 4
- Olinga P., et al. (1997): "Comparison of five incubation systems for rat liver slices using functional and viability parameters". *Journal of pharmacological and toxicological methods* 38, 59.
- op den Dries S., et al. (2013): "Ex vivo normothermic machine perfusion and viability testing of discarded human donor livers". *American journal of transplantation : official journal of the American Society of Transplantation and the American Society of Transplant Surgeons* 13, 1327.
- Ott H.C., et al. (2010): "Regeneration and orthotopic transplantation of a bioartificial lung". *Nat Med* 16, 927.
- Parrish A.R., et al. (1995): "Precision-cut tissue slices: applications in pharmacology and toxicology". *Life Sci* 57, 1887.
- Pelletier J.C., et al. (2009): "(1-(4-(Naphthalen-2-yl)pyrimidin-2-yl)piperidin-4-yl)methanamine: a wingless beta-catenin agonist that increases bone formation rate". *Journal of medicinal chemistry* 52, 6962.
- Petersen T.H., et al. (2010): "Tissue-Engineered Lungs for in Vivo Implantation". *Science* 329, 538.
- Pilaz L.J., et al. (2014): "Live imaging of mitosis in the developing mouse embryonic cortex". *Journal of visualized experiments : JoVE*
- Poon I.K., et al. (2010): "Molecular mechanisms of late apoptotic/necrotic cell clearance". *Cell death and differentiation* 17, 381.
- Rabe K.F., et al. (2007): "Global strategy for the diagnosis, management, and prevention of chronic obstructive pulmonary disease: GOLD executive summary". *Am J Respir Crit Care Med* 176, 532.
- Rausch S.M., et al. (2011): "Local Strain Distribution in Real Three-Dimensional Alveolar Geometries". *Ann Biomed Eng* 39, 2835.
- Rawlins E.L. (2008): "Lung epithelial progenitor cells: lessons from development". *Proc Am Thorac Soc* 5, 675.
- Rawlins E.L., et al. (2008): "Epithelial stem/progenitor cells in lung postnatal growth, maintenance, and repair". *Cold Spring Harbor symposia on quantitative biology* 73, 291.

- Rehberg M., et al. (2014): "Changes in intracellular metabolite pools during growth of adherent MDCK cells in two different media". *Applied microbiology and biotechnology* 98, 385.
- Ressmeyer A.R., et al. (2006): "Characterisation of guinea pig precision-cut lung slices: comparison with human tissues". *Eur Respir J* 28, 603.
- Rice W.L., et al. (2013): "High resolution helium ion scanning microscopy of the rat kidney". *PLoS One* 8, e57051.
- Rock J., et al. (2012): "Endogenous lung regeneration: Potential and limitations". *Am J Respir Crit Care Med* 186, 1213.
- Rock J.R., et al. (2011): "Multiple stromal populations contribute to pulmonary fibrosis without evidence for epithelial to mesenchymal transition". *Proc Natl Acad Sci U S A* 108, E1475.
- Rouwkema J., et al. (2008): "Vascularization in tissue engineering". *Trends in biotechnology* 26, 434.
- Sanderson M.J. (2011): "Exploring lung physiology in health and disease with lung slices". *Pulm Pharmacol Ther* 24, 452.
- Santibanez J.F., et al. (2011): "TGF-beta/TGF-beta receptor system and its role in physiological and pathological conditions". *Clinical science* 121, 233.
- Satoh K., et al. (2005): "Enzymatic detection of precursor cell populations of preneoplastic foci positive for gamma-glutamyltranspeptidase in rat liver". *International journal of cancer Journal international du cancer* 115, 711.
- Schleputz M., et al. (2012): "Neurally Mediated Airway Constriction in Human and Other Species: A Comparative Study Using Precision-Cut Lung Slices (PCLS)". *PLoS One* 7, e47344.
- Schleputz M., et al. (2010): "Electric field stimulation of precision-cut lung slices". *J Appl Physiol* 110, 545.
- Schnorbusch K., et al. (2012): "Precision-cut vibratome slices allow functional live cell imaging of the pulmonary neuroepithelial body microenvironment in fetal mice". *Advances in experimental medicine and biology* 758, 157.
- Seehase S., et al. (2011): "Bronchoconstriction in non-human primates: a species comparison". *J Appl Physiol* 111, 791.
- Semenov M.V., et al. (2007): "SnapShot: Noncanonical Wnt Signaling Pathways". *Cell* 131, 1378.
- Shan J., et al. (2005): "Identification of a specific inhibitor of the dishevelled PDZ domain". *Biochemistry* 44, 15495.
- Shapiro S.D. (2002): "Proteinases in chronic obstructive pulmonary disease". *Biochemical Society transactions* 30, 98.
- Sharafkhaneh A., et al. (2008): "Pathogenesis of emphysema: from the bench to the bedside". *Proc Am Thorac Soc* 5, 475.

- Shi Y., et al. (2012): "Rora is Induced in the Setting of DNA Damage and Promotes Pulmonary Emphysema". *Am J Respir Crit Care Med* 186, 412.
- Shim K. (2011): "Vibratome sectioning for enhanced preservation of the cytoarchitecture of the mammalian organ of Corti". *Journal of visualized experiments : JoVE*
- Smith P.F., et al. (1985): "Dynamic organ culture of precision liver slices for in vitro toxicology". *Life Sci* 36, 1367.
- Sokocevic D., et al. (2013): "The effect of age and emphysematous and fibrotic injury on the re-cellularization of de-cellularized lungs". *Biomaterials* 34, 3256.
- Souidi N., et al. (2013): "Ischemia-reperfusion injury: beneficial effects of mesenchymal stromal cells". *Current opinion in organ transplantation* 18, 34.
- Stockley R.A., et al. (2009): "Burden and pathogenesis of chronic obstructive pulmonary disease". *Proc Am Thorac Soc* 6, 524.
- Sturton G., et al. (2008): "Small airways: an important but neglected target in the treatment of obstructive airway diseases". *Trends Pharmacol Sci* 29, 340.
- Sturton R.G., et al. (2008): "Pharmacological characterization of indacaterol, a novel once daily inhaled 2 adrenoceptor agonist, on small airways in human and rat precision-cut lung slices". *J Pharmacol Exp Ther* 324, 270.
- Takizawa H., et al. (2001): "Increased expression of transforming growth factor-beta1 in small airway epithelium from tobacco smokers and patients with chronic obstructive pulmonary disease (COPD)". *Am J Respir Crit Care Med* 163, 1476.
- Tanjore H., et al. (2011): "Alveolar epithelial cells undergo epithelial-to-mesenchymal transition in response to endoplasmic reticulum stress". *J Biol Chem* 286, 30972.
- Tanjore H., et al. (2013): "β-Catenin in the Alveolar Epithelium Protects from Lung Fibrosis following Intratracheal Bleomycin". *American Journal of Respiratory and Critical Care Medicine* 187, 630.
- Taylor I.W., et al. (2008): "SnapShot: The TGFbeta pathway interactome". *Cell* 133, 378 e1.
- Thiery J.P., et al. (2006): "Complex networks orchestrate epithelial-mesenchymal transitions". *Nature reviews Molecular cell biology* 7, 131.
- Treutlein B., et al. (2014): "Reconstructing lineage hierarchies of the distal lung epithelium using single-cell RNA-seq". *Nature* 509, 371.
- Umachandran M., et al. (2004): "Metabolic and structural viability of precision-cut rat lung slices in culture". *Xenobiotica* 34, 771.
- Vaira V., et al. (2010): "Preclinical model of organotypic culture for pharmacodynamic profiling of human tumors". *Proc Natl Acad Sci U S A* 107, 8352.

- van Diemen C.C., et al. (2006): "Decorin and TGF-beta1 polymorphisms and development of COPD in a general population". *Respir Res* 7, 89.
- Van Scoyk M., et al. (2008): "Wnt signaling pathway and lung disease". *Transl Res* 151, 175.
- Vestbo J., et al. (2013): "Global strategy for the diagnosis, management, and prevention of chronic obstructive pulmonary disease: GOLD executive summary". *Am J Respir Crit Care Med* 187, 347.
- Vickers A.E., et al. (2005): "Precision-cut organ slices to investigate target organ injury". *Expert Opin Drug Metab Toxicol* 1, 687.
- Wagner D.E., et al. (2014): "Comparative decellularization and recellularization of normal versus emphysematous human lungs". *Biomaterials* 35, 3281.
- Wang H., et al. (2003): "Effect of cigarette smoke on fibroblast-mediated gel contraction is dependent on cell density". *Am J Physiol Lung Cell Mol Physiol* 284, L205.
- Wang H., et al. (2014): "Serial optical coherence scanner for large-scale brain imaging at microscopic resolution". *NeuroImage* 84, 1007.
- Wang R., et al. (2011): "Down-regulation of the canonical Wnt beta-catenin pathway in the airway epithelium of healthy smokers and smokers with COPD". *PLoS One* 6, e14793.
- Wang Y., et al. (2013): "miR-375 regulates rat alveolar epithelial cell trans-differentiation by inhibiting Wnt/beta-catenin pathway". *Nucleic acids research* 41, 3833.
- Weyker P.D., et al. (2013): "Lung ischemia reperfusion injury: a bench-to-bedside review". *Seminars in cardiothoracic and vascular anesthesia* 17, 28.
- WHO (Date last updated: October 2013. Date last accessed: June 02 2014): "Factsheet Chronic obstructive pulmonary disease". <http://www.who.int/mediacentre/factsheets/fs315/en/>
- Wilhelm K.R., et al. (2014): "Hyperoxia increases the elastic modulus of alveolar epithelial cells through Rho kinase". *The FEBS journal* 281, 957.
- Willis B.C., et al. (2007): "TGF-beta-induced EMT: mechanisms and implications for fibrotic lung disease". *Am J Physiol Lung Cell Mol Physiol* 293, L525.
- Wohlsen A., et al. (2003): "The early allergic response in small airways of human precision-cut lung slices". *Eur Respir J* 21, 1024.
- Wright J.L., et al. (2008): "Short-term exposure to cigarette smoke induces endothelial dysfunction in small intrapulmonary arteries: analysis using guinea pig precision cut lung slices". *J Appl Physiol* 104, 1462.
- Wyatt T.A., et al. (2012): "Co-exposure to cigarette smoke and alcohol decreases airway epithelial cell cilia beating in a protein kinase C epsilon-dependent manner". *The American journal of pathology* 181, 431.

- Xi Y., et al. (2014): "Inhibition of epithelial-to-mesenchymal transition and pulmonary fibrosis by methacycline". *Am J Respir Cell Mol Biol* 50, 51.
- Yang C., et al. (2014): "Mechanical memory and dosing influence stem cell fate". *Nature materials* 13, 645.
- Yang I.A., et al. (2007): "Inhaled corticosteroids for stable chronic obstructive pulmonary disease". *The Cochrane database of systematic reviews*, CD002991.
- Zemans R.L., et al. (2011): "Neutrophil transmigration triggers repair of the lung epithelium via beta-catenin signaling". *Proc Natl Acad Sci U S A* 108, 15990.
- Zhang M., et al. (2012): "Expression of canonical WNT/beta-CATENIN signaling components in the developing human lung". *BMC developmental biology* 12, 21.
- Zhang N., et al. (2011): "FoxM1 promotes beta-catenin nuclear localization and controls Wnt target-gene expression and glioma tumorigenesis". *Cancer cell* 20, 427.
- Zhang Y.E. (2009): "Non-Smad pathways in TGF-beta signaling". *Cell research* 19, 128.
- Zhao L., et al. (2013): "Transdifferentiation of alveolar epithelial type II to type I cells is controlled by opposing TGF-beta and BMP signaling". *Am J Physiol Lung Cell Mol Physiol* 305, L409.
- Zhou B., et al. (2012): "Interactions between beta-catenin and transforming growth factor-beta signaling pathways mediate epithelial-mesenchymal transition and are dependent on the transcriptional co-activator cAMP-response element-binding protein (CREB)-binding protein (CBP)". *J Biol Chem* 287, 7026.
- Zhou J., et al. (2012): "Local small airway epithelial injury induces global smooth muscle contraction and airway constriction". *J Appl Physiol* 112, 627.
- Zhou S., et al. (2013): "Aging does not enhance experimental cigarette smoke-induced COPD in the mouse". *PLoS One* 8, e71410.
- Zimmerman Z.F., et al. (2012): "Targeting Wnt pathways in disease". *Cold Spring Harbor perspectives in biology* 4

8 APPENDIX

8.1 Acknowledgements

Oliver Eickelberg I like to thank for the opportunity to do my PhD at the Comprehensive Pneumology Center and the helpful discussions during various meetings.

I am very thankful to Melanie Königshoff for the supervision and constant support during my thesis. We had great discussions and it helped me to become a better scientist.

Silke Meiners I want to thanks for her supervision and helpful discussions and advices.

Reinoud Gosens I like to thank for being part of my thesis committee, the great support discussing my work with him, and the advices he gave me.

From the Asklepios Clinics in Gauting I would like to thank Michael Lindner, Ina Koch, Anja Stohwasser, and Diana Steinhart for providing the human samples and the perfect cooperation in general.

Stephanie Kohlmann, Andrea Naujok, Konstanze Heise, Stefan Ambos and all other members of the small animal facility of the CPC I would like to thank for help with animal weighing, ordering, housing, and instillation and especially for being patient and flexible for changes on short notice.

I am especially thankful to Nadine Adam for excellent technical support and help with RNA and protein isolations, genotyping, elastase instillations, immunofluorescence stainings, and generation of 3D *ex vivo* tissue cultures from mice and humans. You have been a great help.

Marlene Stein I would like to thank for the introduction to Western blotting and troubleshooting with the Bioanalyzer.

I would like to thank Maria Neuner for help with the microtome sections and immunohistochemical stainings.

I am thankful to Julia Kipp and Anastasia van denBerg for their patience with ordering stuff and lab organization in general. Keep it running!

Gerald Burgstaller I like to thank for help with all kinds of problems concerning imaging and the imaging post-processing.

Bernd Lentner and Gunther Eder I like to thank for all the small tools they prepared for my special needs.

Ernestine Lusse and Heidi Freimüller I like to thank for keeping the institute running on clean glass supply, autoclaved things, buffers, and all the other small things that you took care of for all of us.

Sarah Vierkotten, Kathrin Mutze, Hoeke Baarsma, Verena Aumiller, and Elisenda Banon-Maneus I like to thank very much for various discussions and help with troubleshooting for all different kinds of experiments. I learned a lot from all of you.

The whole Königshoff Lab I like to thank for the good atmosphere and the helpful discussions. It was a pleasure to work with all of you.

For prove-reading, and their helpful comments I like to thank Sarah Vierkotten, Kathrin Mutze, Hoeke Baarsma, Darcy Wagner, Barbara Berschneider, and Susanne Schäfer. It takes a village to find all mistakes in a text of that length.

Barbara Berschneider, Jens Callegari, Bettina Oehrle, Andrea Schamberger, and Natascha Perera I like to thank for their constant support and their time to have coffee and discussions with me.

All PhD students of the CPC I like to thank for closing all the gaps that I had before talking to them and the great parties we celebrated. Our offices were always a fun place as well.

My friends I like to thank for helping me to have a life next to the thesis and understanding that I also had to work on the weekends.

Johanna Hell I like to thank for her patience with me, her understanding for my strange working hours and support in many ways during my thesis.

I am very grateful to my whole family for their constant support over the last years. Without you, this would never have been possible. Thanks!

8.2 Curriculum vitae

Franziska Elisabeth Uhl

Born July 1, 1982, in Hof, Germany

Educational and professional history

| | |
|-------------------|--|
| Since 10/2014 | Post doctoral associate at the University of Vermont, College of Medicine, Department of Pulmonary Medicine, Laboratory of Daniel J. Weiss, MD, PhD, Burlington, VT, USA |
| 03/2010 – 10/2014 | PhD thesis “Determination of lung regeneration using an <i>ex vivo</i> tissue slice model” with PD Dr. rer. nat. Silke Meiners, in the lab of MD, PhD Melanie Königshoff at the Comprehensive Pneumology Center (CPC), Munich, Germany |
| 05/2007 – 02/2010 | Scientist at the BioCer-Entwicklungs-GmbH, Bayreuth, Germany |
| 05/2006 – 03/2007 | Diploma thesis “Bone Tissue Engineering: Comparison of static and dynamic cultivation of bone marrow stromal cells on differently fabricated hydroxyapatite scaffolds” with Prof. Dr. Günther Ziegler, Friedrich-Baur Institut für Biomaterialien, Bayreuth, Germany |
| 10/2001 – 03/2007 | Diploma in “Environmental and bio engineering (materials and process technology)”, University of Bayreuth, Germany |
| 09/1992 – 06/2001 | Abitur, Schiller-Gymnasium, Hof, Germany |

Awards and sholarships

| | |
|-----------------|--|
| 05/2014 | ATS abstracts scholarship at the annual conferences of the American thoracic society (ATS), San Diego, USA |
| 11/2012 | 2 nd place in the Science Slam Contest at the doctoral students day of the Helmholtz Center Munich |
| 04/2012 | Poster award of the European Respiratory Society (ERS) at the 10th Lung Science Conference (LSC), Estoril, Portugal |
| 04/2012 | Travel grant to attend the 10th Lung Science Conference (LSC) of the European Respiratory Society (ERS) in Estoril, Portugal |
| 03/2010-02/2013 | Helmholtz stipend to conduct the PhD project |
| 11/2008 | Poster award of the Deutsche Gesellschaft für Biomaterialien (DGBM), Hamburg, Germany |

Activities and lectures

| | |
|---------------|--|
| 7.-10.10/2013 | Lecture for the COST training school: training module “building a new lung, de- and recellularisation”, precision-cut lung slices of murine tissue |
| 10/2012 | Lecture for graduate students of the Graduate school Lung Biology and Disease: “lung anatomy” |

| | |
|-----------------|--|
| 06/2011-08/2011 | Participation in the DAAD's RISE scholarship program as supervisor for one undergraduate student from USA for 12 weeks |
| 2010-2011 | Elected Graduate Student Representative from HELENA (Helmholtz Graduate School Environmental Health) |

8.3 Publications and presentations

Publications

1. **F.E. Uhl**, S. Vierkotten, G. Burgstaller, I. Koch, M. Lindner, S. Meiners, O. Eickelberg, M. Königshoff: "Preclinical validation and spatio-temporal imaging of lung repair in human 3D lung tissue cultures". *Eur Respir J*, 2015 Apr 30, in press.
2. D.E. Wagner, **F.E. Uhl**, D.J. Weiss: "Acellular lung scaffolds in lung bioengineering" *Stem Cell Biology, Regenerative Med.: Stem Cells in the Lung*, Springer (2015).
3. D.E. Wagner, **F.E. Uhl**, M. Königshoff, D.J. Weiss: "Ex vivo lung bioengineering". *Stem Cells and Regenerative Medicine Series: Lung Stem Cells in the Epithelium & Vasculature*, Springer (2014).
4. M. Königshoff, **F. Uhl**, R. Gosens: From molecule to man: integrating molecular biology with whole organ physiology in studying respiratory disease. *Pulm Pharmacol Ther*, (2011) 24(5):466-470.
5. S. Schaefer, R. Detsch, **F. Uhl**, U. Deisinger, G. Ziegler: "How Degradation of Calcium Phosphate Bone Substitute Materials is influenced by Phase Composition and Porosity". *Adv Eng Mat* (2011) 13(4):342-350.
6. M. Schumacher, **F. Uhl**, R. Detsch, U. Deisinger, G. Ziegler: "Static and dynamic cultivation of bone marrow stromal cells on biphasic calcium phosphate scaffolds derived from an indirect rapid prototyping technique". *J Mater Sci Mater Med*, (2010) 21(11):3039-3048.
7. R. Detsch, I. Dieser, U. Deisinger, **F. Uhl**, S. Hamisch, G. Ziegler, G. Lipps: "Biofunctionalization of dispense-plotted hydroxyapatite scaffolds with peptides: Quantification and cellular response". *J. Biomed Mater Res A*, (2010) 92(2):493-503.
8. R. Detsch, **F. Uhl**, U. Deisinger, G. Ziegler: "3D-Cultivation of bone marrow stromal cells on hydroxyapatite scaffolds fabricated by dispense-plotting and negative mould technique". *J Mater Sci Mater Med*, (2008) Apr;19(4):1491-6.

Oral presentations

1. **F. Uhl**, G. Burgstaller, I. Koch, M. Lindner, O. Eickelberg, M. Königshoff. "Determination of Wnt/beta-catenin driven lung repair processes in mouse and human lung tissue cultures *ex vivo*". Biochemical determinants of Tissue regeneration, Macclesfield, UK (11.-13.12.2013). selected speaker

2. **F. Uhl**, G. Burgstaller, I. Koch, M. Lindner, O. Eickelberg, M. Königshoff. „The role of Wnt/beta-catenin signalling for lung repair in an *ex vivo* tissue culture model”. 2nd German-French Lung Retreat, Tours, France (16.-19.9.2013).
selected speaker
3. **F. Uhl**, M. Königshoff: “Imaging WNT/beta-catenin signalling in an *ex vivo* tissue culture model of lung repair”. 2nd symposium of the NRS taskforce on animal models in pulmonary research, Utrecht, The Netherlands (10.-11.10.2012).
invited speaker
4. **F. Uhl**, M. Königshoff: “Imaging WNT/beta-catenin signalling in an *ex vivo* tissue culture model of lung repair”. 2nd Munich Lung Conference (MLC), Munich, Germany (5.-6.10.2012).
selected abstract
5. **F. Uhl**, R. Detsch, M. Schumacher, U. Deisinger, G. Ziegler: „Bone Tissue Engineering mit biphasischen über Rapid Prototyping hergestellten Calciumphosphat-Scaffolds.“ Jahrestagung der Deutschen Gesellschaft für Biomaterialien, Hamburg, Germany (20.11.2008 - 22.11.2008).

Poster presentations

1. B. Zvarova, **F.E. Uhl**, N.R. Bonenfant, J.J. Uriarte, W. Chia, Z. Borg, D.J. Weiss, D.E. Wagner. “Residual Detergent Detection and Cell Viability Testing in Decellularized Whole Lungs”. Annual conference of the ATS, Denver, USA (15.-20.05.2015).
2. **F.E. Uhl**, S. Vierkotten, G. Burgstaller, M. Linder, O. Eickelberg, S. Meiners, M. Königshoff. “Preclinical testing of therapeutic Wnt/beta-catenin activation in human 3D lung tissue cultures”. ERS, Munich, Germany (6.-10.9.2014).
3. **F.E. Uhl**, S. Vierkotten, G. Burgstaller, I. Koch, M. Lindner, S. Meiners, O. Eickelberg, M. Königshoff. “Wnt/beta-catenin signalling drives alveolar epithelial cell repair processes in mouse and human lung tissue cultures *ex vivo*”. Annual conference of the ATS, San Diego, USA (16.-21.05.2014).
4. **F. Uhl**, G. Burgstaller, I. Koch, M. Lindner, O. Eickelberg, M. Königshoff. “Determination of Wnt/beta-catenin driven lung repair processes in mouse and human lung tissue cultures *ex vivo*” Biochemical determinants of Tissue regeneration, Macclesfield, UK (11.-13.12.2013).
5. **F. Uhl**, G. Burgstaller, I. Koch, M. Lindner, O. Eickelberg, M. Königshoff. “The role of WNT/ β -catenin signalling for lung repair in an *ex vivo* tissue culture model”. 3rd Munich Lung Conference (MLC), Munich, Germany (2013)
6. **F. Uhl**, G. Burgstaller, O. Eickelberg, M. Königshoff. “Determination of lung repair processes in an *ex vivo* lung tissue culture model”. 2013 Stem Cell Conference, Burlington, Vermont, USA (2013)
7. **F. Uhl**, M. Königshoff: “Imaging WNT/beta-catenin signalling in an *ex vivo* tissue culture model of lung repair” European Respiratory Society, Vienna, Austria (2012)

8. **F. Uhl**, M. Königshoff: "Imaging WNT/beta-catenin signalling in an *ex vivo* tissue culture model of lung repair" 10th Lung Science Conference of the European Respiratory Society, Estoril, Portugal (2012), poster award
9. **F. Uhl**, R. Detsch, U. Deisinger, G. Ziegler: „Bone Tissue Engineering: Einfluss unterschiedlich hergestellter Calciumphosphat-Scaffolds auf die osteogene Stimulierung von Knochenmarkzelle.“ 17. Symposium Verbundwerkstoffe und Werkstoffverbunde, DGM, Bayreuth, Germany (2009)
10. R. Detsch, A. Schlechte, **F. Uhl**, U. Deisinger, G. Ziegler: „Herstellung von vitalen Zell-Alginat Scaffolds via Rapid Prototyping.“ Jahrestagung der Deutschen Gesellschaft für Biomaterialien, Hamburg, Germany (2008), poster award

8.4 Eidesstattliche Versicherung

Uhl, Franziska Elisabeth

Ich erkläre hiermit an Eides statt,
dass ich die vorliegende Dissertation mit dem Thema

“Determination of lung regeneration using an *ex vivo* tissue slice model”

selbständig verfasst, mich außer der angegebenen keiner weiteren Hilfsmittel bedient und alle Erkenntnisse, die aus dem Schrifttum ganz oder annähernd übernommen sind, als solche kenntlich gemacht und nach ihrer Herkunft unter Bezeichnung der Fundstelle einzeln nachgewiesen habe.

Ich erkläre des Weiteren, dass die hier vorgelegte Dissertation nicht in gleicher oder in ähnlicher Form bei einer anderen Stelle zur Erlangung eines akademischen Grades eingereicht wurde.

München, den 06.Oktober 2014



édition scientifique
VVB LAUFERSWEILER VERLAG

VVB LAUFERSWEILER VERLAG
STAUFBENBERGRING 15
D-35396 GIESSEN

Tel: 0641 5599888 Fax: 5599890
redaktion@doktorverlag.de
www.doktorverlag.de

ISBN: 978-3-8359-6351-1



9 783835 963511